CELLULAR AND MOLECULAR MECHANISM OF *LISTERIA* ADHESION PROTEIN-MEDIATED BACTERIAL CROSSING OF THE INTESTINAL BARRIER

by

Rishi Drolia

A Dissertation

Submitted to the Faculty of Purdue University

In Partial Fulfillment of the Requirements for the degree of

Doctor of Philosophy

Department of Food Science

West Lafayette, Indiana

December 2018

THE PURDUE UNIVERSITY GRADUATE SCHOOL
STATEMENT OF COMMITTEE APPROVAL

Dr. Arun K. Bhunia, Chair
Department of Food Science
Dr. Abigail Durkes,
Department of Comparative Pathobiology
Dr. Daoguo Zhou,
Department of Biological Sciences
Dr. Kee-Hong Kim,
Department of Food Science
Dr. Ramesh Vemulapalli,
Department of Comparative Pathobiology

Approved by:

Dr. Arun K. Bhunia,
Head of the Graduate Program

To my brother Ashish and sister Richa, Rest in Peace!

ACKNOWLEDGMENTS

First and foremost, I express my deepest gratitude and thank my major professor Dr. Arun K. Bhunia. I am grateful to him for providing me with the opportunity to work in his lab, believing in me, being patient, giving me excellent suggestions and helping with animal dissections and illustrations used in this dissertation. His guidance and mentorship has been instrumental in development of my independent scientific temperament. He has constantly motivated me to continue improving for a scientific career. The knowledge and experience he has shared is invaluable and will remain with me for my lifetime. His mentorship has prepared me for a successful future in science.

I thank my graduate advisory committee members; Dr. Abigail Durkes, Dr. Daoguo Zhou, Dr. Kee-Hong Kim and Dr. Ramesh Vemulapalli for providing their valuable suggestions and discussion during my committee meetings. I am very grateful to Dr. Abigail Durkes for always taking out time to contribute to the histopathological studies performed in this dissertation. I also pay my sincerest thank to Dr. Jerrold R. Turner at Harvard Medical School to have reviewed a part of this work and for providing the MLCK-knockout mice line.

I was very fortunate to make friends with present and past post-doctoral associates in the lab; Dr. Atul K. Singh, Dr. Shivendra Tenguria and Dr. Krishna Mishra. I thank Atul for his valuable professional advice and scientific discussions. I am indebted to Shivendra and thank him for directly contributing to experiments in the chapter 2 of the dissertation, transmission electron microscopic images (Figure 3.6) and always being available to help with any experiment in the lab be it day or night. I thank Dr. Mishra, for providing valuable professional advice during my graduate study.

I acknowledge the extraordinary cooperation and help with microbiological plating by the graduate students in the Bhunia lab; Celina To, Dongqui Liu, Luping Xu, Manalee Samaddar Marcella Martinez, Tawfiq Alsulami, Valerie Ryan and Xingjian Bai. I would like to recognize the exceptional support of the undergraduate researches in the lab; particularly, Allison Guthrie, Jingyi Ren, Tang Qi, Shangqi Wu and Wen Lv for having helped me with arrangements of large number of animal studies performed to accomplish this work. I also acknowledge Manoj Sawale for help with microbiological plating and Gustavo Moreira for help with cloning.

I thank my graduate school friends and colleagues; Jonathan Kershaw and Malithi Wickramathilaka for critically reading a part of this dissertation; and Preetam Sarkar, for valuable scientific discussions. I also express thanks to members of core facilities at Purdue University; Dr. James Andy Schaber for assistance with confocal microscopy and Donna Brooks, Gabrielle E. Shafer and Victor. Bernal-Crespo for help with histopathology.

I also take this opportunity to thank all the administrative staff of the food science department. A special thanks to the graduate coordinator; Mitzi Barnett, for always willing to help me with graduate school procedures; and Deborah M. Livengood, the purchasing clerk, for helping me with purchasing of chemicals and reagents used in this study.

Lastly, I would like to thank my parents; Harish and Sangeeta Drolia, for their unconditional love and emotional support. Most importantly, I thank my wife; Nishi, without whom this journey would be impossible and for always understanding the late nights and week-ends that is spent in the laboratory or at home writing. I also thank her for assisting with formatting this dissertation.

TABLE OF CONTENTS

LIST OF TABLES

LIST OF FIGURES

LIST OF VIDEOS

ABSTRACT

Author: Drolia, Rishi. PhD
Institution: Purdue University
Degree Received: December 2018
Title:Cellular and Molecular Mechanism of *Listeria* Adhesion Protein-Mediated Bacterial Crossing of the Intestinal Barrier
Committee Chair: Professor Arun K. Bhunia

The crossing of host barriers (intestinal, blood-brain, and placental) is a critical step for systemic infections caused by entero-invasive pathogens. In the intestine, the epithelial cells are the first line of defense against enteric pathogens. *Listeria monocytogenes* is a facultative-intracellular foodborne pathogen that first crosses the intestinal barrier to cause a systemic infection. However, the underlying mechanism is not well understood.

We demonstrate that *Listeria* adhesion protein (LAP) promotes the translocation of *L. monocytogenes* across the intestinal barrier in mouse models (A/J and C57BL/6). Relative to the wild-type (WT; serotype 4b) or the isogenic bacterial invasion protein Internalin A mutant (Δ*inlA*) strain, the *lap*$^{-}$ strain showed significant defect in translocation across the intestinal barrier and colonization of the mesenteric-lymph nodes, liver and spleen in the early phase of infection (24 h and 48 h). LAP induces intestinal epithelial barrier dysfunction for increased translocation as evidenced by increased permeability to 4-kDa FITC-dextran (FD4), a marker of paracellular permeability, in the serum and urine of WT and Δ*inlA*- infected mice and across Caco-2 cell barrier, but not the *lap*$^{-}$ mutant strain. Microscopic examination confirmed localization of the WT and Δ*inlA* strains in the tight junction, a crucial barrier of intestinal paracellular permeability, in the mouse ileal tissue but the *lap*$^{-}$ strain remained confined in the lumen. LAP also upregulates TNF-α and IL-6 in intestinal epithelia of mice and in Caco-2 cells for increased permeability.

Investigation of the underlying molecular mechanisms of LAP-mediated increase in intestinal permeability by using *lap*$^{-}$ mutant strain, purified LAP and shRNA-mediated Hsp60 suppression, we demonstrate that LAP interacts with its host receptor, Hsp60, and activates the canonical NF-κB signaling, which in turn facilitates myosin light-chain kinase (MLCK)-mediated opening of the epithelial barrier via the cellular redistribution of major epithelial junctional proteins claudin-1, occludin, and E-cadherin. Pharmacological inhibition of NF-κB or

MLCK in cells or genetic ablation of MLCK in mice (C57BL/6) prevents mislocalization of epithelial junctional proteins, intestinal permeability and *L. monocytogenes* translocation across the intestinal barrier.

Furthermore, LAP also promotes *L. monocytogenes* translocation across the intestinal barrier and systemic dissemination in a Mongolian gerbil that are permissive to the bacterial invasion proteins; InlA-and InlB-mediated pathways; similar to that in humans. We show a direct LAP-dependent and InlA-independent pathway for *L. monocytogenes* paracellular translocation across the intestinal epithelial cells that do not express luminally accessible E-cadherin. Additionally, we show a functional InlA/E-cadherin interaction pathway that aids *L. monocytogenes* translocation by targeting cells with luminally accessible E-cadherin such as cells at the site of epithelial cell extrusion, epithelial folds and mucus-expelling goblet cells. Thus, *L. monocytogenes* uses LAP to exploit epithelial innate defense in the early phase of infection to cross the intestinal epithelial barrier, independent of other invasion proteins.

This work fills a critical gap in our understanding of *L. monocytogenes* pathogenesis and sheds light to the complex interplay between host-pathogen interactions for bacterial crossing of the crucial intestinal barrier.

CHAPTER 1. REVIEW OF LITERATURE

The following chapter is under revision for publication and is modified from: Drolia, R. and Bhunia, A.K. Crossing the Intestinal Barrier Via *Listeria* Adhesion Protein and Internalin A Trends in Microbiology TIMI-D-18-00177.

Foodborne Listeria monocytogenes Infection

Listeria monocytogenes is an opportunistic and highly invasive foodborne bacterial pathogen. *L. monocytogenes* was first isolated from rabbits (Murray et al. 1926). In the early part of the 20th century, the pathogen was recognized an animal pathogen and found to infect ruminants, predominantly cows and sheep, causing circling disease and abortion. Animals suffer from ataxia, anorexia, depression, lethargy, septicemia, meningitis, head tilt, and encephalitis, which result in the loss of balance and thereby causing the animals to walk in a circle (Brugere-Picoux 2008). *L. monocytogenes* was not recognized as a human foodborne pathogen until early the 1980s, when multiple outbreaks were reported in North America (Schlech et al. 1983; Swaminathan and Gerner-Smidt 2007). Researchers began to link this pathogen's association with soil, manure, decaying vegetation, and environment (Welshimer and Donker-Voet 1971; NicAogáin and O'Byrne 2016) as the primary mode of transmission to foods. *L. monocytogenes* is highly adaptable and uses sophisticated regulatory mechanisms to make the transition from a soil-living saprophyte to an invasive pathogen in humans and animals during foodborne infection (Freitag et al. 2009; Toledo-Arana et al. 2009).

The breaching of barriers such as the host intestinal (Lecuit et al. 2001), blood-brain (Ghosh et al. 2018; Pägelow et al. 2018), and placental (Vázquez-Boland et al. 2017; Lamond and Freitag 2018) is a key mechanism of the intracellular bacterium *L. monocytogenes* (Radoshevich and Cossart 2018). Pregnant women, fetuses, newborn children, adults aged 65

and older, and people with weakened immune systems are most at risk and suffer from severe illnesses including sepsis, meningitis, or encephalitis, often with lifelong consequences. Listeriosis outbreaks are often associated with ready-to-eat (RTE) products including deli meats, hot dogs, liver pâté, smoked fish, soft cheeses prepared from unpasteurized milk, ice cream, coleslaw, and produce such as frozen vegetables, cantaloupe, and apple (Swaminathan and Gerner-Smidt 2007). In the U.S., about 1,600 people are infected each year, causing an estimated 260 deaths (Scallan et al. 2011). Among the foodborne pathogens, *L. monocytogenes* infections result in the highest hospitalization and case fatality rate (20–30%) compared to other pathogens (Scallan et al. 2011; Lomonaco et al. 2015). In 2010, listeriosis resulted in 23,150 illnesses and 5463 deaths worldwide (de Noordhout et al. 2014). Recently, one of the largest outbreaks of listeriosis has been reported in South Africa, with a total of 1060 cases and 216 deaths as of July 26, 2018 (http://www.nicd.ac.za/index.php/listeriosis-outbreak-situation-report/). The estimated infectious dose of *L. monocytogenes* is 10^6–10^7 colony-forming units in primates and susceptible humans (Farber et al. 1996; Smith et al. 2008), but as few as 10^4 organisms could have caused listeriosis in immunocompromised patients in a foodborne outbreak in Finland involving contaminated butter (Maijala et al. 2001). However, in the 2015 ice cream outbreak in the U.S., the FDA estimated that 99.8% of ice cream samples contained <100 most probable number/g, thus implying a very low infectious dose for this pathogen (Pouillot et al. 2016; Buchanan et al. 2017). This further indicates that *L. monocytogenes* has to be highly efficient in crossing the gut epithelial barrier and avoiding the host innate defense for its systemic spread.

Owing to the lack of accurate infectious dose and high mortality among the high-risk groups, the US Food Safety Inspection Service agency has established a zero-tolerance policy in RTE products in 1989, i.e., 0 cells in 5 × 25 g samples. While the rationale for the zero-tolerance

policy has been questioned, in the absence of solid evidence of actual infectious dose, the zero-tolerance policy continues to be enforced. Often, *Listeria*-tainted products are recalled, costing the food industry millions of dollars and a negative impact on brand reputation, thereby inflicting more financial damage. The annual cost of damages due to *L. monocytogenes* in the USA is about US$ 2.8 billion (Hoffmann et al. 2012; Batz et al. 2014). The European Food Safety Authority permits <100 CFU/g of RTE food provided an appropriate antibacterial growth barrier is present, even though the number of confirmed human listeriosis cases is on the rise (Lomonaco et al. 2015; Ricci et al. 2018). Thus, understanding of how *L. monocytogenes* can breach critical host barriers to cause a systemic infection is of foremost importance.

The Anatomy of Intestinal Epithelial Barrier

The crossing of the gastrointestinal barrier is the first and a critical step in the infectious process of a foodborne pathogen.

The mammalian intestine contains as high as 10^{14} commensal bacteria of approximately 100 different species, which form the microbiota. The microbiota not only contributes to digestive, metabolic, and immune functions of the gut, but also competes for colonization with the pathogenic bacteria (Keeney and Finlay 2011; Martens et al. 2018). The gut microbiota can restrict the colonization of pathogenic bacteria by competing for nutrients. For example, the commensal *Escherichia coli* Nissle and HS strains outcompete and diminish the colonization of the pathogenic *E. coli* O157:H7 by competing for carbohydrates (Maltby et al. 2013). Similarly, *E. coli* Nissle inhibits the colonization of the pathogenic bacterium *Salmonella enterica* serovar Typhimurium by competing for iron (Deriu et al. 2013). The commensals in the gut microbiota can also secrete small molecules with bacteriostatic or bactericidal activity to protect against pathogens. For example, the commensal *Enterococcus faecalis* strain carrying a plasmid-encoded bacteriocin

clears the vancomycin-resistant *Enterococcus* (VRE) from the intestinal tract (Kommineni et al. 2015). Finally, the gut microbiota can also modulate the immune system to protect against pathogens. For example, the gut microbiota can combat systemic infections through the induction of protective immunoglobulin G (IgG) antibody response (Zeng et al. 2016) Thus, the microbiota can act as an important barrier by resisting the colonization of pathogenic bacteria.

The intestinal epithelium is a heterogeneous population of five differentiated cell types: **goblet cells** (see Glossary), **enterocytes,** enteroendocrine cells, Paneth cells and tuft cells. These cells have important and distinct functions such as mucus-production, absorption, hormone secretion, antimicrobial peptide (AMP) secretion and taste-chemosensory responses, respectively. The luminal surfaces of the intestinal mucosa are covered with hydrated gel composed of **mucins** secreted by the goblet cells (**Figure 1.1 A**). This layer ranges from 700 μm in the stomach and 150–300 μm in the small and large intestines to prevent large particles and intact bacteria from coming into direct contact with the underlying epithelium (McGuckin et al. 2011). However, bacterial pathogens, such as *L. monocytogenes*, possess different virulence factors such as Internalin (Inl) B, InlC, InlJ, InlL and the *Listeria*-mucin-binding invasin A (*lmo1413*) that binds mucins (Lindén et al. 2008; Mariscotti et al. 2014; Popowska et al. 2017). These virulence factors are covalently bound to the bacterial peptidoglycan via anchoring-domains with an LPXTG motif (Bierne and Cossart 2007). The binding of *L. monocytogenes* to mucins via these virulence factors may allow the bacterium to efficiently penetrate the mucus and facilitate bacterial adhesion or invasion of host cells. In contrast, other bacterial pathogens such as *Clostridium perfringens*, enteroaggregative *E. coli*, enterohemorrhagic *E. coli*, *Shigella flexneri, Vibrio cholerae*, and *Yersinia enterocolitica* possess enzymes that degrade mucins or damage **mucus** (McGuckin et al. 2011).

The intestinal barrier is composed of a single layer of polarized columnar epithelial cells called the enterocytes organized into finger-like projections called villi (**Figure 1.1 A**). These cells are self-renewed every 4–5 days, making the intestinal epithelium a highly dynamic structure (Van Der Flier and Clevers 2009). The intestinal epithelial cells are polarized with the apical surface facing the lumen and the basal surface facing the basement membrane. Epithelial cells are networked together through adhesive contacts called junctions, which join cells together and provide a paracellular seal. The space between two adjacent epithelial cells is called the paracellular space. From the apical to basolateral direction, **tight junctions** (TJs), **adherens junctions** (AJs), and **desmosomes** seal this space (**Figures 1.1 B and 1.1 C**). Together, these three types of intercellular junctions comprise the **apical junctional complex** (**Figure 1.1 A**) (Odenwald and Turner 2017).

TJs are made of peripheral membrane proteins such as zonula occludens (ZO) and different classes of transmembrane proteins such as claudins, occludin, tricellulin, junctional adhesion molecules (JAMs), membrane-associated guanylate kinase, and the polarity complex (PAR) family proteins. TJs regulate the flux of ions and solutes, maintain cell polarity and are the primary determinant of paracellular permeability. TJs are physically associated with the actin and myosin filament and are regulated by a variety of kinases and cytoskeletal proteins. One of the principal mediators of TJ regulation is long **myosin light chain kinase (MLCK)** (Turner et al. 1997; Turner 2009). MLCK is the Ca^{2+} calmodulin-dependent serine-threonine kinase that phosphorylates myosin II regulatory light chain (MLC). The AJs are required for the integrity of the TJs and are located immediately subjacent to the TJs. The AJ has **E-cadherin**, α-catenin, β-catenin, and p120 catenin and it interacts with F-actin. The desmosomes are adhesive junctions that connects adjacent epithelial cells and are located below the AJ. These junctions are composed of multiple protein

subunits consisting of desmoglein, desmocollin, desmoplakin, and are the points where keratin filaments attach to the plasma membrane.

Their basolateral side consists of a basement membrane, which is a thin network made of extracellular matrix proteins. The basement membrane initiates and maintains cell polarity and separates epithelial cells from the underlying **lamina propria**, which contains connective tissue, stromal cells, blood and lymphatic capillaries, and immune cells such as lymphocytes, dendritic cells, or resident macrophages.

The barrier function of the intestine is tightly regulated by the apical junctional complex. However, in compromised conditions such as in response to pathological stimulus, the apical junctional complex can be endocytosed. This endocytosis of the TJ and AJ has been reported to occur via three classic pathways of endocytosis (Utech et al. 2009): **macropinocytosis** of the transmembrane TJ proteins, **clathrin**-coated endocytosis of both TJ and AJ proteins, and **caveolin**-mediated endocytosis of the TJ protein occludin. Thus endocytosis induces the disassembly of the epithelial apical junctional complex.

To establish defined boundaries, the mucosal epithelial cells cover the external surface and line internal compartments to form barriers and to prevent unrestricted passage of bacteria. However, enteric bacterial pathogens have evolved sophisticated mechanisms to circumvent this barrier and efficiently cross the gut mucosa that allows bacteria to spread systemically and cause infectious disease.

Figure 1.1 The anatomy of the mucosal barrier

(A) Hematoxylin and eosin staining showing the morphology of the mouse intestine (left). Scale bar, 25 μm. The panels on the right are enlargements of the boxed areas. Scale bar, 5 μm. The intestine is lined with a single layer of polarized epithelial cells (right) organized into finger-like projections called villi and the underlying lamina propria. The lamina propria is located beneath the basement membrane and contains immune cells, including macrophages, dendritic cells, plasma cells, lamina propria lymphocytes, and neutrophils. Goblet cells (right) that release mucus, and other differentiated epithelial cell types are present.

(B) Transmission electron microscopy showing the tight junction (TJ), adherens junction (AJ), and desmosome (Des) of the mouse ileum. Scale bar, 200 nm. The TJ consists of claudins, zonula occludens (ZO), and occludin that interact with F-actin. The myosin light chain kinase (MLCK) is associated with the perijunctional actomyosin ring. The AJ consists of E-cadherin, α-catenin, β-catenin, and p120 catenin, all of which interact with F-actin. Desmosomes are located beneath the apical junctional complex and are composed of desmoglein, desmocollin, and desmoplakin, and interact with the keratin filaments.

(C) Confocal microscopy images of mouse ileal villi immunostained for ZO-1(red), a TJ protein (left), and E-cadherin (red), an AJ protein (right). Nuclei (blue) are counterstained with DAPI. Scale bar, 10 μm. LP, lamina propria.

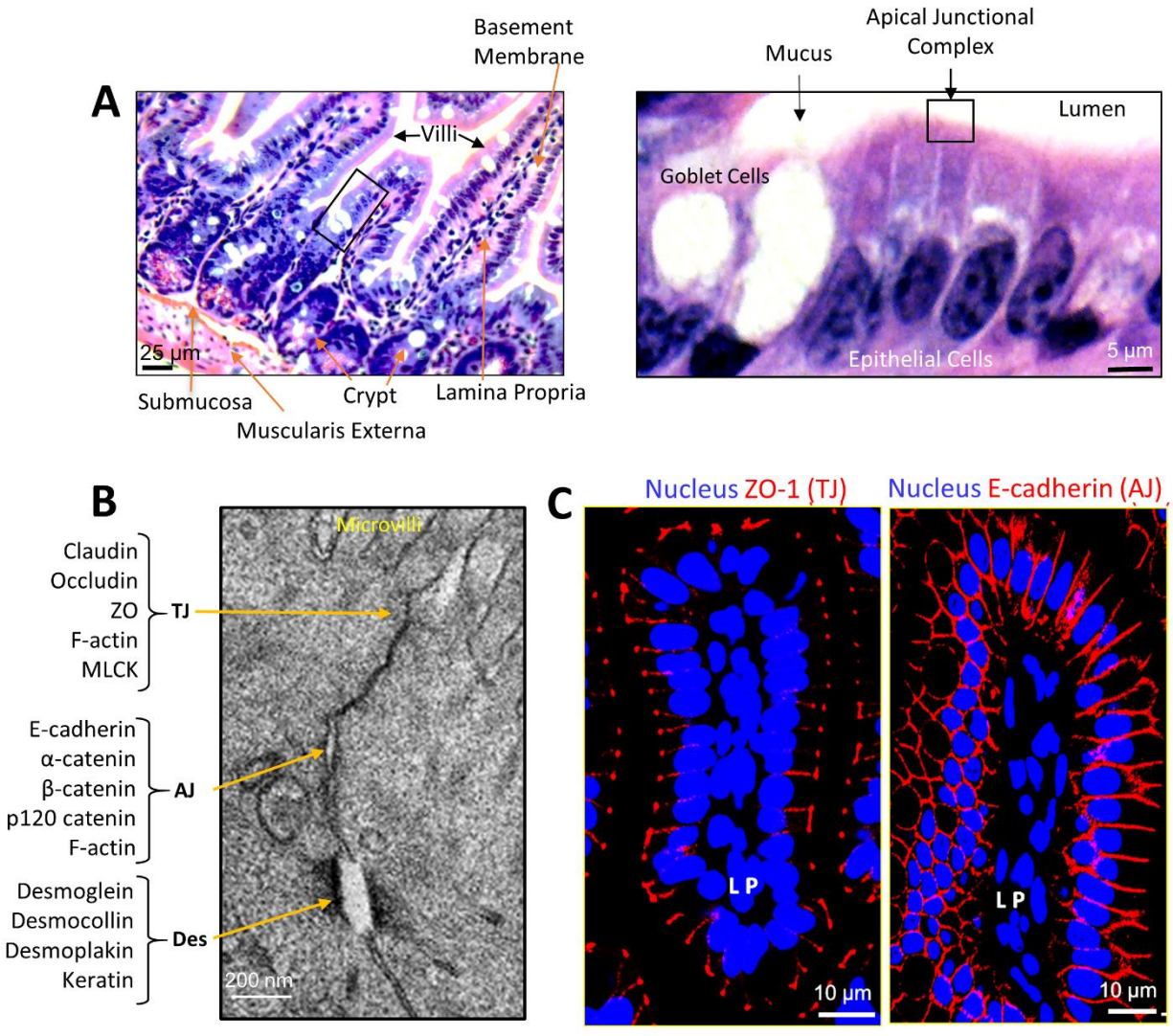
A
Basement Membrane
Villi
25 µm
Submucosa
Crypt
Lamina Propria
Muscularis Externa
Apical Junctional Complex
Mucus
Lumen
Goblet Cells
Epithelial Cells
5 µm
B
Microvilli
Claudin
Occludin
ZO
F-actin
MLCK
TJ
E-cadherin
α-catenin
β-catenin
p120 catenin
F-actin
AJ
Desmoglein
Desmocollin
Desmoplakin
Keratin
Des
200 nm
C
Nucleus ZO-1 (TJ)
Nucleus E-cadherin (AJ)
L P
10 µm
L P
10 µm

L. monocytogenes Pathogenesis and Crossing of the Gut Epithelial Barrier

L. monocytogenes is a facultative intracellular pathogen that invades and multiplies within the cellular compartment, and moves from cell-to-cell (Portnoy et al. 1992). This provides the bacterium a hidden lifestyle and thus is protected from immune cells and antimicrobials. Elegant studies have demonstrated the role of various virulence factors during the intracellular life cycle of *L. monocytogenes*, which has been previously reviewed thoroughly (Portnoy et al. 1992; Bierne et al. 2018; Radoshevich and Cossart 2018). However, the precise mechanism that *L. monocytogenes* employs to cross the intestinal epithelial barrier during the gastrointestinal phase of infection is not fully understood. Although **M** (for microfold) **cells** in the **Peyer's patch** (Marco et al. 1997) and the pathways mediated by the *L. monocytogenes* invasion protein Internalin A (InlA) (Lecuit et al. 2001) aid the crossing of the gut epithelial barrier, the bacterium has been shown to cross the gut barrier in animal models where these two pathways are absent, suggesting the presence of alternate routes (Chiba et al., 2011; Pron et al., 1998) .

The M cell pathway is a passive system, which is used by many enteric pathogens, toxins, biomolecules, or even the resident microbiota. On the other hand, the InlA-mediated pathway is highly specific and it induces membrane protein reorganization to initiate bacterial uptake (Pizarro-Cerdá et al. 2012). *L. monocytogenes* crosses the epithelial barrier by transcytosis and is released into the underlying lamina propria (Nikitas et al. 2011). The bacterium reaches the mesenteric-lymph nodes (MLN) through the lymphatic vessels, disseminates to the liver and spleen via the lymph and blood. It can then spread to secondary target sites of infection such as the central nervous system and the placenta. From the intestine, *L. monocytogenes* can also disseminate to the liver through the hepatic portal vein through a direct route (Melton-Witt et al. 2012).

Multiple reports indicate that *L. monocytogenes* isolates primarily from the environmental or food sources expressing truncated InlA (due to the presence of a premature stop codon in the *inlA* ORF) are less infective in mammalian cell culture or animal models (Olier et al. 2003; Nightingale et al. 2005; Van Stelten et al. 2011). However, more recent studies show that such strains can indeed infect humans (Cruz et al. 2014; Gelbicova et al. 2015; Fravalo et al. 2017) and fetuses of pregnant guinea pigs and mice after oral administration (Holch et al. 2013). These findings provide strong evidence that *L. monocytogenes* also use alternate routes independent of InlA-mediated uptake and the M cell to translocate across the gut barrier.

A recent study has revealed that only a minimal fraction of *L. monocytogenes* in the lymph nodes is intracellular with a vast majority being extracellular (Jones et al. 2015). Additionally, *L. monocytogenes* is primarily associated with monocytes in the intestine and the MLN during the early stages (24–48 h) of infection (Jones and D'Orazio 2017). However, these cells do not serve as an intracellular growth niche, suggesting that intracellular transport in monocytes is not a primary route of dissemination.

The host gut microbiota has an important role during orally acquired listeriosis. Treatment with *Lactobacillus* decreased the invasion capabilities of *L. monocytogenes* in the host intestine (Archambaud et al. 2012). The host gut microbiota interferes with the **microRNA** (miRNA) response upon oral infection with *L. monocytogenes* (Archambaud et al. 2013). In particular, five of miRNA expression variations (in miRNA-143, miRNA-148a, miRNA-200b, miRNA-200c, and miRNA-378) is dependent on the presence of the microbiota (Archambaud et al. 2013). Moreover, a bacteriocin produced by *L. monocytogenes* epidemic strain modulates the host intestinal microbiota for increased host colonization (Quereda et al. 2016). A recent study has identified

intestinal commensal bacteria to enhance resistance against *L. monocytogenes* (Becattini et al. 2017; Becattini and Pamer 2017).

The pattern recognition receptors (PRRs) such as the **toll-like receptors (TLR)** (Kawai and Akira 2011) and the **nucleotide-binding oligomerization domain 2 (NOD2)** (Al Nabhani et al. 2017) in the intestine plays an important role in recognition and elimination of *L. monocytogenes*. Mice lacking MyD88; an intracellular adaptor protein involved in most TLR-mediated signaling, are more susceptible to oral challenge of *L. monocytogenes* (Brandl et al. 2007). The increased susceptibility of the MyD88 knock-out mice to *L. monocytogenes* infection is attributed to the lack of production of the anti-bacterial peptide RegIIIγ (a bactericidal lectin) in these mice. Similarly, mice lacking the NOD2 receptors are more susceptible to oral challenge of *L. monocytogenes* with higher dissemination rates to the liver and spleen (Kobayashi et al. 2005). The increased susceptibility of the NOD2- knockout mice to *L. monocytogenes* infection is attributed to decreased expression of some cryptdins (an antimicrobial peptide) in the small intestine (Kobayashi et al. 2005). A more recent study has also demonstrated an important role of TLR10 of the intestinal epithelial cells in sensing *L. monocytogenes* and eliciting immune responses (Regan et al. 2013).

Therefore, besides the M-cell mediated pathway, the prevailing route for *L. monocytogenes* to cross the intestinal epithelial barrier during the intestinal phase of infection is InlA-mediated transcytosis (**Figure 1.2**) (Radoshevich and Cossart 2018). The following section provides an in-depth review of the M-cell pathway and the InlA-mediated pathway for *L. monocytogenes* translocation across the intestinal barrier.

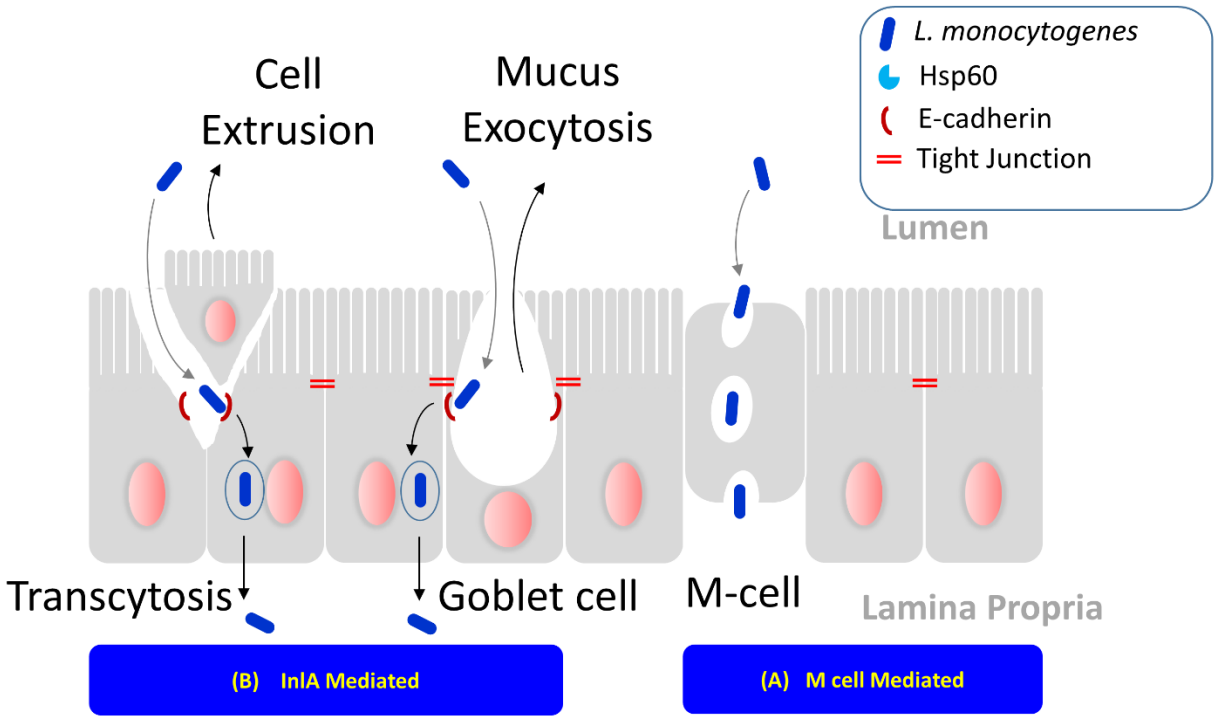

Figure 1.2. Schematic representation showing different routes used by *L. monocytogenes* to cross the gut epithelial barrier.

(**A**) M cell-mediated *L. monocytogenes* translocation occurs in the Peyer's patches.

(**B**) InlA/E-cadherin-mediated *L. monocytogenes* transcytosis, which occurs during epithelial cell extrusion or goblet cell mucus exocytosis, providing access of InlA to E-cadherin at the adherens junction.

M Cells: Exploiting the Natural Immune Surveillance Function

The **mucosal-associated lymphoid tissue (MALT)** comprises immune cells and structured lymphoid tissues. MALT is found in close contact with all mucosa throughout the body. In the intestine, it is termed **gut-associated lymphoid tissue (GALT)**, which consists of both isolated and aggregated lymphoid follicles. These are the sites where antigen recognition and mucosal immune responses are initiated. Marco Aurelio Severino initially described aggregated lymphoid follicles in 1645 in Italy. It was later renamed Peyer's patches after the Swiss pathologist Dr. Johann Conrad Peyer, who provided a detailed description in 1677.

The Peyer's patch is composed of aggregated lymphoid follicles surrounded by a follicle-associated epithelium (FAE) that forms the interface between the GALT and luminal microenvironment. The FAE contains M cells, which are unique epithelial phagocytes that continually sample luminal contents and are located within intestinal villi above isolated or aggregated lymphoid follicles (Ohno 2015). The normal function of M cells is to sample the contents of the lumen of the intestine and present antigens to the immune cells residing in the Peyer's patch. Thus, M cell transcytosis is an important first step in the initiation of a secretory immune response.

Many bacterial enteric pathogens such as rabbit diarrheagenic *E. coli*, *S. enterica* serovar Typhimurium, *S. flexneri*, *V. cholerae*, and *Y. pseudotuberculosis* transits through M cells into the underlying Peyer's patch by taking advantage of the natural immune surveillance function of M cells (Corr et al. 2008; Hase et al. 2009). Like other enteric pathogens, *L. monocytogenes* also uses the M cell-mediated pathway, and the bacterium has been localized within the Peyer's patches in orally infected mice (Marco et al. 1997; Chiba et al. 2011; Drolia et al. 2018). This mechanism is independent of *L. monocytogenes* virulence factor, such as InlA or the pore-forming toxin listeriolysin O (Corr et al. 2006), while another invasion protein, Internalin B (InlB), has been implicated to accelerate listerial invasion into murine M cells on ileal Peyer's patch (Chiba et al. 2011).

However, *L. monocytogenes* also translocates to deeper tissues and organs with similar efficiencies in a rat ligated ileal loop with or without Peyer's patch (Pron et al., 1998). Moreover, in a Peyer's patch-null mouse model, *L. monocytogenes* colonized the ileum and disseminated to the MLN, liver, and spleen (Chiba et al. 2011). Additionally, systemic dissemination of *L. monocytogenes* to the peripheral tissues was also observed by a intrarectal route of infection in the

absence of Peyer's patch in the large intestine (Nishikawa et al. 1998). These findings indicate that *L. monocytogenes* also traverse across the epithelium independently of M cells where other routes of invasion in the gastrointestinal tract are possible.

Internalin A and E-cadherin: Targeting the Adherens Junction

Internalin A (InlA) is the first protein of the Internalin multigene family discovered in 1991 and is involved in the invasion of epithelial cells (Gaillard et al. 1991). InlA is a 80-kDa surface invasion protein containing 15 leucine-rich repeats (LRRs) and signaling peptides, an inter-repeat (IR) region, and an LPXPTG surface anchoring motif at the carboxy-terminal that displays sortage-dependent disulfide covalent bonding with the cell wall peptidoglycan (Bierne et al. 2002; Bierne et al. 2004). The host cell receptor for InlA is E-cadherin (Mengaud et al. 1996). E-cadherin is a major transmembrane protein of 882 amino acids required for AJ formation in epithelial cells. E-cadherin consists of the N-terminal extracellular domain of 555 amino acids, a transmembrane domain of 175 amino acids, and a short intracellular domain of 152 amino acids.

Dynamics of InlA-E-cadherin Interaction

The dynamics of the signaling cascades activated by the InlA-E-cadherin interaction has been well-studied and reviewed (**Figure 4.2)** (Stavru et al. 2011). The binding of InlA to the extracellular domain of E-cadherin results in the recruitment of the junctional proteins α- and β-catenins, p120 catenin a Rho-GAP protein ARHGAP10, a non-conventional myosin VIIa, and a ubiquitous transmembrane protein vezatin. InlA-E-cadherin interaction induces the caveolin-dependent clustering of E-cadherin. The clustering of E-cadherin leads to the activation of the non-receptor tyrosine kinase Src that phosphorylates E-cadherin at residues 753 and 754. The Src-dependent phosphorylation of E-cadherin initiates the release of p120 catenin to the cytoplasm, which induces the activation of the actin nucleator Arp2/3 complex and actin polymerization. This

is followed by recruitment of septin at the site of entry. The Src-dependent phosphorylation of E-cadherin also recruits the ubiquitin-ligase Hakai, which ubiquitinates E-cadherin. E-cadherin ubiquitination induces the recruitment of **clathrin** to form coated-pits for clathrin-mediated bacterial internalization or **caveolin** for clathrin-independent bacterial endocytosis via caveosomes. While the InlA-E-cadherin signaling is important for *L. monocytogenes* invasion into epithelial cells, *L. monocytogenes* efficiently invades cells lacking the intracellular domain of E-cadherin (Ortega et al. 2017). This suggest that the extracellular domain of E-cadherin is sufficient to mediate *L. monocytogenes* invasion (Ortega et al. 2017).

Species Specificity of InlA-E-cadherin Interaction

The InlA-E-cadherin interaction exhibits a host species specificity that is attributed to a variation at the residue 16, at which proline is substituted by glutamic acid in the host species' E-cadherin (Lecuit et al. 1999). Therefore, InlA does not interact with the E-cadherin of InlA-non-permissive hosts such as mice or rats, but it does interact with the E-cadherin of InlA-permissive hosts such as humans, guinea pigs, rabbits, and gerbils (Disson and Lecuit 2013). E-cadherin is located basolaterally at the AJ and is inaccessible to luminal bacteria (Boller et al. 1985). However, two models have been proposed for InlA access to luminal E-cadherin during (i) epithelial cell extrusion and (ii) mucus exocytosis (**Figure 1.2**). (i) During villous epithelial "cell extrusion" (Pentecost et al. 2006), the apical junctional complex proteins are redistributed to the lateral membranes (Marchiando et al. 2011), and thus the extruding cells show a defect in epithelial polarity, which exposes E-cadherin at the cell surface. (ii) InlA access to E-cadherin occurs near the mucus-expelling goblet cells that exposes E-cadherin luminally, where *L. monocytogenes* is internalized and rapidly transcytosed in a vacuole across the epithelial cells and exits into the underlying lamina propria and disseminates systemically (Nikitas et al. 2011). InlA access near

mucus-expelling goblet cells is supported by the observations where the treatment of humanized E-cadherin transgenic mice with IL-33, which increases the number of goblet cells and mucus secretion, also resulted in increased *L. monocytogenes* invasion to the intestinal villi and systemic dissemination to the spleen (Nikitas et al. 2011). Both of these mechanisms for InlA access to E-cadherin relies on the continuous self-renewal ability for eliminating damaged cells and the inherent tissue heterogeneous nature of the intestinal epithelium, respectively. Additionally, phosphoinositide 3-kinase (PI3-K) is constitutively active in the intestine (Gessain et al. 2015). Thus, another invasion protein Internalin B (InlB), which is known to activate PI3-K, is not required for crossing the intestinal barrier (Mansell et al. 2001; Gessain et al. 2015).

Contribution of InlA-E-cadherin Interaction: Lessons from Animal Models

Despite the key role of InlA-E-cadherin interaction in crossing of the intestinal epithelial barrier by *L. monocytogenes*; the intragastric inoculation of an *L. monocytogenes* Δ*inlA* strain resulted in high bacterial burdens in the liver and spleen of wild-type (WT) mice (Bierne et al. 2002), and in the small intestine, cecum, colon, and MLN of transgenic mice expressing humanized E-cadherin (Disson et al. 2008). These observations suggest that the humanized E-cadherin allele is only relevant to InlA-mediated bacterial invasion, and that *L. monocytogenes* uses alternate routes to translocate across the gut mucosa. Furthermore, oral infection of mice with *L. monocytogenes* expressing murinized InlA ($InlA^m$), which binds E-cadherin with high affinity, did not show a significant difference in bacterial burdens in the liver, spleen, and MLN compared to mice that were inoculated with the WT *L. monocytogenes* for up to 48-72 hours post-infection (hpi) (Wollert et al. 2007; Chiba et al. 2011; Bergmann et al. 2013). This further suggests that the InlA-E-cadherin interaction may not be essential for *L. monocytogenes* to cross the intestinal barrier, at least during the early phase of infection. A co-infection study using $InlA^m$, WT, or Δ*inlA*

strains demonstrated that InlA is not required for the establishment of intestinal infection in mice (Bou Ghanem et al. 2012).

Additionally, though the interaction between InlA and E-cadherin in mice and rats is not fully functional (Lecuit et al. 2001), several studies have advocated that *L. monocytogenes* can cross the intestinal barrier and disseminate to the MLN, liver, and spleen following oral infection (Bierne et al. 2002; Czuprynski et al. 2003; Jaradat and Bhunia 2003; Burkholder et al. 2009; Bou Ghanem et al. 2012). These observations are further supported by more recent studies showing that *L. monocytogenes* strains expressing a non-functional InlA (encoding a premature stop codon) can indeed infect human newborns with neonatal listeriosis (Gelbicova et al. 2015), or adults (Cruz et al. 2014; Fravalo et al. 2017) and fetuses of pregnant guinea pigs and mice after oral administration (Holch et al. 2013). Taken together, these observations strongly point to the existence of alternate pathway(s) independent of InlA for *L. monocytogenes* to cross the gut epithelial barrier.

Internalin B and c-Met Interaction

Another important *L. monocytogenes* invasion protein of the internalin multigene family is Internalin B (InlB) (Dramsi et al. 1995), which mediates invasion in the human enterocyte-like Caco-2 and the hepatocyte HepG2 cell lines (Gaillard et al. 1991; Dramsi et al. 1995). InlB is a 63-kDa surface protein that is bound by non-covalent binding to the lipoteichoic acids of bacterial cell wall by the G-W motif (Braun et al. 1997; Jonquieres et al. 1999). The host receptor for InlB is c-Met, a receptor tyrosine kinase (RTK) and the natural receptor for Hepatocyte Growth Factor (HGF) (Shen et al. 2000). Interestingly, the InlB/c-Met interaction also exhibits a species specificity (Khelef et al. 2006). Therefore, InlB does not interact with the c-Met of guinea pigs or rabbits but it does interact with the c-Met of mouse, gerbils and humans. InlB has been shown to

play a role in colonization of the Peyer's patch in wild-type mice, as the Δ*inlB* deletion strains showed a severe defect in invasion through M cells (Chiba et al. 2011). Although, InlB has also been demonstrated to accelerate the intestinal invasion of *L. monocytogenes* expressing murinized InlA ($InlA^m$) (Pentecost et al. 2010); however, InlB has no role in crossing of the intestinal epithelial barrier in host models that are permissive to both InlA and InlB pathways; such as the gerbils or the humanized–E-cad transgenic mice (Disson et al. 2008).

Listeria Adhesion Protein and Heat Shock Protein (Hsp) 60 Interaction

Our group studies the *Listeria* Adhesion Protein (LAP); a 104-kDa alcohol acetaldehyde dehydrogenase, an AdhE homolog (*lmo1634*) that promotes adhesion of only pathogenic *Listeria* species to cell lines of intestinal origin (Pandiripally et al. 1999; Jaradat et al. 2003; Jagadeesan et al. 2010). Analysis of the *lmo1634* locus from F4244, a 4b serotype with genomic sequences from several strains, revealed 99% sequence identity with Clip80459 and F2365 (both 4b serotypes), and 97% sequence identity with EGD-e, EGD, and 10403S (all 1/2a serotypes) (Bailey et al. 2017).

A Bi-functional Adhesin

LAP is a cytosolic bi-functional housekeeping enzyme containing N-terminal acetaldehyde dehydrogenase (ALDH) and C-terminal alcohol dehydrogenase (ADH), and does not contain a leader sequence (Jagadeesan et al. 2010) **(Figure 1.3)**. LAP is present in both pathogenic and nonpathogenic *Listeria* species; and the sequence analysis has revealed ~98% amino acid similarity in LAP from pathogenic (*L. monocytogenes* and *L. ivanovii*) and non-pathogenic species (*L. innocua*, *L. welshimeri*, *L. seeligeri*) (Jagadeesan et al. 2010). However, LAP contributes to the bacterial adhesion to cell lines of intestinal origin only in pathogenic *Listeria* (Jaradat et al. 2003; Jagadeesan et al. 2010) because of inadequate secretion and surface re-association of LAP on non-

pathogenic *Listeria* species (Burkholder et al. 2009; Jagadeesan et al. 2010). LAP is prominently reduced in intracellular and cell-surface protein fractions, and is undetectable in the extracellular milieu of non-pathogenic species. LAP production is maximal during the late logarithmic to stationary phase, and the growth temperature influences its synthesis (Santiago et al. 1999). Nutrient-starving conditions and low glucose (0.4-0.8 g/L) levels increase LAP production (Jaradat and Bhunia 2002). LAP-mediated pathogenesis also depends on the effective secretion of the protein from the bacterium by SecA2, an auxiliary secretion system (Burkholder et al. 2009; Mishra et al. 2011). The oxygen-limiting environment increases the expression of LAP, thus augmenting the pathogenic potential of *L. monocytogenes* as observed in *in vitro* cell culture and mouse models (Burkholder et al. 2009).

Hsp60 is the epithelial receptor for LAP (Wampler et al. 2004). The N-terminal ALDH, specifically the N2 subdomain (Gly224–Gly411), interacts and binds to Hsp60 with high affinity (K_D = 9.5 mM) (Jagadeesan et al. 2011). Hsp60 is a mitochondrial chaperonin and plays a role in protein folding and removal of misfolded proteins from cells. Mammalian Hsp60 activates the innate immune response (Pockley and Henderson 2018), and thus is considered a moonlighting protein (Henderson et al. 2013) possessing two or more distinct biological activities. *L. monocytogenes* infection at low dosage increases plasma membrane and intracellular Hsp60 levels in epithelial Caco-2 cells independent of LAP expression (Burkholder and Bhunia 2010). Furthermore, *L. monocytogenes*-induced membrane Hsp60 expression subsequently facilitates enhanced LAP-mediated *L. monocytogenes* interaction with epithelial cells *in vitro* (Burkholder and Bhunia 2010). Interestingly, Hsp60 also acts as a cell surface receptor for *Staphylococcus aureus* (Dziewanowska et al. 2000) and human immunodeficiency virus (HIV) (Speth et al. 1999).

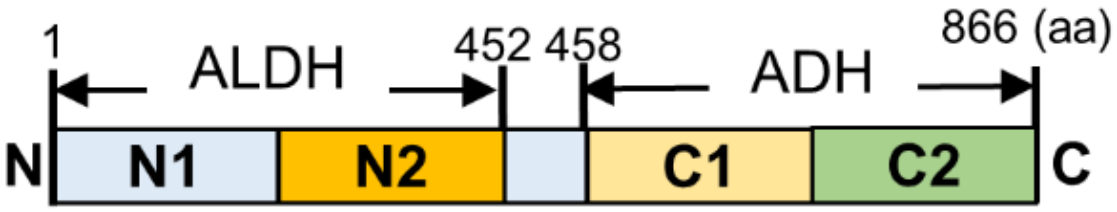

Figure 1.3 Schematic representation of *Listeria* Adhesion Protein

LAP is an alcohol acetaldehyde dehydrogenase enzyme (AAD; 866 aa) consisting of an N-terminal (N1 and N2) acetaldehyde dehydrogenase (ALDH) and a C-terminal (C1 and C2) alcohol dehydrogenase region (ADH).

LAP Promotes *L. monocytogenes* Translocation *In vitro*

LAP was first identified to aid *L. monocytogenes* in adhering to cells of intestinal origin as a potential colonization factor without any apparent invasion function (Pandiripally et al. 1999; Jagadeesan et al. 2010). Later, LAP was found to have a key role in bacterial transepithelial translocation. In a transwell culture device, the mutant strain lacking *lap* (*lap*$^{-}$) showed significantly impaired translocation compared to that of the WT strain across the polarized Caco-2 cell monolayer (Burkholder and Bhunia 2010). However, a strain lacking the InlA (Δ*inlA*) exhibited translocation rates equal to the WT strain (Burkholder and Bhunia 2010), suggesting that LAP-mediated paracellular translocation is independent of InlA-mediated epithelial invasion. Additionally, the translocation phenotype of WT and Δ*inlA* strain was significantly impaired in a Caco-2 cell lines with *Hsp60* knocked-down, but the translocation phenotype of *lap*$^{-}$ strain had no change (Burkholder and Bhunia 2010). Conversely, overexpression of *hsp60* significantly increased translocation of WT and Δ*inlA* but not the *lap*-deficient strain. Therefore, LAP-mediated translocation requires the engagement of its surface receptor Hsp60. Additionally, *L.*

monocytogenes isolates showing high LAP secretion also showed a higher rate of epithelial adhesion and translocation across the Caco-2 epithelial cell barrier (Kim and Bhunia 2013). These findings suggest that interaction of LAP with the host cell receptor Hsp60 is critical for *L. monocytogenes* translocation across the epithelial barrier *in vitro*, and this event can take place independent of InlA. However, whether LAP contributes to *L. monocytogenes* translocation across the intestinal barrier *in vivo* and the underlying cellular and molecular mechanism is not known. Additionally, whether LAP-mediated translocation requires the breaching of cell-cell-junction (a common strategy used by several enteric bacterial pathogens) is not known.

Breaching the Cell-Cell Junction by Bacterial Pathogens

Many enteric bacterial pathogens have evolved different strategies to breach cell-cell-junction for causing intestinal barrier dysfunction and systemic infection (Barreau and Hugot 2014) **(Table 1.1).** Adherent-invasive *E. coli* (AIEC) infects CEABAC10 transgenic mice (expressing human CEACAMs) and increase intestinal paracellular permeability by upregulating the expression of the pore-forming TJ protein Claudin-2 (Denizot et al. 2011). *Campylobacter jejuni* possess the outer membrane vesicle-associated proteolytic activity to cleave occludin and E-cadherin (MacCallum et al. 2005; Elmi et al. 2016). Enteropathogenic *E. coli* (EPEC) employs the type III secretion system (TTSS) effectors, NleA (Thanabalasuriar et al. 2010), EspM (Simovitch et al. 2010), Map (Alto et al. 2006; Singh et al. 2018), and EspF (Yuhan et al. 1997; McNamara et al. 2001; Tapia et al. 2017; Singh et al. 2018) to disrupt TJs for causing diarrheal disease. Recently, EPEC has also been shown to engage EspG1 to target tricellulin (Morampudi et al. 2016) and EspH to target the desmosomes (Roxas et al. 2018). *Helicobacter pylori* uses CagA to cause disorganization of gastric epithelial architecture through inhibition of PAR1 kinase activity (Amieva et al. 2003; Saadat et al. 2007; Wroblewski et al. 2014). More recent work suggest that

other *H. pylori* virulence factors such as; HrtA (Tegtmeyer et al. 2017) and urease (Wroblewski et al. 2009) also cause disruption of cell-cell junction. *Pseudomonas fluorescens* and *Pseudomonas aeruginosa* increases intestinal paracellular permeability in Caco-2 and TC7 cell lines via rearrangements of F-actin microfilaments (Madi et al. 2010). Recent studies have also demonstrated that *P. fluorescens* increases intestinal paracellular permeability by the release of IL-1β by immune cells and the activation of MLCK in the epithelial cells in a NOD2-dependent manner *in vivo* (Alnabhani et al. 2015). *Salmonella enterica* serovar Typhimurium employs SPI-1- secreted effectors (SopB, SopE, SopE2, and SipA) to stimulate Rho family GTPases for the disruption of tight junction structure and function (Boyle et al. 2006). In contrast, the *Salmonella* TTSS effector ArvA is demonstrated to stabilize TJs (Liao et al. 2008; Lin et al. 2016). *S. flexneri* increases paracellular permeability by regulating tight junction-associated proteins (Perdomo et al. 1994; Sakaguchi et al. 2002) and recently, the bacterial secreted Serine Protease A (SepA) has been implicated in this process (Maldonado-Contreras et al. 2017). *Vibrio cholerae* uses the toxins; hemmagglutinin/protease (HAP) and zona occludin toxin (ZOT) to cleave ZO-1 from the intracellular domain of occludin to disrupt barrier function (Wu et al. 2000; Goldblum et al. 2011). Recent work also demonstrates that cholera toxin disrupts barrier functions by mislocalizing E-cadherin, via inhibition of exocyst-mediated trafficking of host proteins to intestinal cell junctions (Guichard et al. 2013). Finally, *Y. pseudotuberculosis* requires the outer membrane protein, YopJ to subvert the signaling of the innate immune receptor Nod2 to induce IL-1β production leading to the disruption of the intestinal epithelial barrier (Marra and Isberg 1997; Meinzer et al. 2012).

Table 1.1. Microbial Pathogens Involved in the Disruption of Epithelial Cell-Cell Junction Barrier

Bacteria	Virulence Factors	Host Targets	Reference(s)
Adherent-invasive *E. coli*	Unknown	Intestinal CEACAMs and Claudin-2	(Denizot et al. 2011)
Campylobacter jejuni	Outer Membrane Vesicles	Occludin and E-cadherin	(Elmi et al. 2016)
Enteropathogenic *E. coli*	NleA	COPII	(Thanabalasuriar et al. 2010)
	EspM	RhoA	(Simovitch et al. 2010)
	Map	Cdc42	(Alto et al. 2006; Singh et al. 2018)
	EspF	Crb3, Occludin,	(McNamara et al. 2001; Tapia et al. 2017; Singh et al. 2018)
	EspG1	Tricellulin	(Morampudi et al. 2016)
	EspH	Rho GTPase, desmoglein-2	(Roxas et al. 2018)
Helicobacter pylori	CagA	ZO-1, PAR1, β-catenin	(Amieva et al. 2003; Saadat et al. 2007; Wroblewski et al. 2014)
	HtrA	Occludin, claudin-8, E-cadherin	(Tegtmeyer et al. 2017)
	Urease	MLCK, ROCK	(Wroblewski et al. 2009)
Pseudomonas aeruginosa	Unknown	F-actin microfilaments	(Madi et al. 2010)
Pseudomonas fluorescens	Unknown	NOD2 signaling, MLCK	(Alnabhani et al. 2015; Al Nabhani et al. 2017)
Salmonella enterica serovar Typhimurium	SipA, SopB, SopE, SopE2	Rho GTPase	(Boyle et al. 2006)
Shigella flexneri	SepA	LIM Kinase 1 (LIMK1), cofilin, ZO-1, ZO-2, E-cadherin and occludin	(Perdomo et al. 1994; Sakaguchi et al. 2002; Maldonado-Contreras et al. 2017)
Vibrio cholerae	HAP and ZOT	ZO-1, occludin	(Wu et al. 2000; Goldblum et al. 2011)
	Cholera toxin	E-cadherin and Notch signaling	(Guichard et al. 2013)
Yersinia pseudotuberculosis	YopJ	NOD2 signaling, activates caspase-1	(Meinzer et al. 2012)

Overall Goals and Hypothesis

This work was undertaken to fill a critical gap in our understanding of *L. monocytogenes* pathogenesis during the intestinal phase of infection. To address this gap my work investigates the role of LAP in *L. monocytogenes* translocation across the intestinal tract in a mouse model that is not permissive to InlA-E-cadherin interaction and a Mongolian gerbil model, the only natural small animal model that is permissive to both InlA and InlB pathways, similar to humans.

The overall hypothesis is that LAP is required for *L. monocytogenes* epithelial barrier crossing and that LAP-mediated translocation requires the breaching of epithelial cell-cell junction.

To prove the hypothesis, two specific aims were addressed:

Aim 1. Determined the role of LAP in *L. monocytogenes* virulence following oral challenge of wild-type and mutant strains (*lap*─ and ΔinlA) in a mouse and the gerbil model.

Aim 2. Investigated the cellular and molecular mechanism for *L. monocytogenes* translocation during the intestinal phase of infection in a Caco-2, mouse and the gerbil model

CHAPTER 2. *LISTERIA* ADHESION PROTEIN INDUCES EPITHELIAL BARRIER DYSFUNCTION FOR BACTEIAL TRANSLOCATION

The following chapter is published and modified from Drolia, R., Tenguria, S., Durkes, A.C., Turner, J.R., and Bhunia, A.K. (2018). *Listeria* Adhesion Protein Induces Intestinal Epithelial Barrier Dysfunction for Bacterial Translocation. Cell Host & Microbe *23*, 470-484.e477.

Abstract

Intestinal epithelial cells are the first line of defense against enteric pathogens yet bacterial pathogens, such as *Listeria monocytogenes,* can breach this barrier. We show that *Listeria* adhesion protein (LAP) induces intestinal epithelial barrier dysfunction to promote bacterial translocation. These disruptions are attributed to production of pro-inflammatory cytokines TNF-α and IL-6, which is observed in mice challenged with WT and isogenic strains lacking the surface invasion protein, Internalin A (Δ*inlA),* but not a *lap*$^{-}$ mutant. Additionally, upon engagement of its surface receptor Hsp60, LAP activates canonical NF-κB signaling, facilitating myosin light-chain kinase (MLCK)-mediated opening of the epithelial barrier via cellular redistribution of the epithelial junctional proteins claudin-1, occludin, and E-cadherin. Pharmacological inhibition of MLCK or NF-κB in cells or genetic ablation of MLCK in mice prevents mislocalization of junctional proteins and *L. monocytogenes* translocation. Thus, *L. monocytogenes* uses LAP to exploit epithelial defenses and cross the intestinal epithelial barrier.

Highlights

1. LAP induces intestinal barrier dysfunction for *L. monocytogenes* translocation

2. LAP activates NF-κB and upregulates TNF-a and IL-6 for increased epithelial permeability

3. LAP interaction with its receptor, Hsp60, is crucial for NF-κB activation

4. LAP activates MLCK for cellular redistribution of claudin-1, occludin, and E-cadherin

Introduction

The breaching of host barriers (intestinal, blood-brain, and placental) is a key mechanism of the intracellular bacterium, *Listeria monocytogenes* during infection (Radoshevich and Cossart 2018). *L. monocytogenes* entry into the epithelial cells is mediated by two invasion proteins, Internalin A (InlA) and Internalin B (InlB) (Dramsi et al. 1995; Lecuit et al. 2001). Following entry, the bacterium resides in a phagosome, which is lysed by listeriolysin O (LLO, encoded by the *hly* gene) to access the cytosol (Portnoy et al. 1988). The bacterium utilizes actin-based motility for cell-to-cell spread where the bacterial ActA protein stimulates cellular actin polymerization via the recruitment of the Arp2/3 complex (Tilney and Portnoy 1989; Kocks et al. 1992). Another virulence protein, Internalin C (InlC), promotes cell-to-cell spread in polarized epithelial cells (Rajabian et al. 2009).

The gastrointestinal tract is the primary route of infection for *L. monocytogenes*, and crossing the intestinal epithelial barrier is the first step. The importance of the InlA-mediated *L. monocytogenes* invasion and crossing of the intestinal epithelial barrier has been reviewed (Radoshevich and Cossart 2018). The host cell receptor for InlA is E-cadherin (Mengaud et al. 1996). The InlA/ E-cadherin interaction exhibits a species specificity that is attributed to a variation at amino acid sequence position 16, at which proline is substituted by glutamic acid in the host species' E-cadherin (Lecuit et al. 1999). Therefore, InlA does not interact with the E-cadherin of

the non-permissive hosts; mouse or rat, but it interacts with the E-cadherin of permissive hosts; humans, guinea pigs, rabbits and gerbils (Lecuit et al. 2001; Disson et al. 2008). E-cadherin is located basolaterally at the adherens junction (AJ) and is inaccessible to bacteria in the intestinal lumen. E-cadherin access is proposed to occur during villous epithelial "cell extrusion" (Pentecost et al. 2006) during which the apical junctional complex proteins are redistributed to the lateral membranes (Marchiando et al. 2011) and around mucus expelling goblet cells (Nikitas et al. 2011). However, a Δ*inlA* mutant, after intragastric (ig) inoculation, showed high bacterial burdens in the liver and spleen of WT mice (Bierne et al. 2002) and in the small intestine, cecum, colon, and MLN of transgenic mice expressing "humanized" E-cadherin (Disson et al. 2008). This suggests that the humanized E-cadherin allele is only relevant to InlA-mediated bacterial invasion and that *L. monocytogenes* use alternate routes to translocate across the gut mucosa. Furthermore, ig-inoculation of *L. monocytogenes* expressing murinized InlA ($InlA^m$) that binds E-cadherin with high affinity did not show significantly higher bacterial burdens in the liver, spleen, MLN and small intestine of mice compared to mice that were ig-inoculated with the WT for up to 48 h pi (Wollert et al. 2007). This suggests that the InlA- E-cadherin interaction may not be essential for *L. monocytogenes* to cross the intestinal barrier, at least during the early phase of infection, which is confirmed in a co-infection study using $InlA^m$, WT or Δ*inlA* in mice (Bou Ghanem et al. 2012).

As stated above, the interaction between InlA and E-cadherin in mice and rats is not fully functional (Lecuit et al. 2001), yet *L. monocytogenes* can cross the intestinal barrier to disseminate to the MLN, liver, and spleen in orally infected mice (Bierne et al. 2002; Czuprynski et al. 2003; Burkholder et al. 2009; Bou Ghanem et al. 2012). Though, the murine M cells in Peyer's patches (PP) are considered the main invasive route for *Listeria* translocation; which relies on InlB (Chiba et al. 2011) without the involvement of InlA or LLO (Corr et al. 2006), in a rat ligated ileal loop

with or without PP or in a PP-null mouse, *L. monocytogenes* translocated to the MLN, liver and spleen (Pron et al. 1998; Chiba et al. 2011) .These findings reinforce *L. monocytogenes* ability to translocate across the intestinal epithelium independent of InlA and M cells.

Our group has identified *Listeria* adhesion protein (LAP), a 104-kDa alcohol acetaldehyde dehydrogenase (*lmo1634*) that promotes adhesion of pathogenic *Listeria* species to cell lines of intestinal origin (Jaradat et al. 2003; Jagadeesan et al. 2010). We identified heat shock protein 60 (Hsp60) as the epithelial receptor for LAP in human enterocyte-like Caco-2 cells (Wampler et al. 2004; Jagadeesan et al. 2011). LAP also promoted translocation across the Caco-2 cell monolayer in a Transwell culture device, as the *lap*$^{-}$ strain exhibited a significantly reduced translocation competency than that of the WT strain, while the Δ*inlA* translocated similarly to that of the WT strain (Burkholder and Bhunia 2010). This translocation phenotype of WT was significantly impaired in an Hsp60-suppressed Caco-2 cell line but the *lap*$^{-}$ strain showed no effect (Burkholder and Bhunia 2010).

The present study investigates whether LAP contributes to translocation of *L. monocytogenes* across the intestinal barrier *in vivo* and elucidates the molecular mechanism by which LAP facilitates bacterial translocation. We used a mouse model, where InlA- E-cadherin interaction is not fully functional and the Caco-2 cell model, where the InlA- E-cadherin interaction is active. We demonstrate that LAP contributes to *L. monocytogenes* translocation into the lamina propria (LP) and systemic dissemination in mice, and across Caco-2 cell barrier by increasing epithelial permeability. Further, we show that the increased epithelial permeability directly correlates with the increased expression TNF-α and IL-6 in mice or cells infected with the WT and the Δ*inlA* strains, but not with the *lap*$^{-}$ strain. By using genetic models and pharmacological inhibitors, we establish that LAP directly binds to Hsp60 to activate canonical NF-κB signaling, thereby

facilitating the myosin light chain kinase (MLCK)-mediated opening of the intestinal cell-cell barrier via the cellular redistribution of the major junctional proteins, claudin-1, occludin and E-cadherin and bacterial translocation in both model systems.

Results

LAP Contributes to Systemic Dissemination and Bacterial Translocation across the Intestinal Barrier

We orally challenged A/J mice with a WT strain F4244 (serotype 4b), an isogenic *lap*-insertion mutant strain (*lap*⁻) and an Δ*inlA* deletion strain, and enumerated *Listeria* in the extra-intestinal tissues at 24 and 48 h pi. The dissemination of *lap*⁻ was significantly impaired in the liver, spleen and MLN (**Figures 2.1A-2.1C**). The *lap*⁻ counts were reduced in the kidneys and was undetectable in blood (**Figures 2.2A and 2.2B**). Histopathology indicated mild-to-moderate multifocal hepatic and splenic necrosis, and neutrophilia in the white and red pulp in spleens of mice challenged with the WT or Δ*inlA* at 48 h pi (**Figures 2.2C and 2.2D**), while these signs were absent in the *lap*⁻-challenged mice. Thus, the *lap*⁻strain exhibits a dissemination defect in trafficking to extra-intestinal sites.

Next, we enumerated *L. monocytogenes* counts in the mucus, epithelial cells and lamina propria fractions of the ileal mucosa at 48 h pi (Bou Ghanem et al. 2012). Relative to the WT strain, the total number of *lap*⁻ bacteria present in the mucus did not change (**Figure 2.1D**); however, a significantly lower *lap*⁻ counts was observed in the epithelial fractions (**Figures 2.1E and 2.1F**), and in the lamina propria (**Figure 2.1G**). Immunostaining of ileal tissue sections confirmed increased bacterial counts in epithelial cells and in the lamina propria of mice challenged with the WT or Δ*inlA* strains (**Figures 2.1H-J and 2.2E**). In contrast, a very few *lap*⁻ bacteria were found on the epithelial cells and were absent in the lamina propria, but predominantly confined to the

lumen. As expected, the *lap*$^{-}$ strain was found in the ileal PP (**Figures 2.2F and 2.2G**). These data suggest that LAP contributes to translocation of *L. monocytogenes* across the intestinal barrier into the underlying lamina propria in a mouse model.

Figure 2.1. LAP contributes *L. monocytogenes* translocation across the intestinal barrier and systemic dissemination.

(A-G) *Listeria* counts (Total CFU) in liver (A), spleen (B), MLN (C), and ileal mucus (D), epithelial cell-intracellular (E), epithelial cell-extracellular (F) and lamina propria (G) of A/J mice (*n*=4-12) at 24 and 48 h pi from three independent experiments. Dashed horizontal lines indicate the detection limit.

(H) Images of ileal villi (48 h pi) stained for ZO-1 (red), *Listeria* (green, arrows) and nucleus (blue). Scale bar, 10 μm. The panels below are enlargements of the boxed areas. Scale bar, 1 μm. White arrows indicate bacteria in the lamina propria and yellow arrows on the epithelial cells or in the lumen.

(I,J) *L. monocytogenes* counts from epithelial cells (I) and lamina propria (J) of villi images (n=75) from 3 mice for each treatment. See also Fig 2.2.

All error bars represent SEM. ****, $P<0.0001$; **, $P<0.01$; *, $P<0.05$; ns, no significance.

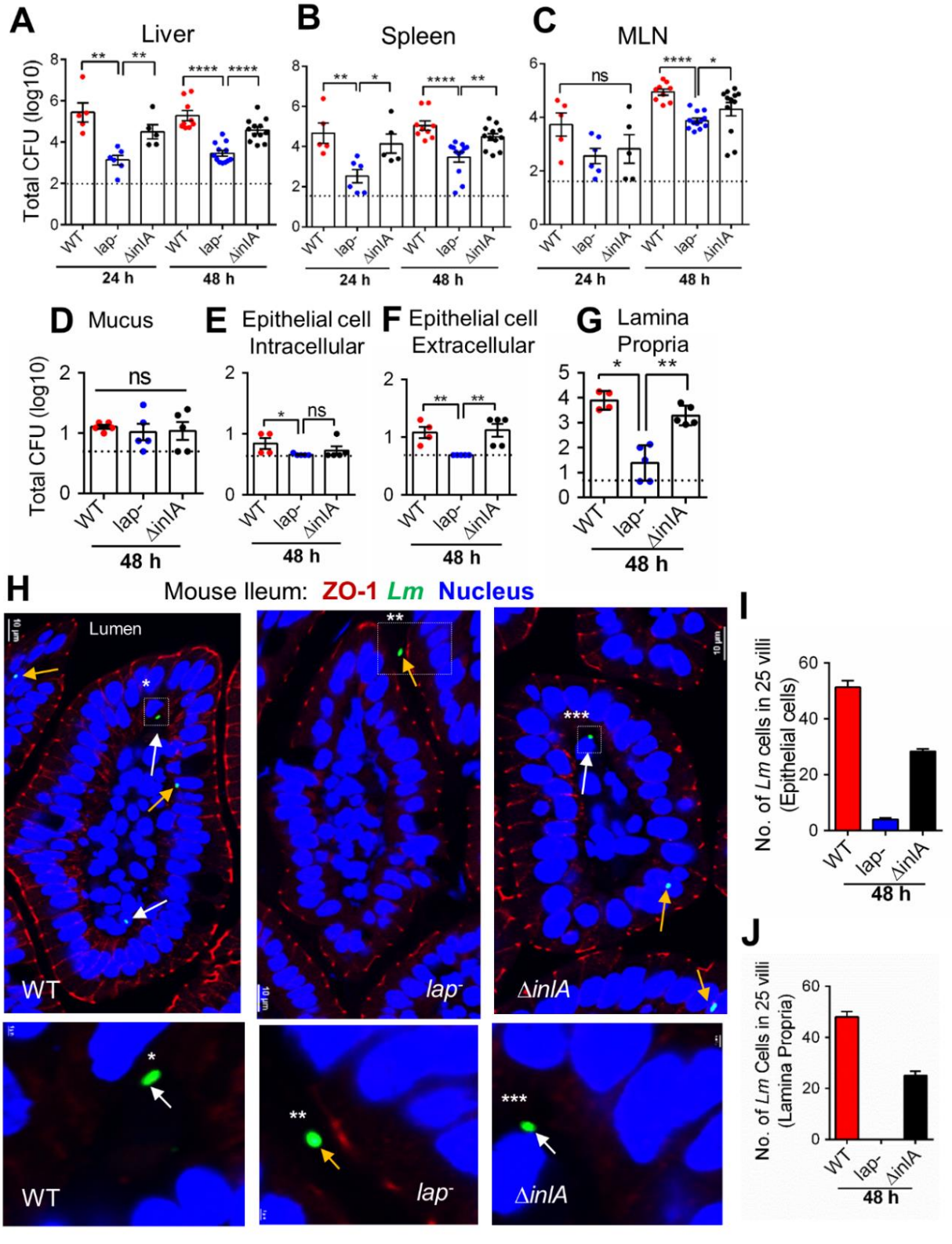
A
Liver
B
Spleen
C
MLN
Total CFU (log10)
WT
lap-
ΔinlA
24 h
48 h
ns
D
Mucus
E
Epithelial cell
Intracellular
F
Epithelial cell
Extracellular
G
Lamina
Propria
H
Mouse Ileum: ZO-1 Lm Nucleus
Lumen
WT
lap-
ΔinlA
I
No. of Lm cells in 25 villi
(Epithelial cells)
J
No. of Lm Cells in 25 villi
(Lamina Propria)

Figure 2.2. *Listeria* infection and microscopic analysis of tissue sections.

(A,B) The dot plot-showing total CFU obtained from kidney **(A)** and blood **(B)** from 8-10 week-old female A/J mice orally challenged with 1×10^8 CFU of *L. monocytogenes* WT, *lap*$^-$ or Δ*inlA* strains from A/J mice (*n*=5) at 24 and 48 h pi. Bars and brackets represent the mean ± SEM, respectively, from three independent experiments. Dashed horizontal lines indicate the limit of detection for each organ/tissue. Statistical significance was determined by using the Mann-Whitney nonparametric test. ns, not significant.

(C,D) Histology score **(C)** and representative light microscopic images of hematoxylin and eosin stained liver and spleen **(D)**, and from control mice (n=3) or from mice (A/J) orally challenged with 1×10^8 CFU of *L. monocytogenes* WT (n=2), *lap*$^-$ (n=5) or *ΔinlA* (n=2) strains 48 h pi. Arrows (yellow) indicate mild-to-moderate multifocal hepatic necrosis in the livers and multifocal areas of necrosis in the spleen of mice challenged with the WT or Δ*inlA* strain.

(E) Confocal immunofluorescence microscopy of fixed paraffin embedded ileal tissue sections, showing multiple villi, immuno-stained for ZO-1 (red), *Listeria* (green, arrows) and DAPI (blue; nucleus) from WT, *lap*$^-$ or Δ*inlA*-challenged mice 48 h pi. Scale bar, 10 µm. White arrows indicate *L. monocytogenes* detected in the lamina propria of WT and Δ*inlA*-challenged mice. Yellow arrows indicate *L. monocytogenes* detected in the lumen or in the epithelial cells. *L. monocytogenes* (yellow arrows) was detected in the lumen of the *lap*$^-$-challenged mice.

(F,G) Confocal immunofluorescence microscopy of mice Peyer's patches in ileal tissue sections orally challenged with *L. monocytogenes* WT, Δ*inlA* or *lap*$^-$ strains. Scale bar, 10 µm (F). Tissues were fixed and were paraffin embedded, sectioned and immunostained for *Listeria* (green, arrows) and DAPI (blue; nucleus). The inset images show enlargements of the boxed areas. Arrows point to the *L. monocytogenes* presence in the Peyer's patches of WT, *lap*$^-$ *or* Δ*inlA* infected mice (F). Graph representing quantitative measurements of an average number of *L. monocytogenes* cells in Peyer's patches per examined microscopic field (n=15 fields) from 3 mice for each treatment (G).

Figure 2.2. continued

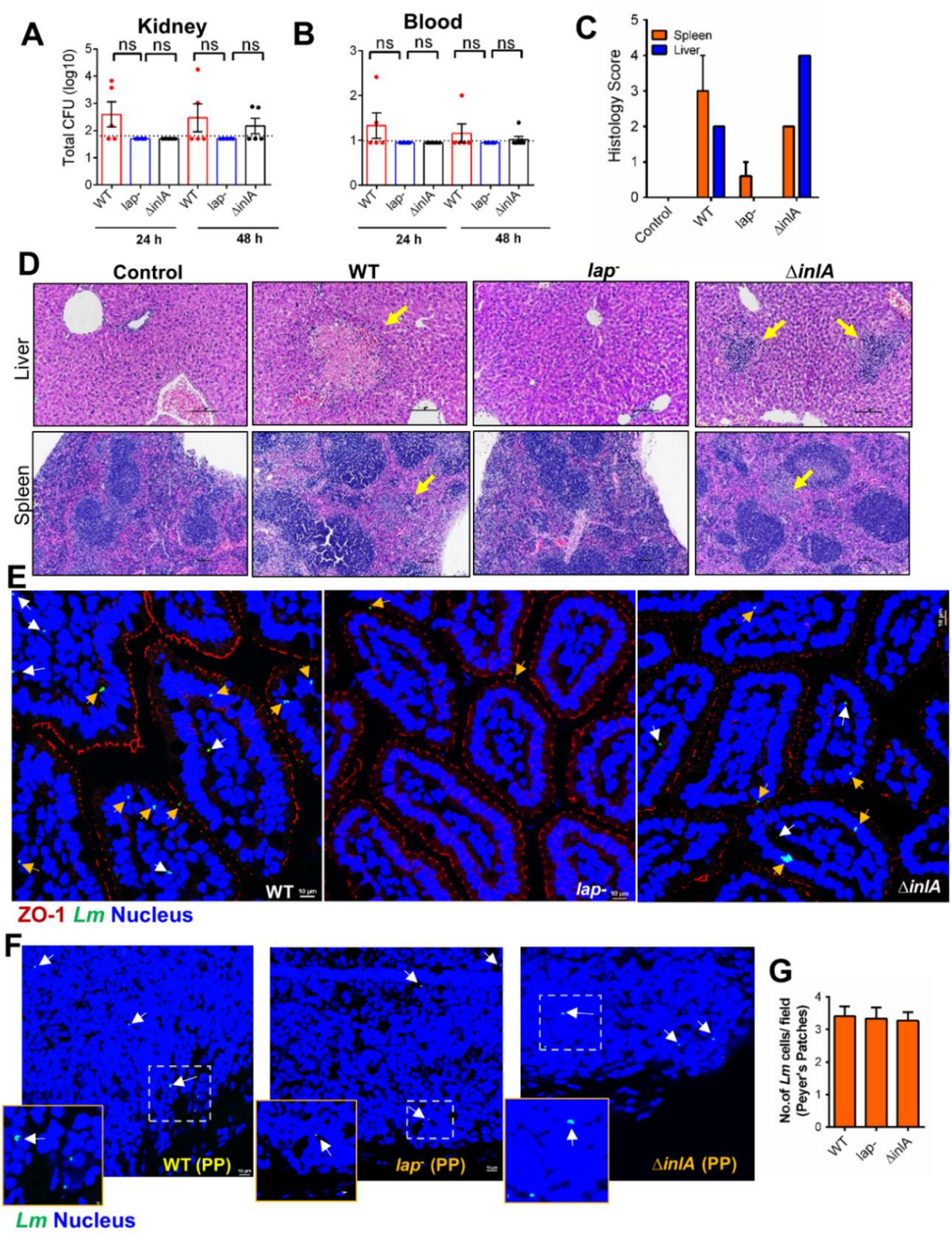

LAP Contributes to Intestinal Barrier Dysfunction

Next, we analyzed intestinal permeability to the paracellular marker, 4-kDa FITC-dextran (FD4), gavaged orally 4-5 h prior to sacrifice, in *Listeria*-infected mice. Relative to the uninfected controls, the FD4 concentrations were significantly increased in the serum, and the urine in WT and Δ*inlA*-challenged mice 48 h pi, while the levels in *lap*$^{-}$-challenged mice were comparable to uninfected controls (**Figures 2.3A** and **2.3B**).

Tight junction (TJ) plays a crucial role in the maintenance of intestinal paracellular permeability. Thus, we examined bacterial localization near TJ. Immunostaining revealed WT and Δ*inlA* co-localization with the TJ protein, ZO-1 at the epithelial cell-cell junction in the ileal tissue (**Figures 2.3C-2.3F, Videos 1-4)**. In contrast, the *lap*$^{-}$ strain was predominantly confined in the lumen of the ileal mucosa **(Figures 2.1H, 2.2E)** and was not found to interact with the TJ (**Figure 2.4A, Video 5)**.

Analysis of translocation phenotypes of mutant strains for other important virulence factors, the Δ*inlB* and the Δ*hly* strains, across the Caco-2 monolayers revealed similar translocation rates to their respective WT strains (**Figure 2.3G)**. By contrast, the *lap*$^{-}$ exhibited a severely attenuated translocation phenotype and the *lap*$^{-}$*lap*$^{+}$ complemented strain restored translocation rates higher than the WT. Furthermore, the attenuated translocation of the *lap*$^{-}$ also correlated with significantly decreased FD4 flux and increased transepithelial electrical resistance (TEER) across Caco-2 cells infected with *lap*$^{-}$ than those infected with the WT (**Figure 2.3H and 2.4B)**. Conversely, the *lap*$^{-}$*lap*$^{+}$ strain showed increased FD4 flux and decreased Caco-2 TEER, equal to the WT. Importantly, the translocation defect observed by the *lap*$^{-}$ strain was not due to decreased cytotoxic effects (**Figure 2.4C**).

To delineate the intracellular role of LAP from its role at the bacterial cell surface, we determined the relevant concentration of LAP available on the bacterial surface during the

infection of Caco-2 cells by using purified recombinant LAP as the standard. Approximately,1 μg of LAP was associated with the cell wall of WT bacteria at 1×10^7 CFU, and an equivalent CFU was used in our translocation assays to achieve a multiplicity of infection (MOI) of 50 (**Figure 2.4D**). Pre-incubation of the *lap*⁻ strain with purified LAP (*lap*⁻ +LAP), at a concentration that is available on the bacterial surface (1 μg), resulted in a strong association of the protein with the bacterial cell wall (**Figure 2.4E**) and rescued the translocation defect of the *lap*⁻ strain across the Caco-2 barrier (**Figure 2.3G**).

Additionally, treatment of Caco-2 monolayers with LAP significantly reduced TEER, when LAP was added to the apical, basolateral or both the compartments (**Figure 2.4F**) and TEER value reduced progressively with increasing concentration of LAP (**Figure 2.3I**). Consequently, FD4 permeability increased, equivalent to TNF-α as a positive control, over a 72-h period (**Figure 2.3J**). Collectively, these data confirm that the LAP increases epithelial permeability and suggest a positive correlation between LAP-mediated epithelial permeability and *Listeria* translocation in a mouse and human Caco-2 cell models.

Figure 2.3. LAP contributes to intestinal barrier dysfunction.

(A,B) 4-kDa FITC-dextran (FD4) permeability through the intestinal epithelium of uninfected (control) and *L. monocytogenes*–infected A/J mice in serum (A) and urine (B).

(C-F) *L. monocytogenes* localization in the mouse ileal epithelial cell junction (48 h pi). ZO-1 (red), *Listeria* (green; arrows) and nucleus (blue) infected with WT (C,D) or Δ*inlA* (E,F). Merged images show co-localization of *L. monocytogenes* and ZO-1 (arrow), and *L. monocytogenes* exiting the epithelial cell (D,F, arrows) and in the lamina propria (LP) (D, yellow arrow). Scale bar, 1 µm.

(G,H) *L. monocytogenes* WT (F4244 and 10403s) and their isogenic mutant strains translocation across Caco-2 cell barrier or *lap*$^{-}$ with exogenously added recombinant LAP (*lap*$^{-}$+LAP: 1 µg/ml, 2 µg/ml), and *L. innocua* (G). (H) FD4 flux (Y1 axis) and bacterial translocation (Y2 axis) after treatment with *Listeria* (MOI 50).

(I,J) Purified LAP pre-treatment effect on the Caco-2 TEER (I) and FD4 permeability (J). Human TNF-α (10 ng/ml) was used as a control. See also Fig 2.4 and Videos 1, 2, 3, 4 and 5.

All error bars represent SEM (n= 5-7). ***, $P<0.001$; **, $P<0.01$; ns, no significance.

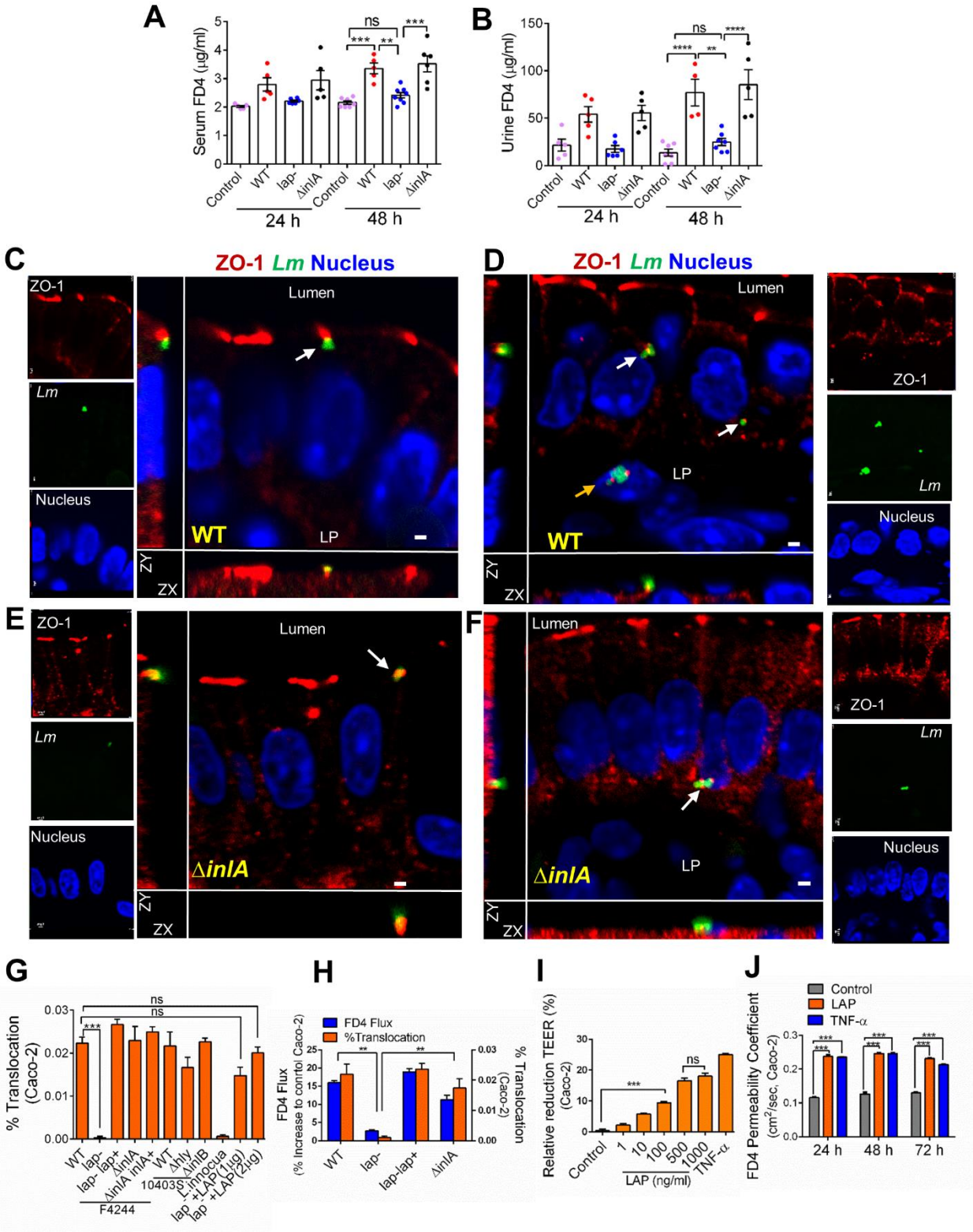
A
Serum FD4 (μg/ml)
Control
WT
lap-
ΔinlA
24 h
48 h
B
Urine FD4 (μg/ml)
C
ZO-1 Lm Nucleus
Lumen
WT
LP
ZY
ZX
D
E
ΔinlA
F
G
% Translocation (Caco-2)
F4244
10403S
L.innocua
lap- +LAP(1μg)
lap- +LAP(2μg)
H
FD4 Flux
%Translocation
(% Increase to conrtol Caco-2)
I
Relative reduction TEER (%) (Caco-2)
LAP (ng/ml)
TNF-α
J
Control
LAP
TNF-α
FD4 Permeability Coefficient (cm²/sec, Caco-2)
24 h
48 h
72 h

Videos 1-5

Video 1. Related to Fig 2.3. Localization of *L. monocytogenes* WT in the mouse ileal epithelial tight junction (Video Link).
Images ileal tissue sections immunostained for ZO-1 (red), *Listeria* (green) and DAPI (blue; nucleus) from *L. monocytogenes* WT-challenged A/J mice 48 h pi, acquired as a z stack and assembled as a three-dimensional reconstruction. This video demonstrates co-localization of WT cell (green) with ZO-1 (red) in mouse ileal epithelial cell TJ

Video 2. Related to Fig 2.3. Localization of *L. monocytogenes* WT in the mouse ileal epithelial tight junction (exiting the cell junction) and in the lamina propria (Video Link)
Images of ileal tissue sections immunostained for ZO-1 (red), *Listeria* (green) and DAPI (blue; nucleus) from *L. monocytogenes* WT-challenged A/J mice 48 h pi, acquired as a z stack and assembled as a three-dimensional reconstruction. This video demonstrates (a) co-localization of *L. monocytogenes* WT strain (green) with ZO-1 (red) in mouse ileum at the epithelial cell-cell junction (b) *L. monocytogenes* exiting the cell junction and (c) *L. monocytogenes* in the lamina propria.

Video 3. Related to Fig 2.3. Localization of *L. monocytogenes ΔinlA* in the mouse ileal epithelial tight junction (Video Link).
Images of paraffin-embedded ileal tissue sections immunostained for ZO-1 (red), *Listeria* (green) and DAPI (blue; nucleus) from *L. monocytogenes* Δ*inlA* -challenged mice 48 h pi, acquired as a z stack and assembled as a three-dimensional reconstruction. This video demonstrates co-localization of *L. monocytogenes* Δ*inlA* strains (green) with ZO-1 (red) in mouse ileal epithelial cell TJ.

Video 4. Related to Fig 2.3. Localization of *L. monocytogenes ΔinlA* in the mouse ileal epithelial tight junction (exiting the cell junction) (Video Link).
Images of paraffin-embedded ileal tissue sections immunostained for ZO-1 (red), *Listeria* (green) and DAPI (blue; nucleus) from *L. monocytogenes* Δ*inlA* -challenged A/J mice 48 h pi, acquired as a z stack by confocal microscopy and assembled as a three-dimensional reconstruction. This video demonstrates (a) co-localization of *L. monocytogenes* Δ*inlA* strains (green) with ZO-1 (red) in mouse ileum at the epithelial cell-cell junction and (b) *L. monocytogenes* exiting the cell junction.

Video 5. Related to Fig 2.3. Localization of *L. monocytogenes lap—* in the lumen of mouse ileal tissue (Video Link).
Images of ileal tissue sections immunostained for ZO-1 (red), *Listeria* (green) and DAPI (blue; nucleus) from *L. monocytogenes lap*$^{-}$ -challenged A/J mice 48 h pi acquired as a z stack and assembled as a three-dimensional reconstruction. This video demonstrates the presence of *L. monocytogenes lap*$^{-}$ strain in the lumen of ileal tissue with no apparent association with the epithelial cell TJ.

Figure 2.4. Analysis of tight junction protein (ZO-1) staining, TEER analysis, Caco-2 cell viability by LDH release assay, titration of the relevant concentration of LAP that is available on the bacterial surface and LAP binding to the surface of *L. monocytogenes.*

(A) Confocal immunofluorescence microscopy images of 5 µm thick, ileal tissue sections immunostained for ZO-1 (red), *Listeria* (green, arrows) and DAPI (blue; nucleus) from *lap*$^{-}$ -challenged mice 48 h pi. Scale bars, 1 µm. No *lap*$^{-}$ strain was found to be co-localized with the tight junction protein ZO-1(red). Separated channels are shown individually to the left of the merged images. The X-Z and Y-Z cross-sections were produced by orthogonal reconstructions from the z-stack scanning. Pictures are representative of five different fields from two mice.

(B) Analysis of epithelial permeability by measuring the transepithelial electrical resistance (TEER) across Transwell grown uninfected (control) Caco-2 cells or cells infected apically with *L. monocytogenes* WT, *lap*$^{-}$, *lap*$^{-}$ *lap*$^{+}$ and Δ*inlA* strains (MOI 50, 2 h pi). The data were normalized to uninfected controls and then expressed as the mean % change ± SEM from three independent experiments (n=6). ***, $P<0.001$; **, $P<0.01$, ns, no significance.

(C) Analysis of cell viability by an LDH release assay in culture supernatants of Caco-2 cells infected with WT, *lap*$^{-}$, *lap*$^{-}$ *lap*$^{+}$, Δ*inlA*, Δ*inlA inlA*$^{+}$ strains (MOI 50, 2 h pi) grown on Transwell filter-insert. The data are representative of two independent experiments analyzed in triplicate (n=6) and represent the mean ± SEM. ns, no significance.

(D) Titration of the relevant concentration of LAP that is available on the bacterial surface during infection of Caco-2 cells. (Top panel) Western blot analysis of total LAP and InlA expression in cell wall-associated fractions from $1x10^{9}$, $1x10^{8}$, $1x10^{7}$ CFU of *L. monocytogenes* WT, after 16 h of growth. The anti-LAP mAb-H7 was used to detect LAP and the anti-InlA mAb-2D12 was used to detect InlA. Purified LAP (0.5 µg, 1 µg or 2 µg, as quantified by BCA assay), was used as a standard. (Bottom panel) The mean antibody-reaction intensity values were calculated from measurements of reaction intensity (pixel) for bands. Densitometry report represents the mean ± SEM of three independent experiments. ns, no significance.

(E) Analysis of purified LAP binding to the surface of *L. monocytogenes*. Western blot analysis of cell wall-associated LAP from *L. monocytogenes* WT, *lap*$^{-}$, *lap*$^{-}$ *lap*$^{+}$ strain or *lap*$^{-}$ strain that was incubated with 1 µg or 2 µg of purified LAP for 30 min at room temperature as described in STAR Methods section and analyzed after immunoblotting with the LAP-specific mAb.

(F) Effect of recombinant purified LAP on the filter-insert grown Caco-2 TEER after LAP (1 µg/ml) pre-treatment of the apical (AP), basolateral (BL), or combined apical and basolateral compartments for 48 h. Data represent mean ± SEM from three independent experiments (n=6).

Statistical significance for plots B,C,D, and F was determined by using the one-way ANOVA test followed by a Tukey's multiple comparisons ***, $P<0.001$; **, $P<0.01$; ns, no significance.

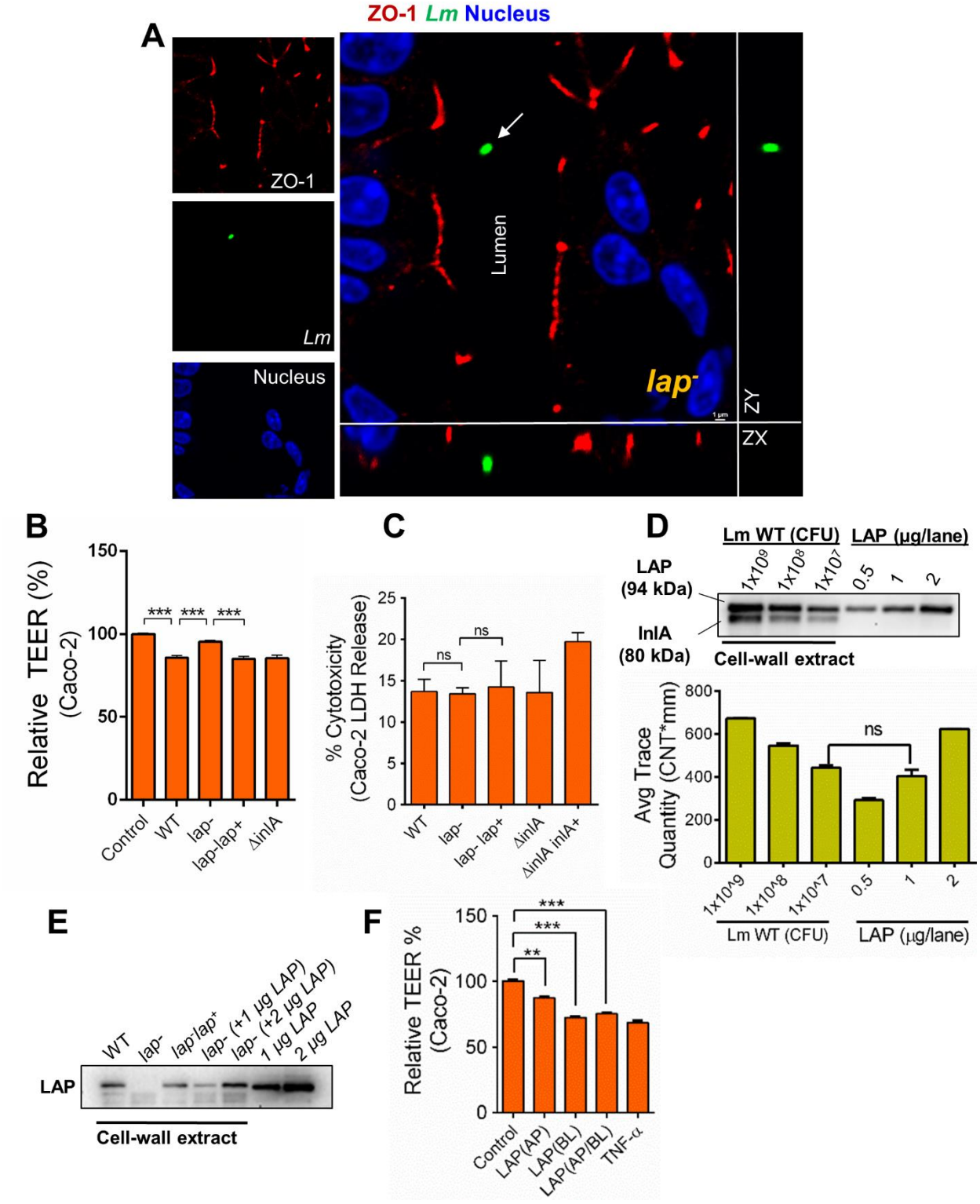
A
ZO-1 Lm Nucleus
ZO-1
Lm
Nucleus
Lumen
lap-
ZY
ZX
B
Relative TEER (%) (Caco-2)
150
100
50
0
***
***
***
Control
WT
lap-
lap-lap+
ΔinlA
C
% Cytotoxicity (Caco-2 LDH Release)
25
20
15
10
5
0
ns
ns
WT
lap-
lap- lap+
ΔinlA
ΔinlA inlA+
D
Lm WT (CFU)
LAP (μg/lane)
LAP (94 kDa)
InlA (80 kDa)
1x10^9
1x10^8
1x10^7
0.5
1
2
Cell-wall extract
Avg Trace Quantity (CNT*mm)
800
600
400
200
0
ns
1x10^9
1x10^8
1x10^7
0.5
1
2
Lm WT (CFU)
LAP (μg/lane)
E
WT
lap-
lap-lap+
lap- (+1 μg LAP)
lap- (+2 μg LAP)
1 μg LAP
2 μg LAP
LAP
Cell-wall extract
F
Relative TEER % (Caco-2)
150
100
50
0
***
***
**
Control
LAP(AP)
LAP(BL)
LAP(AP/BL)
TNF-α

LAP Upregulates TNF-α and IL-6 Expression in Intestinal Cells

Cytokines play a crucial role in the modulation of inflammatory responses in the gastrointestinal tract, and pro-inflammatory cytokines, such as TNF-α, IL-1β, IL-6, IL-8, and IFN-γ, induce disturbances in the intestinal cell-cell junction barrier, which promotes increased epithelial permeability and penetration of luminal antigens (Ma et al. 2004). *L. monocytogenes* upregulates IL-8, MCP1, GM-CSF, and TNF-α in epithelial cells (Jung et al. 1995), and the intestinal host response is InlA-independent (Lecuit et al. 2007). Therefore, we compared the expression of 40 inflammatory mediators in culture supernatants of Caco-2 cells infected with WT or *lap*⁻ using a cytokine dot-blot array (**Figure 2.6A**). Densitometry of the arrays revealed that TNF-α, IL-6, IL-8, and IFN-γ, and the chemokine MCP-2 were downregulated, in particular, TNF-α and IL-6 by 26±1% and 47±2%, respectively, when infected with the *lap*⁻ compared to the WT (**Figures 2.6A and 2.6B, Table 2.2)**. The *lap*⁻ strain produced significanly lower TNF-α and IL-6 than the WT in Caco-2 cells (**Figures 2.5A and 2.5B**). Treatment of Caco-2 cells with purified LAP produced high levels of TNF-α and IL-6 without causing any cytotoxic effects (**Figures 2.5A, 2.5B and 2.6C**). In the ileal mucosa, levels of TNF-α and IL-6 transcripts (mRNA) and proteins were also significantly higher in mice infected with WT and Δ*inlA* than those infected with the *lap*⁻ (**Figures 2.5C-2.5H**).

Histopathology of ileal tissue revealed significantly increased numbers of polymorphonuclear and mononuclear cells infiltrating the base of the villous lamina propria, and increased involvement of the submucosa, in mice challenged with the WT and Δ*inlA* than the *lap*⁻ strain at 24 h and 48 h pi (**Figures 2.5I and 2.5J**). These data suggest that LAP contributes to TNF-α and IL-6 production in Caco-2 cells and mouse ileal mucosa.

Figure 2.5. LAP upregulates TNF-α and IL-6 expression in intestinal cells.

(A,B) ELISA analysis of human TNF-α (A) and IL-6 (B) in Caco-2 cell supernatants (n=4-6), and mouse TNF-α (C) and IL-6 (D) in mouse (n=3-4) ileal tissues at 48 h pi. *L. innocua* (nonpathogen) and the purified LAP (1 μg/ml) were used as controls (A,B).

(E-H) Analysis of mRNA levels for TNF-α at 24 h (E) and 48 h (F) pi and IL-6 at 24 h (G) and 48 h (H) pi in the ileal mucosa of mice (n=3-4) and values were normalized to *gapdh* with the average for untreated samples set at 1.

(I,J) Histology score of ileal tissue sections at combined 24 h and 48 h pi (I), and representative H&E stained images (J) (scale bar, 50 μm) from control uninfected mice (n=6) or *Listeria* infected mice (n=10-11). Polymorphonuclear and mononuclear cells (arrows) infiltrating the base of the villous lamina propria are evident (J). See also Fig 2.6 and Table 1.1.

All error bars represent SEM. ****, $P<0.0001$; ***, $P<0.001$; **, $P<0.01$; *, $P<0.05$; ns, no significance.

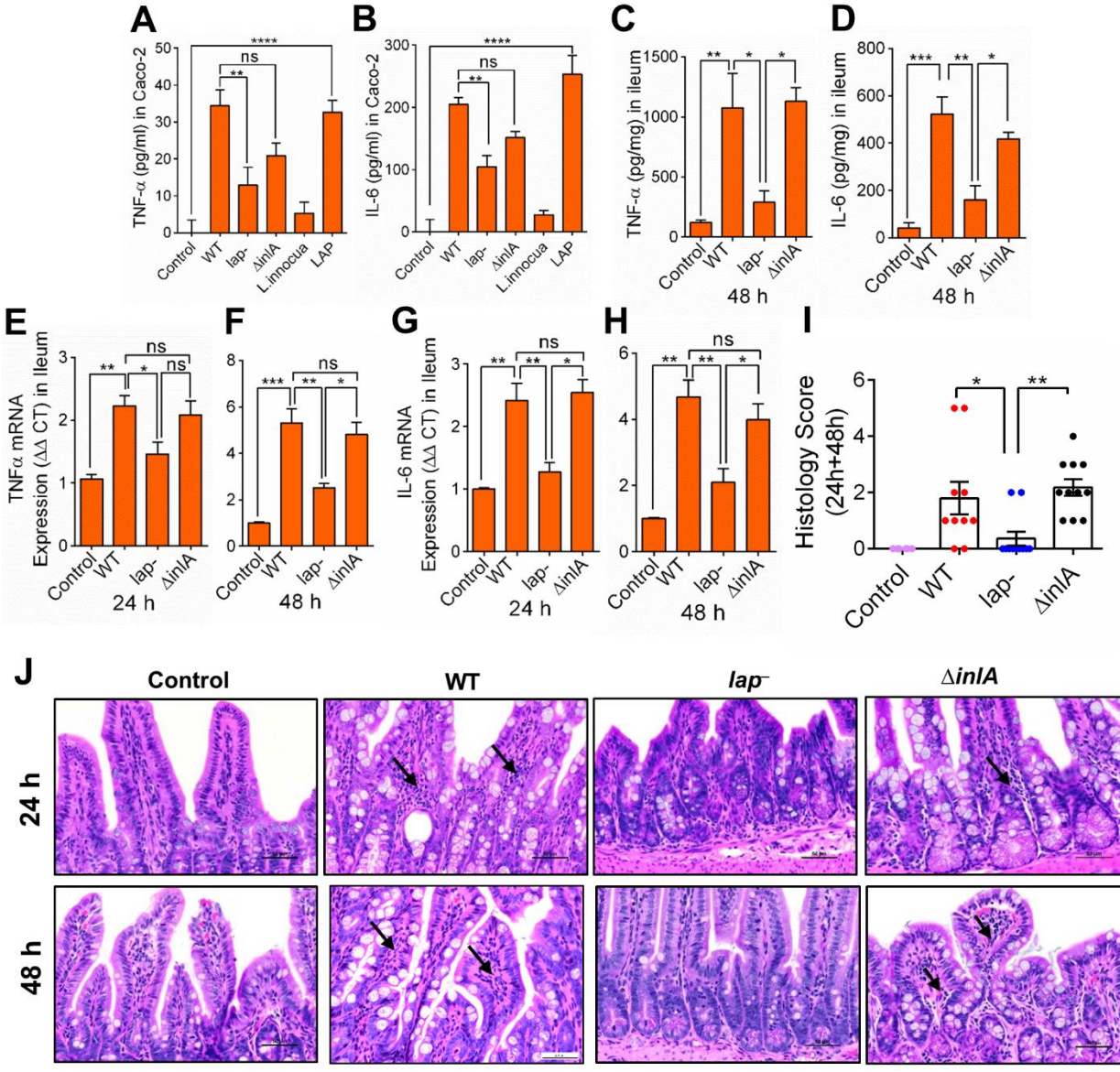
A
TNF-α (pg/ml) in Caco-2
Control
WT
lap-
ΔinlA
L.innocua
LAP
B
IL-6 (pg/ml) in Caco-2
C
TNF-α (pg/mg) in ileum
48 h
D
IL-6 (pg/mg) in ileum
48 h
E
TNFα mRNA Expression (ΔΔ CT) in Ileum
24 h
F
48 h
G
IL-6 mRNA Expression (ΔΔ CT) in Ileum
24 h
H
48 h
I
Histology Score (24h+48h)
J
Control
WT
lap–
ΔinlA
24 h
48 h

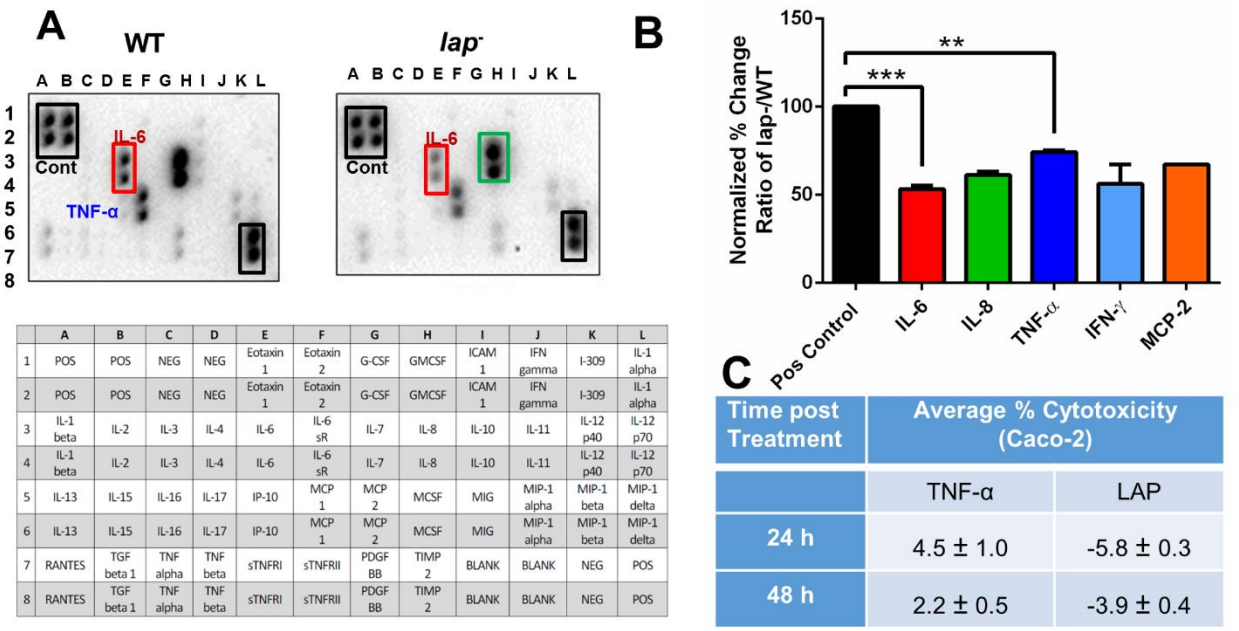

	A	B	C	D	E	F	G	H	I	J	K	L
1	POS	POS	NEG	NEG	Eotaxin 1	Eotaxin 2	G-CSF	GMCSF	ICAM 1	IFN gamma	I-309	IL-1 alpha
2	POS	POS	NEG	NEG	Eotaxin 1	Eotaxin 2	G-CSF	GMCSF	ICAM 1	IFN gamma	I-309	IL-1 alpha
3	IL-1 beta	IL-2	IL-3	IL-4	IL-6	IL-6 sR	IL-7	IL-8	IL-10	IL-11	IL-12 p40	IL-12 p70
4	IL-1 beta	IL-2	IL-3	IL-4	IL-6	IL-6 sR	IL-7	IL-8	IL-10	IL-11	IL-12 p40	IL-12 p70
5	IL-13	IL-15	IL-16	IL-17	IP-10	MCP 1	MCP 2	MCSF	MIG	MIP-1 alpha	MIP-1 beta	MIP-1 delta
6	IL-13	IL-15	IL-16	IL-17	IP-10	MCP 1	MCP 2	MCSF	MIG	MIP-1 alpha	MIP-1 beta	MIP-1 delta
7	RANTES	TGF beta 1	TNF alpha	TNF beta	sTNFRI	sTNFRII	PDGF BB	TIMP 2	BLANK	BLANK	NEG	POS
8	RANTES	TGF beta 1	TNF alpha	TNF beta	sTNFRI	sTNFRII	PDGF BB	TIMP 2	BLANK	BLANK	NEG	POS

Time post Treatment	Average % Cytotoxicity (Caco-2)	
	TNF-α	LAP
24 h	4.5 ± 1.0	-5.8 ± 0.3
48 h	2.2 ± 0.5	-3.9 ± 0.4

Figure 2.6. Comparison of the expression of inflammatory mediators in culture supernatants of Caco-2 cells infected with WT or *lap*⁻ bacteria and analysis of the cytotoxic effect of purified recombinant LAP.

(A,B) (**Top panel**) Array displaying the cytokine (40) expression profiles in Caco-2 cell supernatants infected with *L. monocytogenes* WT (left) or *lap*⁻ (right) using a semi-quantitative membrane-based human inflammation array 3 (Ray Biotech). The array is representative of two independent experiments with each spot in duplicate (n=4). (**Bottom panel**) Map of human inflammation array 3 **(A)**. Bar graph depicting the densitometry analysis of spots corresponding to IL-6, IL-8, TNF-α, IFN-γ, and MCP-2 from arrays **(B)**. The data were normalized to array-specific positive controls and then expressed as the mean % change ± SEM from two independent experiments (n=4).

(C) Analysis of the cytotoxic effect of purified recombinant LAP, if any, on Caco-2 cells. Negative (-) values indicate that % cytotoxicity was less than the untreated control. Human TNF-α (10 µg/ml) was used as a control. The data represent mean (% cytotoxicity) ± SEM (n=6).

Statistical significance for plot B was determined by using the one-way ANOVA test followed by a Tukey's multiple comparisons. ***, $P<0.001$; **, $P<0.01$.

LAP Contributes to *Listeria*-induced NF-κB Activation for Increased Epithelial Permeability

NF-κB is a central regulator of pro-inflammatory cytokines, including TNF-α and IL-6 (Oeckinghaus et al. 2011), and it is strongly activated in Caco-2 cells upon *L. monocytogenes* infection independent of invasion (Baldwin et al. 2003), thus we examined whether LAP contributes to NF-κB(p65) activation. We observed significantly lower levels of nuclear p65 and P-p65 in the *lap*⁻ infected cells relative to the WT or Δ*inlA* infected cells at 30 min pi (**Figures 2.7A and 2.7B**). The total cellular p65 was not changed in the WT, *lap*⁻ or Δ*inlA* infected cells (**Figure 2.8A)**. Purified LAP treatment also increased IKKα level in the cytosol, and p65 and P-p65 in the nucleus in a concentration-dependent manner (**Figures 2.7C and 2.7D**). Therefore, LAP contributes to *Listeria*-induced NF-κB activation in Caco-2 cells.

NF-κB is inactive in unstimulated cells and remains associated with the inhibitors of κB (IκB, IκBα and IκBβ) in the cytoplasm. Treatment of Caco-2 cells with LAP rapidly degraded IκBα within 15 min and the most were degraded within 45 min, while phospho-IκBα (P-IκBα) concomitantly appeared at 15 min (**Figures 2.7E** and **2.8B**). The IκBα degradation paralleled with a significant increase in nuclear p65 and P-p65 at 30 min pi (**Figures 2.7F and 2.8C**). Treatment of Caco-2 cells with human TNF-α exhibited a similar IκBα degradation kinetics and a concomitant increase in cytosolic P-IκBα and nuclear p65 and P-p65 levels (**Figures 2.7E and 2.7F, 2.8B and 2.8C**). Immunostaining confirmed p65 sequestration in the nucleus after 30 min of LAP or TNF-α treatment (**Figure 2.7G**). Thus, LAP in Caco-2 cells stimulates IκBα degradation and facilitates rapid translocation of p65 to the nucleus, a hallmark of NF-κB activation.

Analysis of intestinal epithelial cells (IECs) of mice infected with WT or Δ*inlA* revealed increased NF-κB activity; as immunostaining confirmed nuclear abundance of p65 and P-p65 in IECs (**Figures 2.7H-2.7J**). In contrast, the *lap*⁻ infected mice showed the presence of a very low

nuclear positive p65 and P-p65 cells and most of the p65 were sequestered in the cytoplasm of IECs.

L. monocytogenes-induced NF-κB pathway is the most dominant host response in macrophage, which is the major resident cell in lamina propria; therefore, we verified the ability of LAP to activate NF-κB in the murine macrophage RAW 264.7-NF-κB-luciferase reporter cell line. LAP activated NF-κB in a concentration-dependent manner (**Figure 2.8D**). Likewise, purified recombinant InlB protein activated NF-κB in RAW 264.7 cells, but InlA was neutral (**Figures 2.8E and 2.8F**). Heat (**Figure 2.8F**) and proteinase-K (**Figures 2.8G and 2.8H**) abolished, while polymyxin-B (**Figures 2.8I and 2.8J**) treatment retained the NF-κB activation ability of LAP and InlB indicating susceptibility of these proteins to thermal denaturation and proteolytic enzymes, and absence of LPS contamination, respectively. Pretreatment of LAP with an anti-LAP mAb also significantly reduced LAP-mediated NF-κB response (**Figure 2.8K**). Besides, the *lap*⁻ strain showed lower NF-κB activity than the WT strain **(Figure 2.8L)**. Collectively, these results suggest that LAP activates NF-κB in Caco-2 cells, IEC's of mice and murine macrophage cell line (RAW 264.7), while InlA is unresponsive (this study). InlB does not activate NF-κB in epithelial cell lines (Caco-2, HeLa, Hep G2, LoVo), however, it activates NF-κB in macrophage (Mansell et al. 2000). Likewise, among the other virulence proteins, LLO activates NF-κB in HEK293 cell line (Tsuchiya et al. 2005) and in endothelial cells of transgenic mice (Kayal et al. 2002), while InlC interferes with NF-κB activation in murine macrophages *in vivo* (Gouin et al. 2010).

We next examined whether pretreatment of Caco-2 cells with the NF-κB inhibitors, BAY or PDTC could prevent LAP-induced epithelial permeability. Both inhibitors significantly inhibited LAP-mediated NF-κB activation (**Figures 2.8M**), restored Caco-2 TEER (**Figure 2.8N**), and reduced WT and Δ*inlA* translocation by 80-90% across Caco-2 cell barrier (**Figures 2.7K and**

2.7L). Both inhibitors independently did not affect Caco-2 TEER (**Figures 2.8O and 2.8P**) and more importantly, did not affect WT invasion of Caco-2 cells (**Figures 2.8Q and 2.8R**). As a positive control, we pretreated Caco-2 cells with cytochalasin D that inhibits actin polymerization, bacterial invasion and cell-to-cell spread (Tilney and Portnoy 1989) but increases tight junction permeability (Stevenson and Begg 1994). Pretreatment of Caco-2 cells with cytochalasin D induced a very low TEER (**Figure 2.8S**) and markedly increased the translocation competencies of the WT and the isogenic *lap*$^{-}$, *lap*$^{-}$ *lap*$^{+}$ and Δ*inlA* across the Caco-2 cell barrier (**Figures 2.8T**), despite a low observed invasion (**Figures 2.8U**). Neutralization of TNF-α and IL-6 with antibodies also restored purified LAP-mediated drop in Caco-2 TEER (**Figure 2.8V)**. Taken together, these data demonstrate that LAP-mediated NF-κB activation is critical during *L. monocytogenes*-induced epithelial permeability.

Figure 2.7. LAP contributes to *Listeria*-induced NF-κB activation for increased epithelial permeability.

(A,B) Immunoblot and densitometry plots (n=3) of *Listeria*-induced p65 (A) and P-p65 (B) levels in the nuclear extracts of uninfected (Control) Caco-2 cells or infected with *L. monocytogenes* and *L. innocua* (MOI 50, 30 min). TBP (TATA-binding protein) is a nuclear loading control.

(C,D) Immunoblot and densitometry plots (n=3) showing IKK-α levels in the cytosolic extracts (C), and of p65 and P-p65 in the nuclear extracts (D) of LAP-treated (30 min) Caco-2 cells.

(E,F) Immunoblots showing time-dependent expression of IκBα and P-IκBα in the cytosolic extracts (E) and p65 and P-p65 in the nuclear extracts (F) of Caco-2 cells treated with LAP (1 μg/ml) or TNF-α (10 ng/ml).

(G) Images of Caco-2 cells treated with LAP (1 μg/ml) or human TNF-α (10 ng/ml) for 30 min stained for p65 (green) and the nuclei (blue). Arrows show the nuclear localization of p65. Scale bar, 20 μm.

(H,I) Images of ileal villi stained for p65 (H, green) and P-p65 (I, green) and the nuclei (blue) from uninfected (control) or mice infected with *Listeria* 48 h pi (see Fig 1). Arrows indicate the nuclear localization of p65 and P-p65. Scale bar, 10 μm.

(J) Enumeration of IEC per villus (n=10-15 villi from 2-3 mice/treatment) positive for p65 and P-p65 in the nucleus of Fig H and I.

(K,L) *Listeria* (MOI 50) translocation through Caco-2 cell barrier following pretreatment with BAY (10 μM, 30 min) (K) or with PDTC (100 μM, 30 min) (L) (n=6). See also Fig 2.8.

All error bars represent SEM. ***, $P<0.0001$; **, $P<0.001$.

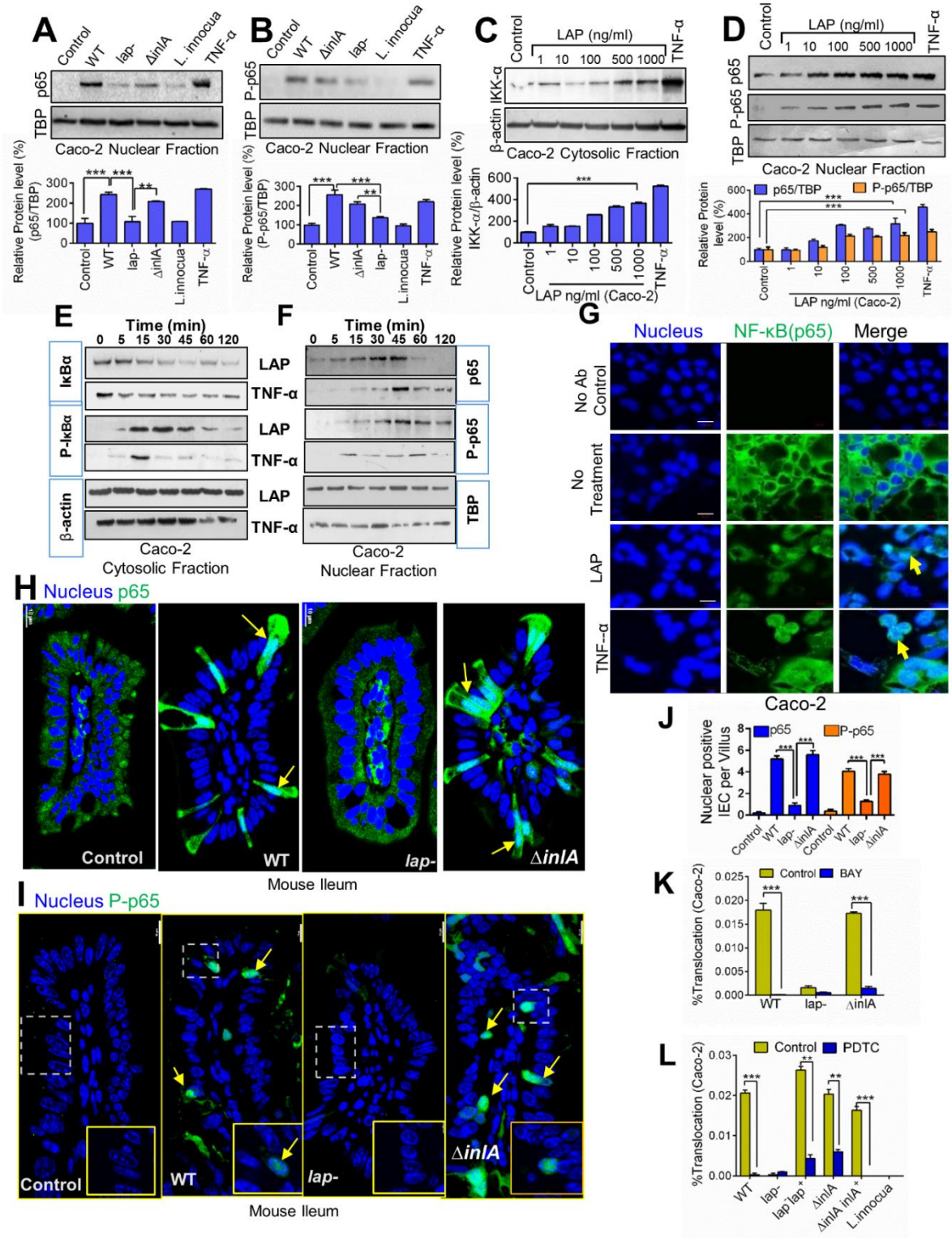
A
Control
WT
lap-
ΔinlA
L. innocua
TNF-α
p65
TBP
Caco-2 Nuclear Fraction
Relative Protein level (%) (p65/TBP)
B
P-p65
Relative Protein level (%) (P-p65/TBP)
C
LAP (ng/ml)
1 10 100 500 1000
IKK-α
β-actin
Caco-2 Cytosolic Fraction
Relative Protein level (%) IKK-α/β-actin
LAP ng/ml (Caco-2)
D
P-p65 p65
p65/TBP
P-p65/TBP
Relative Protein level (%)
E
Time (min)
0 5 15 30 45 60 120
IκBα
P-IκBα
β-actin
LAP
TNF-α
Caco-2 Cytosolic Fraction
F
p65
P-p65
TBP
Caco-2 Nuclear Fraction
G
Nucleus
NF-κB(p65)
Merge
No Ab Control
No Treatment
LAP
TNF-α
Caco-2
H
Nucleus p65
Control
WT
lap-
ΔinlA
Mouse Ileum
I
Nucleus P-p65
J
Nuclear positive IEC per Villus
K
Control
BAY
%Translocation (Caco-2)
L
PDTC
lap+
ΔinlA inlA+

Figure 2.8. Analysis of LAP-mediated NF-κB activation, and effect of inhibitors on epithelial barrier function and bacterial invasion and translocation in Caco-2 cell model.

(A) Immunoblot analysis showing no marked changes of the total cellular p65 expression levels in the whole-cell lysate of Caco-2 cells infected with *L. monocytogenes* WT, Δ*inlA*, *lap*⁻, and *L. innocua* (MOI 50, 30 min). TBP (TATA-binding protein), uninfected cells (control), and TNF-α (10 ng/ml) were used as loading, baseline, and positive controls, respectively (**top panel).** Densitometry reports of p65 levels after normalization to TBP (**bottom panel**). Immunoblots are representative of 3 independent experiments and densitometry report represent the mean ± SEM of three independent experiments.

(B,C) Densitometry reports of time-dependent IκBα and P-IκBα levels following treatment with purified recombinant LAP (1 μg/ml; **A, top panel**) or TNF-α (10 ng/ml; **B, bottom panel**) in cytoplasmic extract after normalization to the levels of β-actin and p65 and P-p65 following treatment with purified recombinant LAP (1 μg/ml; **C, top panel**) or TNF-α (10 ng/ml; **C, bottom panel**) in nuclear extracts after normalization to the levels of TBP. Densitometry report represents the mean ± SEM of three independent experiments.

(D) Analysis of dose-dependent NF-κB activation by purified recombinant LAP in RAW 264.7 luciferase reporter macrophage cell line. Cells were treated with LAP purified from either from *E. coli* BL21 or ClearColi (1-2500 ng/ml) and LPS (500 ng/ml) for 6 h, and luciferase activity was measured. In Clear Coli, two of the secondary acyl chains of the normally hexa-acylated LPS have been deleted, thus eliminating a key determinant of endotoxicity. The data represent mean ± SEM of three independent experiments (n=6).

(E) Verification of purity and identity of recombinant InlA, InlB and LAP proteins by Coomassie blue staining (top panel) and Western blot (bottom panel). Each well was loaded with 2.5 μg of purified protein in SDS-PAGE (12.5%- polyacrylamide), electrophoretically separated in gel, and Coomassie stained (left panel) or immunoprobed with protein-specific antibodies (top panel). Purified LAP shows two bands. The upper band is the full-length LAP (*lmo1634*, consists of two enzymes, acetaldehyde dehydrogenase (ALDH) and alcohol dehydrogenase (ADH), called alcohol acetaldehyde dehydrogenase) and the lower band (~50 kDa) is predicted to be alcohol dehydrogenase, which tends to separate from the acetaldehyde dehydrogenase when analyzed in SDS-PAGE. Mass-spectrometry analysis of the 50-kDa band reported it as LAP (*lmo1634*).

(F) Analysis of NF-κB activation in RAW 264.7 luciferase reporter macrophage cell line by purified recombinant LAP, InlA or InlB (1 μg/ml each) treated with or without heat treatment (100°C, 10 min). The data represent mean ± SEM of three independent experiments (n=6).

(G) Coomassie blue stained gel showing recombinant (undigested) or proteinase-K digested purified LAP, InlA or InlB proteins.

Figure 2.8. continued

(H) Analysis of NF-κB activation in RAW 264.7 luciferase reporter macrophage cell line by purified recombinant LAP, InlA or InlB (1 µg/ml each) pre-treated with or without proteinase-K treatment (1 µg/ µg of protein, 30 min, and 37°C). The data represent mean ± SEM of three independent experiments (n=6).

(I) Analysis of LPS (endotoxin) levels in purified recombinant proteins from *E. coli* BL21 after passing through the polymyxin B column. The endotoxin activities in purified recombinant LAP, InlA and InlB were determined using the LAL Endotoxin Assay Kit. The value for LAP is representative of two independent experiments and is reported as mean of endotoxin level (ng/µg) ± SD). The analysis of InlA and InlB is reported as values from a single analysis.

(J) Analysis of NF-κB activation in RAW 264.7 luciferase reporter macrophage cell line by purified recombinant LAP, InlA or InlB (1 µg/ml each) treated with or without polymyxin B (10 µg/ml) for 1 h prior to exposure to cells for 6 h. The data represent mean ± SEM of three independent experiments (n=6).

(K) Analysis of NF-κB activation of purified recombinant LAP in RAW 264.7 luciferase reporter macrophage cell line by pre-incubating with anti-LAP mAb which reduced luciferase activity, whereas isotype control mouse IgG (1 µg/ml each, 1 h, 37°C) had no effect. The data represent mean ± SEM of three independent experiments (n=6).

(L) Analysis of NF-κB activation in RAW 264.7 luciferase reporter macrophage cell line infected with WT, *lap*$^{-}$, *lap*$^{-}$ *lap*$^{+}$, Δ*inlA* strains (MOI 10, 6 h). Uninfected cells (control) were used as a baseline control. The data represent mean ± SEM of three independent experiments (n=6).

(M) Western blot (**left panel**) showing suppression of LAP-mediated NF-κB activation by NF-κB inhibitors, PDTC or BAY. PDTC (100 µM, 30 min pretreatment) or BAY (10 µM, 30 min pretreatment) significantly reduced the levels of p65 in the nuclear extracts in Caco-2 cells treated with LAP (1 µg/ml, 30 min) or human TNF-α (100 ng/ml, 30 min) compared to the untreated cells. Densitometry reports (**right panel**) of p65 levels after normalization to TBP (loading control) are presented below the immunoblots. Immunoblots are representative of three independent experiments. Densitometry report represent the mean ± SEM of three independent experiments.

(N) Effect of NF-κB inhibitors, PDTC or BAY pre-treatment on TEER of Transwell filter-insert grown Caco-2 cells treated with recombinant purified LAP (1 µg/ml, 24h). Pre-treatment of Caco-2 cells with NF-κB inhibitors, PDTC (100 µM, 30 min, pretreatment) or BAY (10 µM, 30 min, pretreatment) restored LAP-mediated drop in Caco-2 TEER. The data represent the mean ± SEM of three independent experiments (n=3)

Figure 2.8. continued

(O,P) TEER values of Transwell filter-insert grown Caco-2 cells before and after treatment with NF-κB inhibitors, PDTC (100 μm, 30 min) **(O)** or BAY (10 μm, 30 min) **(P)**. Both NF-κB inhibitors used independently did not affect Caco-2 TEER. The data represent the mean ± SEM of three independent experiments (n=3).

(Q,R) Analysis of *L. monocytogenes* WT invasion of Caco-2 cells pretreated **(Q)** BAY (10 μM, 30 min) or with PDTC (100 μM, 30 min) **(Q)**. Both NF-κB inhibitors did not affect intracellular invasion of *L. monocytogenes* WT. The data represent three independent experiments (n=3).

(S) TEER values for Transwell filter-insert grown Caco-2 cells pre-treated with or without Cytochalasin D (1 μg/ml, for 1 h) (n=3).

(T,U) Analysis of *L. monocytogenes* (WT, *lap*$^{-}$, *lap*$^{-}$ *lap*$^{+}$, Δ*inlA* strains, MOI 50) translocation across **(T)** and invasion into **(U)** Caco-2 cells pretreated with or without cytochalasin D (1 μg/ml, 1 h). The data represent three independent experiments (n=6).

(V) Effect of TNF-α, or IL-6 neutralizing antibodies on TEER of on Transwell filter-insert grown Caco-2 cells treated with anti-TNF-α (1 μg/ml, maintained 24 h during treatment) or anti-IL-6 (1 μg/ml, maintained 24 h during treatment) neutralizing antibodies or added together (n=6). Neutralizing antibodies restored recombinant purified LAP (1 μg/ml, 24 h treatment)-mediated drop in TEER. Recombinant purified LAP was added to the apical side and neutralizing antibodies were added to apical and basolateral side.

Statistical significance for plots A,B,C,D,F,H,J,K,L,M,N,T,U and V was determined by using the one-way ANOVA test followed by a Tukey's multiple comparisons, for plots O,P,Q,R and S using the unpaired t-test. The error bars represent SEM. ***, $P<0.001$; **, $P<0.01$, *, $P<0.05$; ns, no significance.

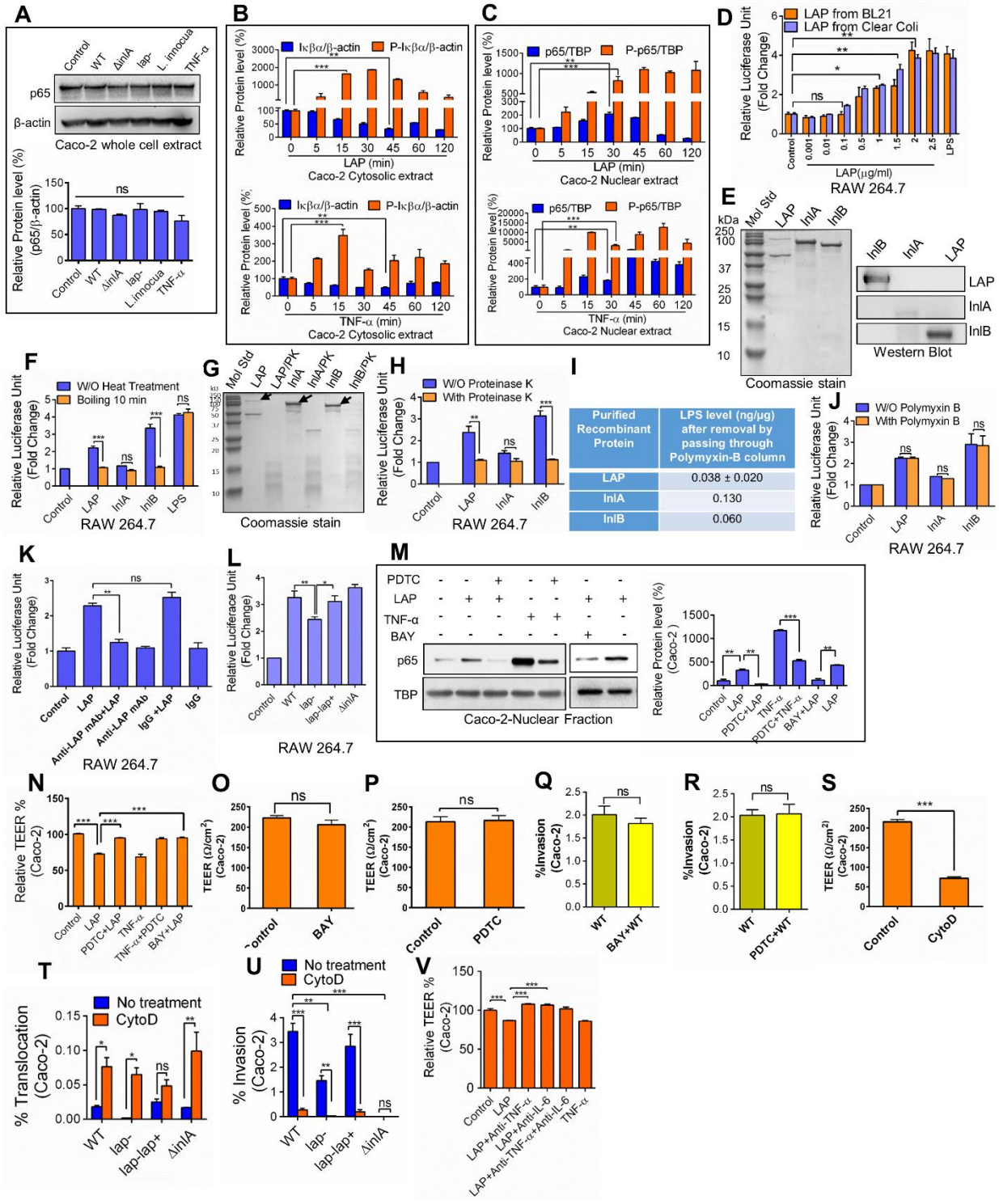
A
Control
WT
ΔinlA
lap-
L. innocua
TNF-α
p65
β-actin
Caco-2 whole cell extract
Relative Protein level (%) (p65/β-actin)
ns
B
Iκβα/β-actin
P-Iκβα/β-actin
Relative Protein level (%)
LAP (min)
Caco-2 Cytosolic extract
TNF-α (min)
Caco-2 Cytosolic extract
C
p65/TBP
P-p65/TBP
LAP (min)
Caco-2 Nuclear extract
TNF-α (min)
Caco-2 Nuclear extract
D
LAP from BL21
LAP from Clear Coli
Relative Luciferase Unit (Fold Change)
LAP(μg/ml)
RAW 264.7
E
Mol Std
LAP
InlA
InlB
kDa
Coomassie stain
Western Blot
F
W/O Heat Treatment
Boiling 10 min
Relative Luciferase Unit (Fold Change)
RAW 264.7
G
Mol Std
LAP
LAP/PK
InlA
InlA/PK
InlB
InlB/PK
Coomassie stain
H
W/O Proteinase K
With Proteinase K
RAW 264.7
I
Purified Recombinant Protein
LPS level (ng/μg) after removal by passing through Polymyxin-B column
LAP
0.038 ± 0.020
InlA
0.130
InlB
0.060
J
W/O Polymyxin B
With Polymyxin B
RAW 264.7
K
Control
LAP
Anti-LAP mAb+LAP
Anti-LAP mAb
IgG +LAP
IgG
RAW 264.7
L
Control
WT
lap-
lap-lap+
ΔinlA
RAW 264.7
M
PDTC
LAP
TNF-α
BAY
p65
TBP
Caco-2-Nuclear Fraction
Relative Protein level (%) (Caco-2)
Control
LAP
PDTC+LAP
TNF-α
PDTC+TNF-α
BAY+LAP
LAP
N
Relative TEER % (Caco-2)
Control
LAP
PDTC+LAP
TNF-α
TNF-α+PDTC
BAY+LAP
O
TEER (Ω/cm²) (Caco-2)
Control
BAY
P
TEER (Ω/cm²) (Caco-2)
Control
PDTC
Q
%Invasion (Caco-2)
WT
BAY+WT
R
%Invasion (Caco-2)
WT
PDTC+WT
S
TEER (Ω/cm²) (Caco-2)
Control
CytoD
T
No treatment
CytoD
% Translocation (Caco-2)
WT
lap-
lap-lap+
ΔinlA
U
No treatment
CytoD
% Invasion (Caco-2)
WT
lap-
lap-lap+
ΔinlA
V
Relative TEER % (Caco-2)
Control
LAP
LAP+Anti-TNF-α
LAP+Anti-IL-6
LAP+Anti-TNF-α+Anti-IL-6
TNF-α

LAP-mediated Activation of NF-κB is Dependent on the Hsp60 Receptor

Hsp60 acts as an IKK-interacting protein and mediates NF-κB-dependent signaling via interaction with IKKα/β in the cytoplasm (Chun et al. 2010). Hsp60 is the receptor for LAP, and to determine the contribution of Hsp60 in *Listeria*-mediated NF-κB activation, we used Hsp60 knockdown (*hsp60*::shRNA, ~70% knock-down) Caco-2 cells (Burkholder and Bhunia 2010) (**Figures 2.10A and 2.10B**) and determined the levels of IKK-β in the cytoplasmic, and p65 and P-p65 in the nuclear fraction in *Listeria*-infected or purified LAP-treated cells. Knock-down of Hsp60 resulted in significant decreases of *L. monocytogenes lap* (**Figure 2.9A**) or purified LAP-mediated (**Figure 2.9B)** IKK-β, p65 and P-p65 expression and p65 nuclear translocation (**Figure 2.9C**). Additionally, blocking of surface Hsp60 with an anti-Hsp60-specific mAb prior to purified LAP treatment showed a significant reduction in LAP-mediated IKK-β and p65 expression in Caco-2 cells (**Figure 2.9D**). Therefore, LAP (ligand) and Hsp60 (receptor) interaction contribute to *Listeria*-induced NF-κB activation in Caco-2 cells.

To examine the possible interactions between Hsp60 and IKK in Caco-2 cells, we next immunoprecipitated IKKβ from purified LAP-treated or -untreated Caco-2 cell lysates. Immunoblotting the lysates revealed co-precipitation of Hsp60 and IKK-β in LAP-treated cell lysates (**Figure 2.9E**). Reverse immunoprecipitation using an anti-Hsp60 antibody also co-precipitated IKK-β and Hsp60 in the LAP-treated cell lysates (**Figure 2.9F**). Thus, Hsp60 ultimately resides in the IKK complex in LAP-treated Caco-2 cells. Analysis of the subcellular distribution of Hsp60 and IKK-β indicated that purified LAP treatment did not change the total cellular Hsp60 levels but decreased the membrane Hsp60 and increased the cytosolic Hsp60 levels significantly (**Figure 2.10C**). However, LAP-treatment increased total cellular and cytosolic IKK-β levels significantly (**Figure 2.10C**). Thus, LAP induces internalization of

surface expressed Hsp60 in Caco-2 cells, which may facilitate interaction of Hsp60 with the IKK-complex.

The primary function of Hsp60 is to act as a molecular chaperone within the cell cytoplasm and mitochondrial matrix. We have previously (Burkholder and Bhunia 2010), and also in this study (**Figure 2.10C**) demonstrated membrane localization of Hsp60 in Caco-2 cells. In the mouse intestine, Hsp60 has been localized at high levels in the crypts and the villi (Berger et al. 2016). Here, we confirmed apical and the plasma membrane localization of Hsp60 in the villi of mouse ileal tissue by immunostaining and Western blotting (**Figures 2.10D and 2.10E**). These results suggest that apically expressed surface Hsp60 is accessible to bacteria located in the intestinal lumen.

Figure 2.9. LAP-induced NF-κB activation is Hsp60 receptor dependent.

(A,B) Immunoblot and densitometry plots (n=3) of cytosolic IKK-β and Hsp60 and nuclear p65 and P-p65 in vector control shRNA (Control::shRNA) or *hsp60* knockdown (hsp60::shRNA) Caco-2 cells after infection with *Listeria* (MOI 50, 30 min) or no infection (Control) (A). Panel B is same as panel A except the Caco-2 cells were treated with purified LAP (1 μg/ml) or human TNF-α (10 ng/ml) for 30 min (B).

(C) Localization of p65 (green), Hsp60 (red) and nucleus (blue) in vector-control shRNA (Control shRNA) or *hsp60* knockdown (hsp60::shRNA) Caco-2 cells treated with purified LAP (1 μg/ml), TNF-α (10 ng/ml) or untreated (Control) for 30 min. In LAP and TNF-α treated Control cells, p65 is in the nucleus (white arrows) while in the cytoplasm of *hsp60* knockdown cells (dark arrows). Scale bar, 10 μm.

(D) Immunoblot and densitometry plots (n=3) of cytosolic IKK-β and nuclear p65 in Caco-2 cells incubated with anti-Hsp60 mAb (1 μg/ml, 1 h) to block surface Hsp60 prior to LAP (1 μg/ml, 30 min) treatment.

(E,F) Immunoblots showing the interaction of Hsp60 with IKK-β in LAP (1 μg/ml, 30 min)-treated Caco-2 cells. IKK-β (E) or Hsp60 (F) were immunoprecipitated from Caco-2 cell lysates and immunoprobed with anti-Hsp60 (E) or anti-IKKβ (F) mAb. Arrows (E, F) indicate co-precipitated IKK-β and Hsp60, respectively, in the LAP-treated cells. The 10% input lane (E,F) represents Caco-2 lysate without immunoprecipitation (IP). The IP: No Ab lane (E,F) represents IP reactions without addition of antibody. Rabbit IgG (IP: IgG lane) (E) or normal mouse IgG (IP: IgG lane) **(F)** was used as an isotype control IP reaction. See also Fig 2.10.

All error bars represent SEM. ***, $P<0.0001$; **, $P<0.001$; *, $P<0.05$.

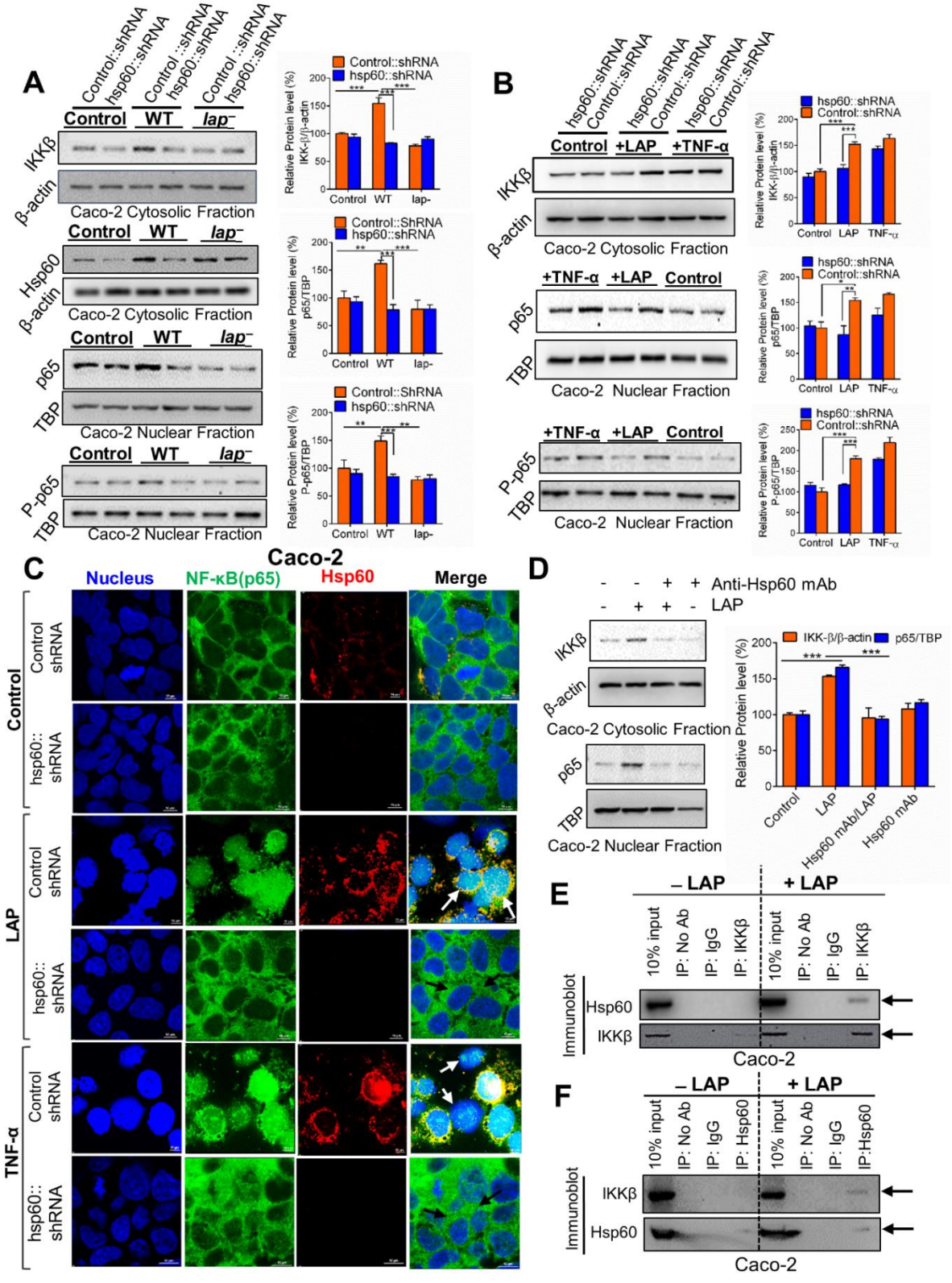
A
Control::shRNA
hsp60::shRNA
Control
WT
lap⁻
IKKβ
β-actin
Caco-2 Cytosolic Fraction
Hsp60
p65
TBP
Caco-2 Nuclear Fraction
P-p65
Relative Protein level (%)
IKK-β/β-actin
p65/TBP
P-p65/TBP
B
+LAP
+TNF-α
Control
C
Caco-2
Nucleus
NF-κB(p65)
Hsp60
Merge
LAP
TNF-α
D
Anti-Hsp60 mAb
LAP
Hsp60 mAb/LAP
Hsp60 mAb
E
– LAP
+ LAP
10% input
IP: No Ab
IP: IgG
IP: IKKβ
Immunoblot
F
IP: Hsp60

Figure 2.10. Confirmation of shRNA-mediated Hsp60 knockdown in Caco-2 cells, sub-cellular distribution of IKK-β and Hsp60 proteins in Caco-2 cells and confocal immunofluorescence microscopy and immunoblots for Hsp60 distribution in mouse intestine.

(A,B) Immunoblot analysis confirming Hsp60 knockdown in Caco-2 cells (*hsp60*::shRNA) relative to vector control (control::shRNA) cells. Both membrane **(A)** and cytosolic Hsp60 **(B)** levels was markedly lower (~70%) in Hsp60 knock-down (*hsp60*::shRNA) Caco-2 cells relative to the vector control (control::shRNA) cells. Densitometry reports of Hsp60 levels after normalization to β-Actin from three independent experiments are presented to the right of each blot.

(C) Immunoblot showing the sub-cellular distribution of IKK-β and Hsp60 proteins in the total (left panel), the membrane (middle panel) and the cytosolic (right panel) fractions from Caco-2 cells treated with purified recombinant LAP(1 µg/ml, 30 min) relative to control (untreated) cells. Densitometry reports of protein levels after normalization to β-actin (loading control) is presented to the right of each panel, which represent mean ± SEM of three independent immunoblot experiments. Immunoblot depicts no significant changes in the total Hsp60 levels (left panel), a significant decrease in the membrane Hsp60 levels (middle panel) and a significant increase in the cytosolic Hsp60 (right panel) levels following LAP (1 µg/ml, 30 min) treatment, relative to untreated cells. Immunoblot also shows a significant increase in total (left panel) and cytosolic IKK-β (right panel) protein levels following LAP (1 µg/ml, 30 min) treatment while IKK-β levels were undetectable in the membrane fraction (middle panel).

(D) Confocal immunofluorescence microscopy of ileal tissue sections from uninfected (control) A/J mouse immunostained for Hsp60 (red), F-actin (white, pseudo-color) and DAPI (blue; nucleus). Bars, 10 µm. Separated channels and merged images are shown individually. The far right panel (enlarged) shows enlargements of the boxed areas in the merged image. Bars, 1 µm. Hsp60 was detected apically and in addition to the cytoplasm, in the plasma membrane (arrows, enlarged image) of intestinal epithelial cells, as evidenced by co-localization of Hsp60 (red) with F- actin (white) in the mouse ileal tissue sections. Pictures are representative of five different fields from three mice.

(E) Immunoblot showing the sub-cellular distribution of Hsp60 protein in the membrane (**left panel**), the cytosol (**right panel**) fractions from purified ileal intestinal epithelial cells (IEC) from two representative uninfected (Control) A/J mice. E-cadherin in the membrane fraction (left panel) was used as a positive control. The same extract was probed with antibodies against cytosolic marker MEK-1/2, and membrane marker Pan-cadherin, which confirmed the absence of detectable MEK-1/2 levels in the membrane fraction (**left panel**) and absence of detectable Pan-cadherin levels in the cytosolic fraction (**right panel**).

Statistical significance for panel C was determined by using the unpaired *t*-test. **, $P<0.01$.

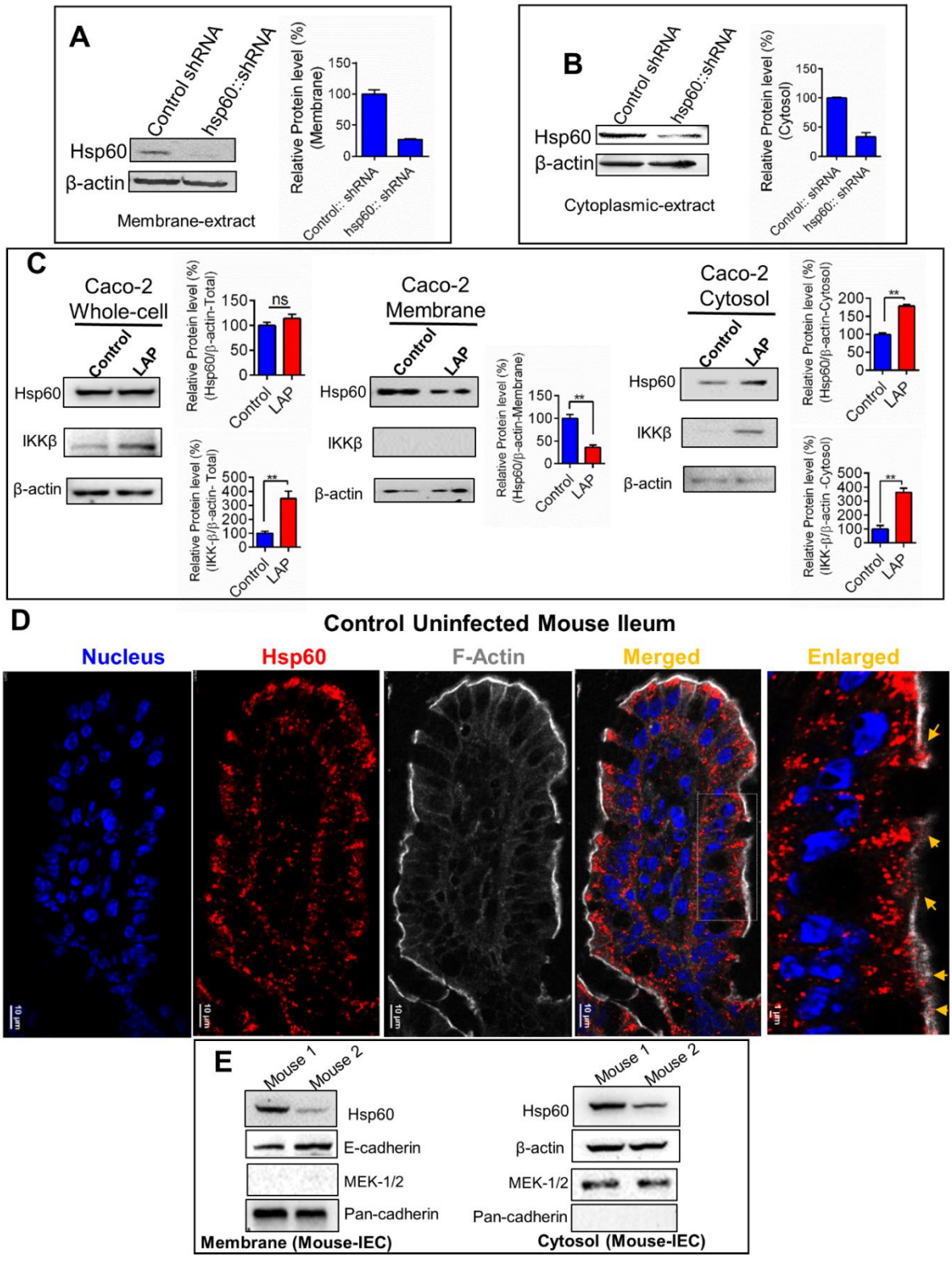
A
Control shRNA
hsp60::shRNA
Hsp60
β-actin
Membrane-extract
Relative Protein level (%) (Membrane)
Control:: shRNA
hsp60:: shRNA
B
Control shRNA
hsp60::shRNA
Hsp60
β-actin
Cytoplasmic-extract
Relative Protein level (%) (Cytosol)
C
Caco-2 Whole-cell
Control
LAP
Hsp60
IKKβ
β-actin
Relative Protein level (%) (Hsp60/β-actin-Total)
ns
Relative Protein level (%) (IKK-β/β-actin- Total)
Caco-2 Membrane
Relative Protein level (%) (Hsp60/β-actin-Membrane)
Caco-2 Cytosol
Relative Protein level (%) (Hsp60/β-actin-Cytosol)
Relative Protein level (%) (IKK-β/β-actin -Cytosol)
D
Control Uninfected Mouse Ileum
Nucleus
Hsp60
F-Actin
Merged
Enlarged
E
Mouse 1
Mouse 2
Hsp60
E-cadherin
MEK-1/2
Pan-cadherin
Membrane (Mouse-IEC)
β-actin
Cytosol (Mouse-IEC)

LAP induces Junctional Protein Dysregulation for Increased Epithelial Permeability and *L.monocytogenes* Translocation

MLCK phosphorylates myosin II regulatory light chain (MLC) which regulates paracellular permeability via cytoskeleton rearrangement and modulates TJ protein expression (Hecht et al. 1996; Clayburgh et al. 2005). Moreover, pro-inflammatory cytokines can induce tight junction dysfunction via activation of MLCK (Ma et al. 2005). We observed a time-dependent increase in MLCK expression with purified LAP-treatment and MLCK and P-MLC expression during *L. monocytogenes* infection in Caco-2 cells (**Figure 2.11B**).

Next, we analyzed the time-dependent distribution of TJ (claudin-1, occludin, ZO-1) and AJ (E-cadherin and β-catenin) proteins in the detergent-insoluble and-soluble fractions from Caco-2 cells infected with WT. In the detergent-insoluble fractions, the WT strain significantly reduced the expression of occludin, claudin-1 and E-cadherin at 45 min pi than the uninfected control without significant alterations in the expression of ZO-1 and β-catenin (**Figure 2.12A**). While in the detergent-soluble fractions, a concomitant increased expression of occludin at 60 min pi and claudin-1 and E-cadherin at 45 min pi was observed (**Figure 2.12B**). The total protein levels of claudin-1, occludin, ZO-1, E-cadherin and β-catenin in WT-infected Caco-2 cells did not change, at all-time points during infection (5-120 min pi) (**Figure 2.12C**). Therefore, infection of Caco-2 cells with the WT strain caused a sub-cellular redistribution of occludin, claudin-1 and E-cadherin without affecting the total cellular junctional protein levels.

Analysis of cell junction proteins of Caco-2 cells with WT and Δ*inlA* infection at 45 min pi revealed significantly decreased expression of occludin and claudin-1 in the detergent-insoluble fractions (**Figure 2.11C**) and increased total cellular MLCK and P-MLC expression compared to the uninfected cells (**Figure 2.11D**). Notably, E-cadherin expression was also significantly reduced in WT (~88%) and Δ*inlA* (~20%) infected cells (**Figure 2.11C**). In contrast, the expression

of these proteins in the *lap*⁻-infected cells were similar to uninfected Caco-2 cells. Thus, LAP contributes to the subcellular redistribution of occludin claudin-1 and E-cadherin, and increased expression of MLCK and P-MLC in Caco-2 cells and the direct interaction between InlA and E-cadherin also contributes to E-cadherin internalization not only in Caco-2 cells (this study) but also in Jeg-3 cells (Bonazzi et al. 2008).

We next examined whether pretreatment of Caco-2 cells with the NF-κB inhibitor, BAY or the MLCK inhibitor, PIK could prevent LAP-mediated junctional protein mislocalization. Both inhibitors prevented *L. monocytogenes*-induced redistribution of occludin, claudin-1, and E-cadherin (**Figure 2.11C**) and decreased the total MLCK and P-MLC expression to baseline levels (**Figures 2.11D**). These inhibitors independently had no effect on the expression of these junctional proteins (**Figure 2.11C**) or Caco-2 TEER (**Figures 2.6O, 2.12D and 2.12E**). Additionally, consistent with our observations with the NF-κB inhibitors, (**Figures 2.5K and 2.5L**), the MLCK inhibitors, PIK or ML-9 significantly reduced the translocation competencies of WT and Δ*inlA* across the Caco-2 cell barrier (**Figures 2.11E and 2.12F**) and restored purified LAP-mediated drop in Caco-2 TEER (**Figure 2.12G**) without affecting invasion of WT in Caco-2 cells (**Figures 2.12H and 2.12I**). Additionally, knockdown of Hsp60, the receptor of LAP, also prevented *L. monocytogenes* LAP-induced redistribution of occludin, claudin-1, and E-cadherin (**Figures 2.11F and 2.12J-L)** and restored the drop in Caco-2 TEER significantly (**Figures 2.12M).**

Analysis of ileal IEC's of mice infected with WT and Δ*inlA* revealed reduced occludin, claudin-1, and E-cadherin expression in the detergent-insoluble fractions (**Figure 2.11G**) and increased total cellular MLCK and P-MLC expression (**Figure 2.11H**) but not in mice challenged with the *lap*⁻ strain. Immunostaining of the ileal tissue sections confirmed membrane

mislocalization of occludin, claudin-1, and E-cadherin and increased expression of P-MLC in IEC's of mice challenged with the WT and Δ*inlA*, but not by the *lap*$^{-}$ strain (**Figure 2.11I**). Collectively, these results indicate that LAP induces MLCK expression resulting in phosphorylation of MLC, which in turn promotes the MLCK-triggered opening of the epithelial barrier via cellular redistribution (mislocalization) of occludin, claudin-1, and E-cadherin.

Figure 2.11. LAP induces junctional protein dysregulation through MLCK activation.

(A,B) Immunoblot and densitometry plots (n=3) of MLCK (A,B), P-MLC (B) or MLC (B) in the whole-cell lysate of Caco-2 cells treated with purified LAP (1 μg/ml) (A) or WT (B).

(C,D) Immunoblot and densitometry plots (n=3) of proteins from the detergent-insoluble fraction (C) and whole cell lysate of Caco-2 cells infected with *Listeria*, or pre-treated with MLCK inhibitor, PIK (150 μM) or NF-κB inhibitor, BAY (10 μM) prior to infection with WT.

(E) Translocation (n=6) of *Listeria* through Caco-2 monolayers pretreated with MLCK inhibitor, PIK (150 μM).

(F) Immunoblots of cell junction proteins in the detergent-insoluble fraction of control or *hsp60* knockdown Caco-2 cells infected with *Listeria* or uninfected (Control).

(G,H) Immunoblot and densitometry plots of cell junction proteins in the detergent-insoluble fraction (G), and MLCK, P-MLC and MLC in whole-cell lysates (H) of purified ileal IEC from two mice (A/J) (see Fig 1) at 48 h pi.

(**I**) Images of the mouse (A/J) ileal villi sections (48 h pi) showing membrane localization of occludin, claudin-1, E-cadherin (red) and P-MLC (green). White arrows represent normal presentation while yellow arrows represent alterations or mislocalization. Nuclei (blue). Scale bar, 50 μm. LP, Lamina Propria. See also Fig 2.12.

Caco-2 cell infection (MOI 50, 45 min). All error bars represent SEM. ***, $P<0.001$; **, $P<0.01$, *, $P<0.05$; ns, no significance.

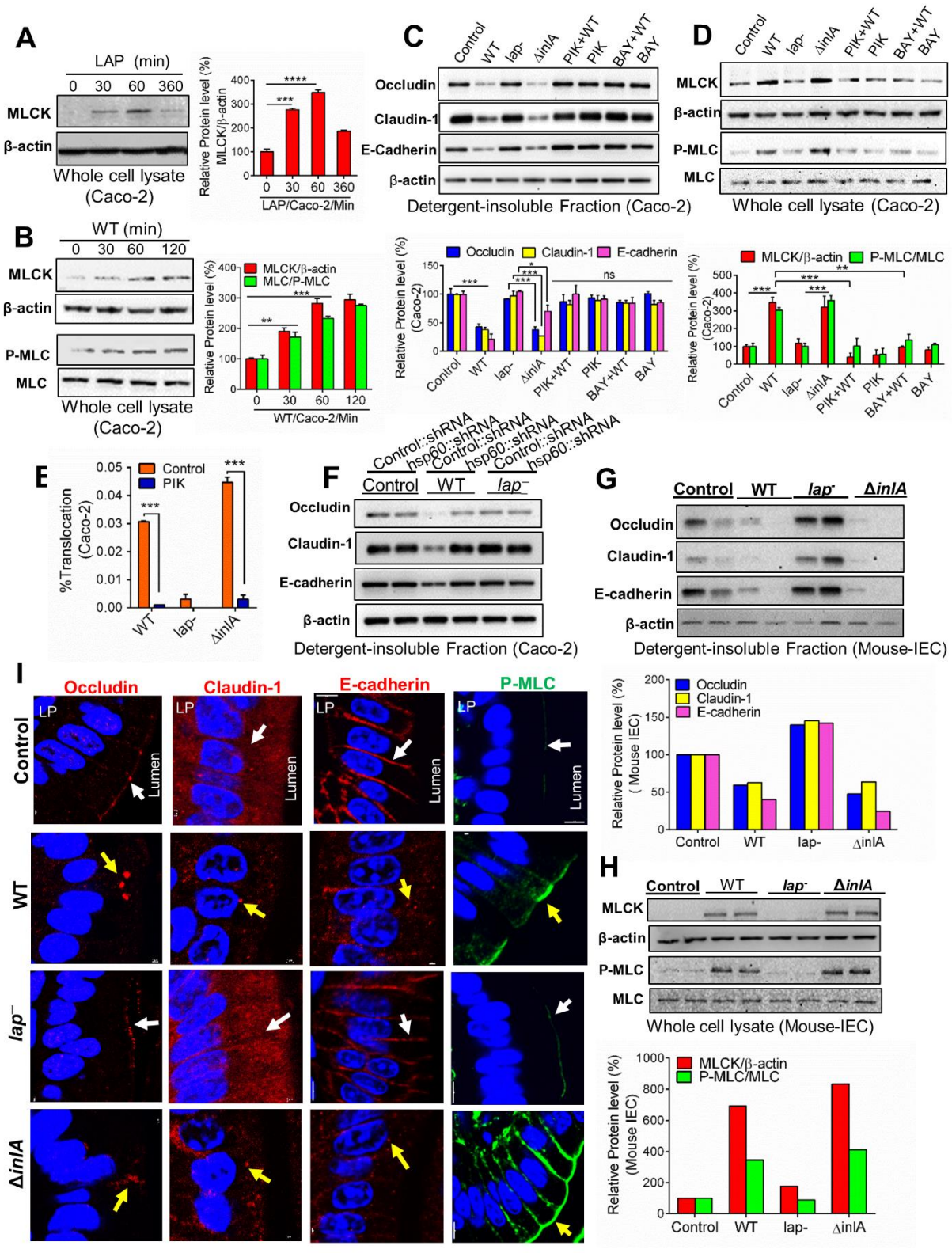
A
LAP (min)
0 30 60 360
MLCK
β-actin
Whole cell lysate (Caco-2)
Relative Protein level (%) MLCK/β-actin
LAP/Caco-2/Min
B
WT (min)
0 30 60 120
MLCK
β-actin
P-MLC
MLC
Whole cell lysate (Caco-2)
MLCK/β-actin
MLC/P-MLC
WT/Caco-2/Min
C
Control WT lap- ΔinlA PIK+WT PIK BAY+WT BAY
Occludin
Claudin-1
E-Cadherin
β-actin
Detergent-insoluble Fraction (Caco-2)
D
Control WT lap- ΔinlA PIK+WT PIK BAY+WT BAY
MLCK
β-actin
P-MLC
MLC
Whole cell lysate (Caco-2)
Occludin Claudin-1 E-cadherin
Relative Protein level (%) (Caco-2)
MLCK/β-actin P-MLC/MLC
E
Control PIK
%Translocation (Caco-2)
WT lap- ΔinlA
F
Control::shRNA hsp60::shRNA
Control WT lap⁻
Occludin
Claudin-1
E-cadherin
β-actin
Detergent-insoluble Fraction (Caco-2)
G
Control WT lap- ΔinlA
Occludin
Claudin-1
E-cadherin
β-actin
Detergent-insoluble Fraction (Mouse-IEC)
I
Occludin Claudin-1 E-cadherin P-MLC
Control
WT
lap⁻
ΔinlA
LP
Lumen
Relative Protein level (%) (Mouse IEC)
Occludin
Claudin-1
E-cadherin
Control WT lap- ΔinlA
H
Control WT lap- ΔinlA
MLCK
β-actin
P-MLC
MLC
Whole cell lysate (Mouse-IEC)
MLCK/β-actin
P-MLC/MLC
Relative Protein level (%) (Mouse IEC)
Control WT lap- ΔinlA

Figure 2.12. Analysis of transepithelial electrical resistance (TEER) and invasion of *L. monocytogenes* WT strain to Caco-2 cells pretreated with MLCK inhibitor, ML-9, and PIK.

(A,B) Immunoblot showing the time-dependent sub-cellular distribution of TJ (occludin, claudin-1, and ZO-1) and AJ (E-cadherin and β-catenin) proteins in the detergent-insoluble (membrane-rich) **(A)** and detergent-soluble **(B)** fractions from Caco-2 cells infected with the WT strain (MOI 50). Densitometry reports of junctional protein levels after normalization to β-Actin (loading control) is presented in the **right panels** of **A** and **B**, which represent mean ± SEM of three independent immunoblot experiments. Immunoblot shows significant decrease in claudin-1, occludin, and E-cadherin protein expression levels in the detergent-insoluble fractions at 45 min pi (A) and concomitant increase in the expression of claudin-1 and E-cadherin at 45 min pi, and of occludin at 60 min pi in the detergent-soluble fraction (B) relative to uninfected cells (0 min). Immunoblots are representative of three independent experiments.

(C) Immunoblot showing time-dependent analysis of TJ (occludin, claudin-1, and ZO-1) and AJ (E-cadherin and β-catenin) proteins levels in the whole-cell extracts (total protein) from Caco-2 cells infected with the WT strain (MOI 50). Densitometry reports of junctional protein levels after normalization to β-actin (loading control) is presented in the **right panel** of **C** which represent mean ± SEM of three independent immunoblot experiments. Immunoblot shows no significant changes in the levels of occludin, claudin-1 and ZO-1, E-cadherin and β-catenin proteins in the whole-cell lysates during the 120 min time, relative to uninfected cells (0 min). Immunoblots are representative of three independent experiments.

(D,E) TEER values of filter-insert grown Caco-2 cells before and after treatment with MLCK inhibitors, PIK (150 μM, 30 min pre-treatment and maintained during 2-h infection) **(D)** or ML-9 (20 μM, 30 min) **(E)**. Both MLCK inhibitors did not affect Caco-2 TEER. The data are representative of three independent experiments (n=3) and reported as mean ± SEM.

(F) Decreased translocation of the *L. monocytogenes* WT, *lap*$^{-}$ *lap*$^{+}$, Δ*inlA*, and Δ*inlA inlA*$^{+}$ strains, pretreated with MLCK inhibitor, ML-9 (20 μM, 30 min pre-treatment) through Caco-2 cell monolayers grown on Transwell filter-inserts infected at an MOI of 50. The data represent the mean ± SEM of three independent experiments (n=6).

(G) Effect of MLCK inhibitors, PIK (150 μM 30 min pretreatment and maintained during 24 h period) or ML-9 (20 μM, 30 min pre-treatment and maintained during 24 h period) on TEER of Transwell filter-insert grown Caco-2 cells treated with recombinant purified LAP (1 μg/ml). Treatment of Caco-2 cells with MLCK inhibitors, PIK or ML-9 restored LAP-mediated drop in Caco-2 TEER. The data represent the mean ± SEM of three independent experiments (n=6).

(H,I) Analysis of *L. monocytogenes* WT invasion of Caco-2 cells pretreated with MLCK inhibitors, PIK (150 μM, 30 min pre-treatment and maintained during 2-h infection) **(H)** or ML-9 (20 μM, 30 min) **(I)**. Both MLCK inhibitors did not affect intracellular invasion of *L. monocytogenes* WT. The data represent the mean ± SEM of three independent experiments (n=3).

Figure 2.12. continued

(J-L) Densitometry reports for immunoblots in Fig. 6F showing restoration of occludin **(J)**, claudin-1**(K)** and E-cadherin **(L)** protein levels, in the detergent-insoluble fraction of Caco-2 cells with *hsp60* knocked-down (*hsp60*$^{-}$) infected with *L. monocytogenes* WT or *lap*$^{-}$ strain (MOI 50, 30 min), relative to *L. monocytogenes* WT infected vector control shRNA (control) cells. Densitometry reports represent mean ± SEM of three independent immunoblot experiments.

(M) Analysis of epithelial permeability by measuring the TEER across filter-insert grown vector control Caco-2 cells (Vector Control::shRNA) or with *hsp60* knocked-down (hsp60::shRNA) infected apically with *L. monocytogenes* WT and *lap*$^{-}$ (MOI 50, 2 h). The data were normalized to uninfected controls and expressed as the mean % change ± SEM from three independent experiments, n=6. ***, $P<0.001$; **, $P<0.01$, ns, no significance.

Statistical significance for plots A-C was determined by using the two-way ANOVA test followed by a Dunnett's post hoc test, for plots D,E,H and I by Student *t* test, for plots F,G,J,K,L and M, a two-way ANOVA test followed by a Tukey's multiple comparisons. ****, $P<0.0001$; ***, $P<0.001$; **, $P<0.01$.

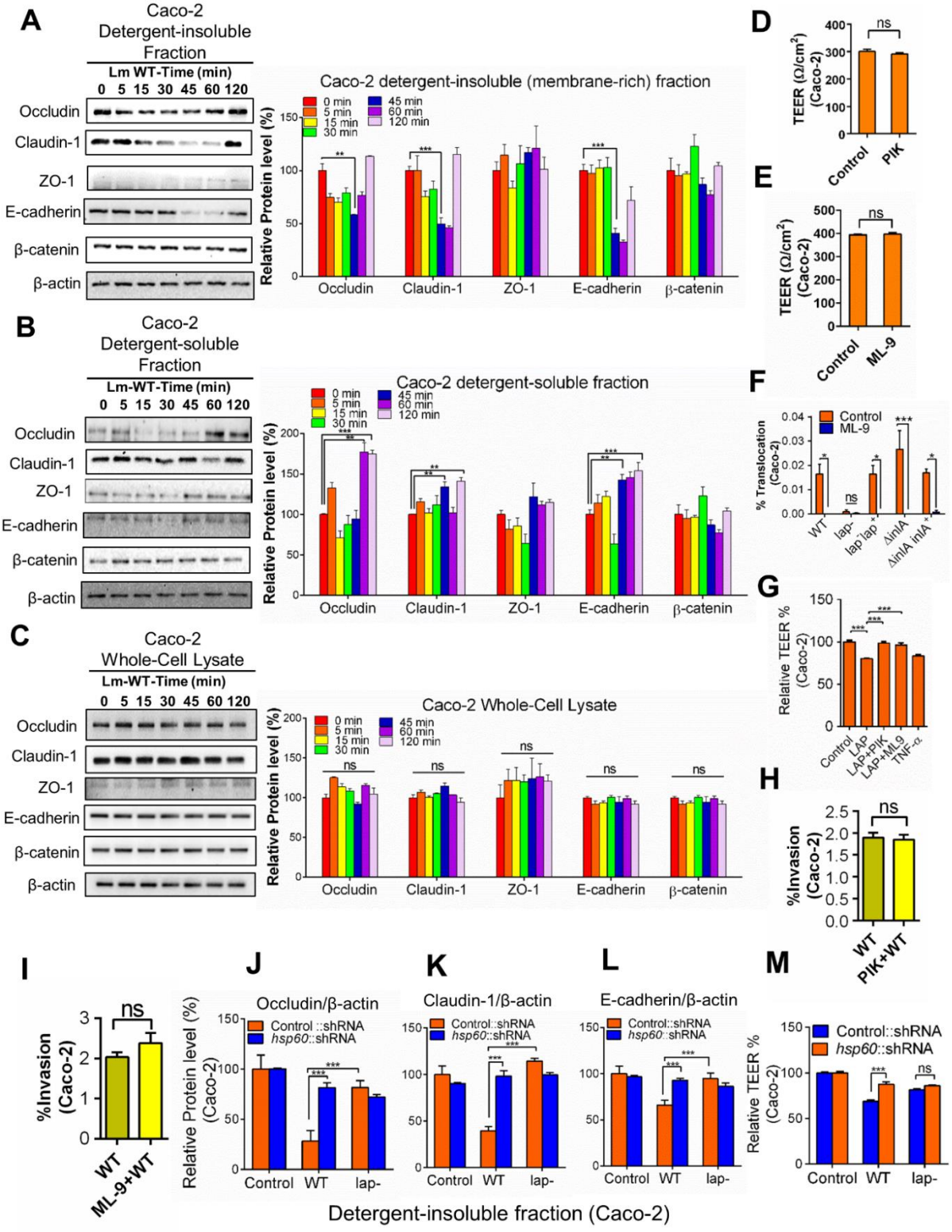
A
Caco-2
Detergent-insoluble
Fraction
Lm WT-Time (min)
0 5 15 30 45 60 120
Occludin
Claudin-1
ZO-1
E-cadherin
β-catenin
β-actin
Caco-2 detergent-insoluble (membrane-rich) fraction
0 min
5 min
15 min
30 min
45 min
60 min
120 min
Relative Protein level (%)
Occludin
Claudin-1
ZO-1
E-cadherin
β-catenin
B
Caco-2
Detergent-soluble
Fraction
Lm-WT-Time (min)
0 5 15 30 45 60 120
Caco-2 detergent-soluble fraction
C
Caco-2
Whole-Cell Lysate
Caco-2 Whole-Cell Lysate
D
TEER (Ω/cm²)
(Caco-2)
ns
Control
PIK
E
Control
ML-9
F
% Translocation
(Caco-2)
Control
ML-9
WT
lap-
lap lap+
ΔinlA
ΔinlA inlA+
G
Relative TEER %
(Caco-2)
Control
LAP
LAP+PIK
LAP+ML9
TNF-α
H
%Invasion
(Caco-2)
WT
PIK+WT
I
%Invasion
(Caco-2)
WT
ML-9+WT
J
Occludin/β-actin
Control ::shRNA
hsp60::shRNA
Relative Protein level (%)
(Caco-2)
Control
WT
lap-
K
Claudin-1/β-actin
L
E-cadherin/β-actin
M
Relative TEER %
(Caco-2)
Detergent-insoluble fraction (Caco-2)

L. monocytogenes Translocation and Epithelial Permeability did not Increase in MLCK Knockout Mice

We orally challenged MLCK knockout mice lacking the 210-kDa long chain ($MLCK^{-/-}$) and its parental strain (C57BL/6 mice, $MLCK^{+/+}$) with WT, *lap*⁻ or Δ*inlA* and enumerated bacterial burdens in the intestinal and extra-intestinal tissues at 48 h pi. The bacterial burden in the liver, spleen and the MLN of the $MLCK^{+/+}$ mice challenged with the *lap*⁻ or the $MLCK^{-/-}$ mice challenged with either the WT or the *lap*⁻ were significantly reduced than those in the same tissues of the $MLCK^{+/+}$ mice that were challenged with WT or Δ*inlA* (**Figures 2.13A-2.13C**). In the mucus, WT, *lap*⁻ or Δ*inlA* counts were similar for both $MLCK^{+/+}$ and $MLCK^{-/-}$ mice **(Figure 2.13D)**. In the epithelial cell of both the $MLCK^{+/+}$ and $MLCK^{-/-}$ mice, WT counts were similar, but the *lap*⁻ count was significantly reduced (**Figures 2.13E and 2.13F)** suggesting that the epithelial intracellular invasion of *L. monocytogenes* was not affected in $MLCK^{-/-}$ mice. As expected, the *lap*⁻ counts in lamina propria were significantly lower than the WT or Δ*inlA* in $MLCK^{+/+}$ mice; however, both *lap*⁻ and WT strain showed similar but significantly reduced translocation to the lamina propria in $MLCK^{-/-}$ mice relative to $MLCK^{+/+}$ mice (**Figure 2.13G**). Thus, *L. monocytogenes* in the $MLCK^{-/-}$ mice exhibits a defect in translocating from the ileal mucosa to the underlying lamina propria and systemic dissemination possibly due to decreased translocation in this mouse strain.

We measured FD4 permeability, to assess whether decreased bacterial translocation correlates with decreased epithelial permeability in $MLCK^{-/-}$ mice. *Listeria*-infected $MLCK^{+/+}$ mice that received FD4 orally 4-5 h before sacrifice displayed significantly increased FD4 in the sera and the urine in WT and Δ*inlA*-infected mice compared to the *lap*⁻ -infected or uninfected mice (**Figures 2.13H and 2.13I**). In the $MLCK^{-/-}$ mice, there were no significant differences in

the FD4 levels in the sera and urine of mice challenged with the WT or the *lap*⁻ strain or in the uninfected controls.

Immunostaining of ileal tissues confirmed membrane mislocalization of occludin, claudin-1 and E-cadherin, and increased expression of P-MLC in $MLCK^{+/+}$ in IECs of mice challenged with WT and Δ*inlA*, but not with the *lap*⁻ strain or the $MLCK^{-/-}$ mice challenged with either the WT or *lap*⁻ (**Figure 2.13J**). Therefore, the translocation defect of the *lap*⁻ strain to the lamina propria is also observed in the C57BL/6 mouse strain (besides A/J strain) and MLCK contributes to LAP-induced junctional protein dysregulation, epithelial barrier dysfunction and *L. monocytogenes* translocation.

Figure 2.13. *L. monocytogenes* translocation and epithelial permeability did not increase in MLCK knockout mice.

(A-G) *Listeria* counts (Total CFU) in liver (A), spleen (B), MLN (C), and ileal mucus (D), epithelial cell intracellular (E), epithelial cell-extracellular (F) and lamina propria (G) of wild-type C57BL/6 ($MLCK^{+/+}$) or MLCK knock-out ($MLCK^{-/-}$) mice (*n*=4-7 male and female) at 48 h pi. Dashed lines indicate the limit of detection.

(H,I) Analysis of FD4 permeability through the intestinal epithelium of uninfected (Cont) and WT, *lap*$^{-}$ and Δ*inlA*–infected $MLCK^{+/+}$ or the $MLCK^{-/-}$ mice (n= 5-7) in serum (A) and urine (B) at 48 h pi.

(J) Images of the mouse (C57BL/6, $MLCK^{+/+}$ and $MLCK^{-/-}$) ileal villi sections (48 h pi) showing membrane localization of occludin, claudin-1, E-cadherin (red) and P-MLC (green). White arrows represent normal presentation while yellow arrows represent alterations or mislocalization. Nuclei (blue). Scale bar, 50 μm. LP, Lamina Propria.

All error bars represent SEM. ***, $P<0.001$; **, $P<0.01$; *, $P<0.05$; ns, no significance.

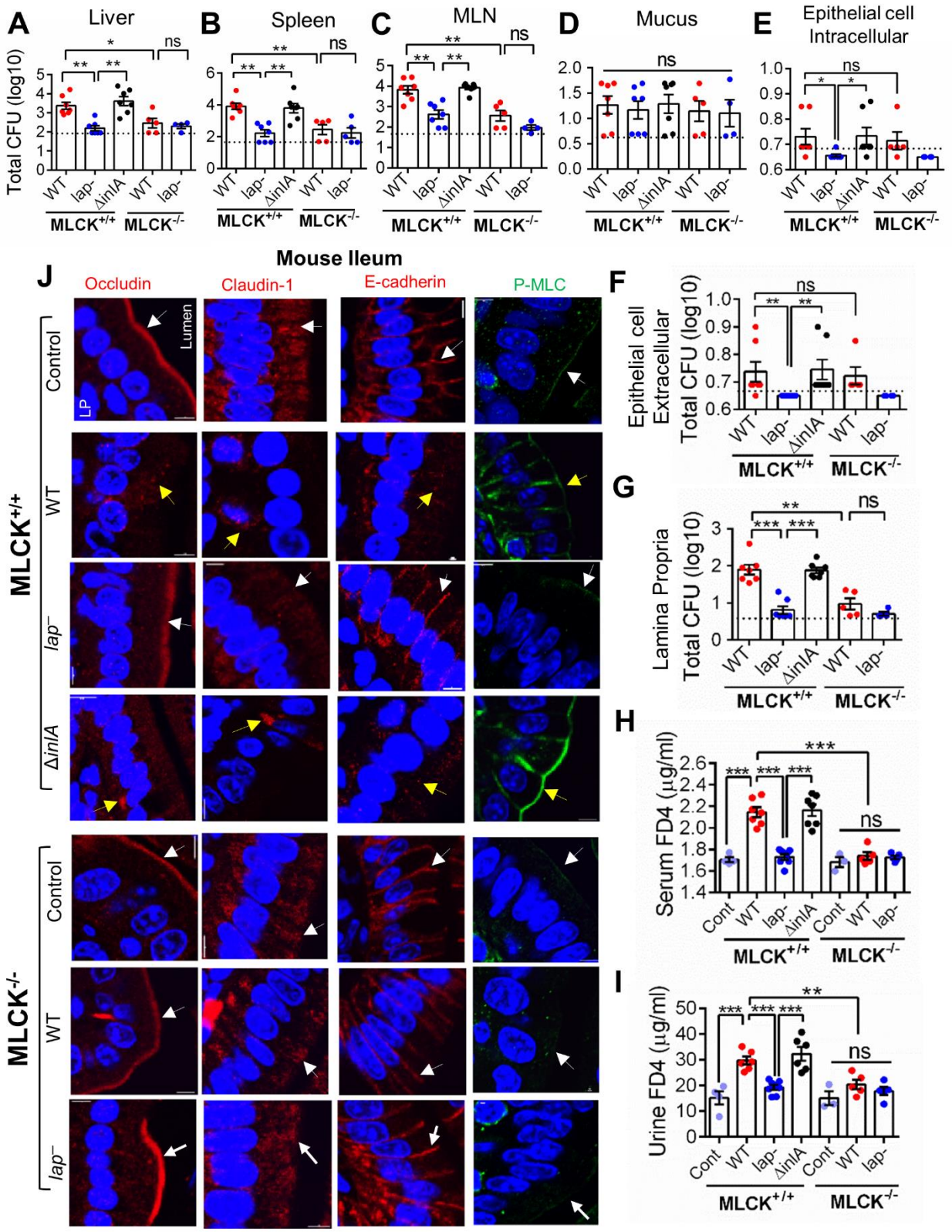
A
Liver
B
Spleen
C
MLN
D
Mucus
E
Epithelial cell
Intracellular
Total CFU (log10)
WT
lap-
ΔinlA
MLCK+/+
MLCK-/-
ns
J
Mouse Ileum
Occludin
Claudin-1
E-cadherin
P-MLC
Lumen
LP
Control
WT
lap−
ΔinlA
MLCK+/+
MLCK-/-
F
Epithelial cell
Extracellular
Total CFU (log10)
G
Lamina Propria
Total CFU (log10)
H
Serum FD4 (μg/ml)
Cont
I
Urine FD4 (μg/ml)

Discussion

The precise mechanism by which *L. monocytogenes* crosses the epithelial barrier during the gastrointestinal phase of infection is not fully understood. Previous work demonstrated that *L. monocytogenes* used two pathways: InlA-mediated uptake and the M cell transcytosis (Pron et al. 1998; Corr et al. 2006). However, recent studies have demonstrated that *L. monocytogenes* expressing non-functional InlA (encoding a premature stop codon) infected fetuses of pregnant guinea pigs and mice after oral administration (Holch et al. 2013) and human newborns with neonatal listeriosis (Gelbicova et al. 2015). Additionally, in a PP-null mouse, *L. monocytogenes* colonized the ileum and disseminated to the MLN, liver and spleen in a ligated loop assay (Chiba et al. 2011). These findings provide a strong evidence that *L. monocytogenes* also uses alternate routes to translocate across the gut barrier.

Here, we used a mouse model in combination with the human Caco-2 cell model. We established that LAP contributes to translocation of *L. monocytogenes* from the intestinal lumen, across the gut epithelium into the underlying LAP and subsequent systemic dissemination in a mouse model. By using both model systems, we show that LAP binding to Hsp60 activates canonical NF-κB signaling, which facilitates MLCK-mediated opening of the intestinal epithelial barrier via the cellular redistribution of the major TJ proteins (claudin-1 and occludin) and AJ protein (E-cadherin) and increases intestinal permeability. Furthermore, LAP-mediated epithelial cytokine production (TNF-α, IL-6) in the early phase (24-48 h) of infection promotes epithelial barrier dysfunction to facilitate *L. monocytogenes* translocation and to avoid the innate immune defenses without showing an overt inflammatory response.

We were intrigued that the LAP-Hsp60 interaction contributed to NF-κB activation despite the primary role of mitochondrial Hsp60 to act as a molecular chaperone and assist in the folding of imported proteins to their native conformation. Increasing evidence also supports a role for

eukaryotic Hsp60 in "moonlighting," which is the property of proteins possessing two or more distinct biological activities. Extracellular eukaryotic Hsp60 is recognized by TLR2 and TLR4 (Vabulas et al. 2001), which leads to NF-κB activation, and plays a role in innate immunity. We and others have demonstrated that Hsp60 acts as a cell surface receptor for *Staphylococcus aureus* (Dziewanowska et al. 2000), HIV (Speth et al. 1999), and *L. monocytogenes* (Wampler et al. 2004). Cytosolic Hsp60 also regulates apoptosis activity in cancer cells (Xanthoudakis et al. 1999) and cell survival functions by interacting with IKK in the cytoplasm and activating NF-κB (Chun et al. 2010). Our results suggest that membrane or surface-expressed Hsp60 at the intestinal interface exhibits an immune sensor function that leads to NF-κB activation. Intestinal epithelial TLR2 and TLR10 (Regan et al. 2013) and NOD2 (Kobayashi et al. 2005) also activate NF-κB at the intestinal interface following *L. monocytogenes* infection. Therefore, one question remains: why must a LAP-Hsp60 interaction that activates NF-κB happen to increase epithelial permeability with all of these redundant pathways? One possible explanation is that the relative distribution of these receptors in the intestine contributes to the differences in the levels of NF-κB activation according to their respective ligands. Notably, we observed earlier a dramatic increase in apical Hsp60 expression following *L. monocytogenes* infection in Caco-2 cell plasma membranes (Burkholder and Bhunia 2010). In this study, we observed high Hsp60 expression in the membrane of mouse IEC's. NOD2 is not expressed in Caco-2 cells (Hisamatsu et al. 2003), and Caco-2 cells are not responsive to TLR2 or TLR4 agonists because of the low expression of TLR2, the absence of TLR4, and the high expression of the Toll inhibitory protein, Tollip (Abreu et al. 2003). An alternate explanation is that the interaction of LAP with Hsp60, in addition to NF-κB activation, may also elicit other signal transduction pathways that contribute to increased paracellular

permeability. The present study reveals a moonlighting function of LAP-Hsp60 interaction and links to a wider phenomenon of bacterial recognition during innate immunity.

Our data suggest that in the intestinal phase of infection, the *L. monocytogenes* LAP activates NF-κB and exploits the epithelial innate defenses to cross the intestinal epithelial barrier. Strikingly, *L. monocytogenes* has also evolved mechanisms to counter innate response to overcome host defense. The InlC interferes with innate immune responses in murine macrophages *in vivo* (Gouin et al. 2010), thus after translocation to lamina propria , *L. monocytogenes* may use InlC to dampen immune responses for the systemic spread. This well-orchestrated regulation of NF-κB-mediated response at different stages of infection may allow an efficient spread of *L. monocytogenes* to peripheral tissues.

Here, we demonstrate that during *L. monocytogenes* infection, LAP activates MLCK to redistribute junctional proteins, claudin-1, occludin, E-cadherin to facilitate *L. monocytogenes* translocation across the gut epithelium in the early stage of infection (24-48 h). InlA uses E-cadherin as the receptor, but it is intriguing to learn that *L. monocytogenes* infection redistributes E-cadherin to facilitate bacterial translocation. In the absence of InlA– E-cadherin -mediated uptake (in a mouse model); the bacterium can use LAP-Hsp60-mediated translocation pathway to gain access for successful infection (**Figure 2.14**). This flexibility may make the bacterium far less susceptible to clearance by the innate immune defense by providing easier access to the lamina propria. Our results from Caco-2 cells (functional InlA- E-cadherin) further suggest that LAP-Hsp60-mediated translocation may be an important precursor event for InlA-dependent epithelial translocation that provides access to E-cadherin in the AJ of the permissive model (**Figure 2.14**). Alternatively, LAP-Hsp60-mediated translocation may serve as an active mechanism for InlA-independent translocation in InlA-permissive hosts such as humans, rabbits, guinea pigs and

gerbils in addition to epithelial invasion via “villous cell extrusion” (Pentecost et al. 2006) and at the empty goblet cell junction (Nikitas et al. 2011).

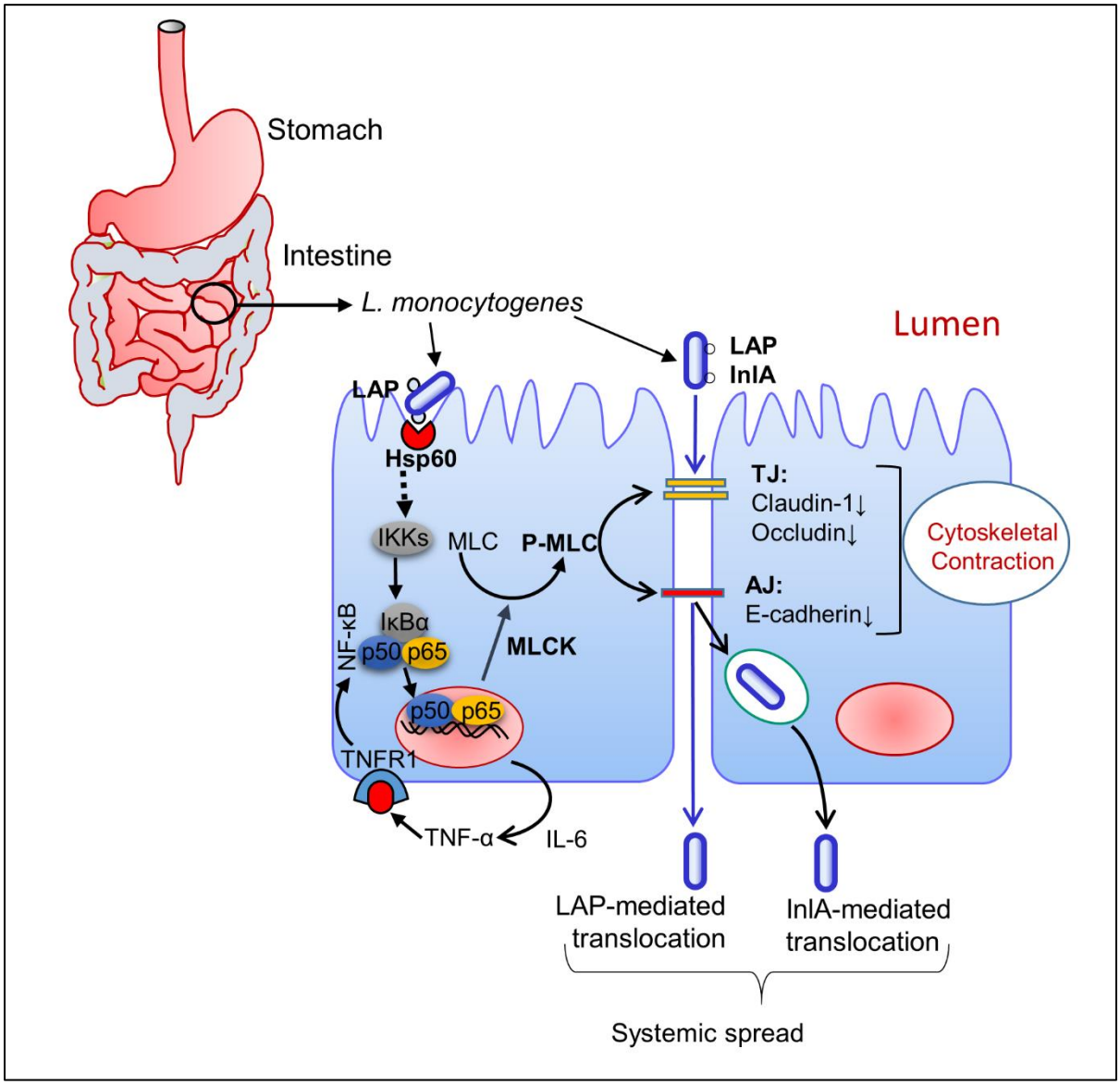

Figure 2.14. Proposed model of the LAP-mediated translocation of *L. monocytogenes* through the intestinal epithelial barrier.

L. monocytogenes uses LAP to induce the epithelial barrier dysfunction through activation of NF-κB and MLCK and promotes its translocation across the intestinal epithelium. At the same time, it may facilitate an interaction between InlA and E-cadherin at the adherens junction (AJ) for intracellular translocation in permissive hosts, such as humans and guinea pigs.

Author Contributions

Rishi Drolia and Dr. Arun K. Bhunia designed the experiments, performed the experiments, interpreted the data and wrote the manuscript. Shivendra Tenguria performed the experiment, Dr. Jerrold R. Turner supplied MLCK$^{-/-}$ mice, reagents, and assisted with the study, and Dr. Abigail C. Durkes assisted with histopathology. All authors reviewed the published manuscript.

Declaration of Interest

A utility patent has been filed on Oct 4, 2018. Drolia, R., Samaddar, M., Bhunia, A. K. Enhanced Drug Delivery across Epithelial Barrier.

Experimental Model and Subject Details

Mice. A/J mice (female, 8-10 week-old; Jackson Laboratory) that are highly sensitive to oral *L. monocytogenes* challenge (Czuprynski et al. 2003; Burkholder et al. 2009) were used. The use of A/J mice allowed us to use a 10^8 CFU (10-fold lesser inoculum) to cause a systemic infection. For experiments with C57BL/6 mice, 6-8 week-old, male or female, wild-type C57BL/6 (MLCK$^{+/+}$), or the 210-kDa MLCK$^{-/-}$ mice (Clayburgh et al. 2005), bred in our facility were used. Mice were housed in individual cages, provided *ad libitum* feed and water, and acclimatized for 5 days (A/J) before the experiments. On the day of the challenge, food and water were removed from the cages 5 h prior to oral gavage to prevent mechanical blockage of the *Listeria* inoculum by food in the stomach, which may cause the inoculum to aspirate into the lungs. The 6-h grown *L. monocytogenes* WT, *lap*$^{-}$, and *ΔinlA* strains, each resuspended in 200 µl of phosphate-buffered saline (PBS, pH 7.4) containing approximately 1×10^8 CFU for A/J mice and 1×10^9 CFU for C57BL/6 MLCK$^{+/+}$or the MLCK$^{-/-}$ mice were administered orally to randomly selected mice using a stainless steel ball-end feeding needle (Popper). The control mice received only PBS. The food

was returned 1 h pi, and the mice were sacrificed 24 h and 48 h pi using CO_2 asphyxiation. All animal procedure (IACUC Protocol no. 1201000595) was approved by the Purdue University Animal Care and Use Committee, who adheres to the recommendations of the Guide for the Care and Use of Laboratory Animals published by the National Institutes of Health.

Bacterial strains and growth conditions. The bacterial strains are listed in the **Table 2.1**. *L. monocytogenes* F4244 (WT) serovar 4b, the isogenic *lap*-deficient insertion mutant KB208 (*lap*$^{-}$), the *lap*-complemented CKB208 (*lap*$^{-}$ *lap*$^{+}$)(Jagadeesan et al. 2010), the Δ*inlA* in-frame deletion mutant (AKB301) and its complement (Δ*inlA inlA*$^{+}$; AKB302) (Burkholder and Bhunia 2010), the 10403s WT strain serovar 1/2a, and the in-frame deletion mutant strains, Δ*hly* (DP-L2161) and the Δ*inlB* (DP-L4406) were used. The 10403s and its derivative strains were kindly provided by Dr. Portnoy at UC-Berkeley. All of the *L. monocytogenes* strains were grown in Tryptic soy broth containing 0.6% yeast extract (TSBYE; BD Bioscience) at 37°C with shaking for 12-16 h unless otherwise indicated. The *lap*$^{-}$ strain was grown in TSBYE containing erythromycin (Em; 5 µg/ml) at 42°C, the *lap*$^{-}$*lap*$^{+}$ strain in TSBYE containing Em (5 µg/ml) and chloramphenicol (Cm; 5 µg/ml) at 37°C, and the Δ*inlA inlA*$^{+}$ strain in TSBYE containing Cm (5 µg/ml) at 37°C. *L. innocua* F4248 was grown in TSBYE at 37°C for 12-16 h.

Cell lines. The human colon carcinoma Caco-2 cell line (ATTC # HTB37) from 25-35 passages were cultured in Dulbecco's Modified Eagle's medium (DMEM) (Thermo Fisher Scientific) supplemented with 4 mM L-glutamine, 1 mM sodium pyruvate and 10% fetal bovine serum (FBS; Atlanta Biologicals). Caco-2 cells presenting stable suppression of *hsp60* mRNA and Caco-2 presenting a non-targeting control shRNA vector were previously developed using shRNA (Burkholder and Bhunia 2010) and cultured in DMEM supplemented with 4 mM L-glutamine, 1 mM sodium pyruvate, 10% FBS and 800 µg/ml Geneticin; G418. The NF-κB luciferase reporter

cell line (Novus Biologicals) was cultured in DMEM supplemented with 4 mM L-glutamine, 1 mM sodium pyruvate, 10% FBS, 100 U/ml penicillin, 100 µg/ml streptomycin and 3 µg/ml puromycin. All cell lines were maintained at 37°C with 5% CO_2.

Method Details

Enumeration of *L. monocytogenes* in mouse organs

The organs were harvested aseptically and homogenized using a tissue homogenizer in 4.5 ml (spleen, MLN, kidney) or 9 ml (liver) of buffered- *Listeria* enrichment broth (BLEB) containing 0.1% Tween 20 and selective antimicrobial agents (Neogen). To enumerate *Listeria*, the samples were serially diluted in PBS and plated onto modified Oxford (MOX; Neogen) agar plates. In specific experiments, small sections of liver, spleen and ileal tissue samples (1 cm) were cut into two parts, with one part fixed overnight in 10% formalin for histopathology or immunostaining and the other stored in RNAlater (Thermo Fisher Scientific) for gene expression analysis. Urine excreted voluntarily during CO_2 asphyxiation was collected in a plastic bag. Blood was collected using a 1 ml syringe with a 21G needle by cardiac puncture. To enumerate the *Listeria* in the blood, 50 µl of blood was diluted with 450 µl of BLEB immediately following collection and samples were serially diluted and plated as above.

To enumerate bacteria in the mucus, epithelial cell and the lamina propria fractions from the ileal tissue, a previously described protocol (Bou Ghanem et al. 2012) with minor modifications was used. Briefly, for separation of the mucus fraction, the ileum section (10 cm) was first flushed with sterile PBS, visible Peyer's patches were removed and cut longitudinally. The tissue sections were then washed three times by incubating for 2 min in a tube containing 3 ml of 6 mM N-acetylcysteine (Sigma-Aldrich) and then shaken vigorously before transferring to a fresh tube. The washes (9 ml) were pooled and centrifuged for 20 min at 12,000 xg. The pellets

were resuspended in 0.5 ml of PBS, vortexed and serial dilutions were plated on MOX agar plates. To enumerate bacteria in the epithelial fraction, the ileal tissue from above were cut into small pieces (1 cm each) with a scalpel and incubated at 37°C with shaking in a tube containing 5 ml of RPMI (Invitrogen) supplemented with 5 mM EDTA, and 1 mM DTT for a total of 3 times. Each time, the tissues were transferred to fresh tubes containing 5 ml of RPMI supplemented with 5 mM EDTA, and 1 mM DTT. The combined three washes (15 ml) was centrifuged at low speed (1,200x g) to pellet the cells. The cell pellets and the supernatant fluids were processed separately to enumerate the intracellular and extracellular bacteria in the epithelial fraction. To enumerate intracellular bacteria, the pellet from either the epithelial fraction or the lamina propria fraction (extraction protocol mentioned below) was suspended in 5 ml of RPMI-5 containing 25 μg/ml gentamicin and the single cell suspension was incubated at 37°C with 5% CO_2 for 30 min to kill any extracellular *L. monocytogenes.* The single cell suspension was then centrifuged at low speed (1,200x g) to pellet the cells and the pellets were washed twice in PBS. The pellets were then suspended in 0.5 ml PBS, vortexed to lyse the cells, serially diluted and plated on MOX agar plates. To quantify extracellular bacteria the supernatant from the washes of the epithelial cell fraction or the lamina propria fraction (extraction protocol mentioned below) was pooled and centrifuged at 12,000 x g for 20 min. The pellets were then resuspended in 0.5 ml PBS, vortexed and plated on MOX agar plates. To enumerate bacteria in the lamina propria fraction, the DTT and EDTA from the intestinal pieces were removed by two successive washes in 25 ml sterile PBS. The tissue pieces were then incubated in a sterile tube of digestion solution containing 4 ml of RPMI supplemented with 5% FBS and 1 mg/ml type IV collagenase and 40 μg/ml DNAse I (both from Worthington) at 37°C for 40 min with shaking. This step was repeated in a fresh tube containing the digestion solution until the tissue pieces were completely dissolved. The combined digestion

solution was centrifuged at low speed (1,200x g) to pellet the cells. The pellet and the supernatant were processed as described above to enumerate the intracellular and extracellular bacteria in the lamina propria fraction.

Immunofluorescence staining and confocal microscopy

The mouse ileal-tissue sections were fixed with 10% formalin and embedded in paraffin. The tissues were sectioned (5 µm- thick), deparaffinized, and rehydrated for antigen retrieval by immersing the slides in boiling sodium citrate buffer (10 mM, pH 6.0) for 10 min. The tissue sections were permeabilized and blocked with PBS containing 0.3% Triton X-100 (Sigma-Aldrich) and 3% normal goat serum (Cell signaling) and immunostained with specific antibodies (**Table 2.1**) by incubating overnight at 4°C. Following antibody incubation, slides were rinsed with PBS (3 cycles, 5 min), and were incubated with FITC or Alexa Fluor 555-conjugated secondary antibody for 2 h at room temperature followed by washing three times with PBS (3 cycles, 5 min). The nuclei were stained with DAPI (500 ng/ml; Cell signaling) and slides were mounted in ProLong antifade reagent (Cell Signaling). The p65 and P-p65 nuclear positive cells were counted and expressed as average nuclear positive cells per villus. Images are representative of five different fields from 2-3 mice per treatment.

For antibody labeling in cells, Caco-2 cells were grown to 40-50% confluence in four-chambered slides (Millipore). At the end of the treatment, the cells were fixed with 3.7% formaldehyde in PBS for 20 min and permeabilized and blocked with PBS containing 0.3% Triton X-100 and 3% BSA (Sigma-Aldrich) for 1 h at room temperature and then incubated with respective antibodies (**Table 2.1**) overnight at 4°C. Following antibody incubation, the cells were washed with PBS (3 cycles, 5 min) and incubated with FITC or Alexa Fluor 555-conjugated

secondary antibody for 2 h at room temperature. The nuclei were stained with DAPI (500 ng/ml; Cell signaling) and slides were mounted in ProLong antifade reagent (Cell Signaling).

All images were acquired using a Nikon A1R confocal microscope (equipped with 405nm/Argon/561nm lasers) using a Plan APO VC 60X/1.40 NA oil immersion objective with the Nikon Elements software (Nikon Instruments Inc.) at the Purdue Bindley Bioscience Imaging Facility. The X-Z and Y-Z cross-sections were produced by orthogonal reconstructions from z-stack scanning at 0.15µm intervals taken with 60X objective in 5 µm thick paraffin embedded tissue section. Three-dimensional reconstructions were performed using Nikon elements software (Nikon Instruments Inc.).

Analysis of *in vivo* intestinal permeability

The mice were orally gavaged with non-metabolizable 4 kDa FITC-labeled dextran (FD4; 15 mg/100 µl, Sigma-Aldrich) 4-5 h prior to sacrifice. Serum and urine (50 µl each), collected above, were mixed with an equal volume of PBS, and fluorescence was measured (Em: 485 nm; Ex: 520 nm; Spectramax, Molecular Devices) and the FD4 concentration was calculated using a standard curve generated by serially diluting FD4 in PBS. The serum and urine from the mice that were uninfected and not administered FD4 were used to determine the background levels.

Epithelial permeability, bacterial translocation, invasion and pharmacological inhibitors

Caco-2 cells were grown as monolayers on Transwell inserts with 3.0 µm pores (Corning-Costar) for up to 14-21 days. TEER was measured to monitor the monolayer integrity (Millicells Voltmeter, Millipore). A TEER value of at least 200 Ω/cm^2 (±10) was used as the basal value to monitor the monolayer integrity (Burkholder and Bhunia 2010). Bacterial cells were washed three times in PBS and resuspended in DMEM-FBS (10%) at an MOI of ~50 and were added to the apical side of the Transwell system, and after 2 h incubation period at 37°C in 5% CO_2, the liquid

was collected from the basal well, and then translocated bacteria were enumerated by plating (Burkholder and Bhunia 2010). For analysis of FD4 flux, non-metabolizable 4 kDa FITC-labeled dextran (FD4; 5 mg/ml, Sigma-Aldrich) was added with bacteria (MOI, ~50) resuspended in DMEM-FBS (10%) and added to the apical side. After 2 h incubation at 37°C in 5% CO_2, the liquid was collected from the basal well and fluorescence was measured (Em: 485 nm; Ex: 520 nm; Spectramax, Molecular Devices). For pharmacological inhibition of NF-κB, Caco-2 cells were pretreated with inhibitors (PDTC, 100 μM, R&D Systems; BAY-11-7085,10 μM, Sigma) for 30 min. For inhibition of MLCK, Caco-2 cells were pretreated with inhibitors (ML-9, 20 μM, Sigma; Dreverse PIK (Owens et al. 2005),150 μM) for 30 min. In specified experiments, ML-9 and Dreverse PIK (permeant peptide inhibitor of kinase) were maintained for the duration of the experiment. For inhibition of actin polymerization, Caco-2 cells were pretreated with Cytochalasin D (1 μg/ml; Sigma-Aldrich) for 1 h. For neutralization of cytokines (TNF-α and IL-6), Caco-2 cells were incubated with anti-TNF-α (Cell signaling), anti-IL-6 (Thermo-Fisher) antibodies (1 μg/ml each) or together for 24 h.

For re-association of externally added LAP to the *lap*⁻ mutant, bacteria were harvested from 1 ml of overnight grown culture, and the pellet was washed three times in PBS before the addition of 1 or 2 μg/ml of purified LAP. The mixture was incubated for 30 min at 30°C with continuous shaking and then pelleted, washed five times in the PBS, resuspended in DMEM, and used in the aforementioned translocation assay.

To determine the effect of LAP on Caco-2 permeability at specified time points (0, 24, 48 and 72 h) following incubation with recombinant purified LAP, 500 μl of FD4 (1 mg/ml in DMEM) was added to the apical side and the fluorescence readings (Em: 485 nm; Ex: 520 nm; Spectramax,

Molecular Devices) for the basal medium (100 µl) were measured. Human TNF-α (10 ng/ml, R&D Systems) was added to both apical and basal sides and used as a positive control.

For bacterial invasion analysis, monolayers were washed with PBS after 1 h of infection (MOI, ~50) and incubated with DMEM-FBS (10%) containing gentamicin (50 µg/ml) for 1 h. Caco-2 cells were lysed with 0.1% Triton X, and the internalized bacteria were enumerated by plating.

Caco-2 cell viability assay

To determine Caco-2 viability, cell culture supernatants from Caco-2 cells infected with WT, *lap*$^{-}$, *lap*$^{-}$*lap*$^{+}$, Δ*inlA* and Δ*inlA inlA*$^{+}$ strains (MOI ~50, 2h) grown on Transwell inserts or treated with the purified recombinant LAP for 24 or 48 h were assayed for lactate dehydrogenase release (Thermo Fisher Scientific). Two controls were included for calculation of percent cytotoxicity (LDH release). The low control consisted of supernatant from untreated Caco-2 cells with no exposure to bacteria. High control was from cells treated with 0.1% Triton X-100 for one minute.

Recombinant protein purification

Recombinant proteins (LAP and InlB) containing endogenous His, S and Trx tags derived from the pET-32a/pET28 cloning vector (Novagen) from *E. coli* BL21 or ClearColi (Lucigen) were purified using a Ni-affinity column. In ClearColi, LPS lacks secondary acyl chain thus eliminating endotoxicity. Briefly, for LAP purification, *E. coli* BL21 or ClearColi were each grown in 1 L LB broth (BD) with ampicillin (50 µg/ml) for 3 h at 37°C. For InlB purification, *E. coli* pET28b-1 was grown in 1 L LB containing 30 µg/ml of kanamycin at 37°C for 3 h, and IPTG (1 mM) induced at 20°C for 12 h. After sonication (total 7 min, with cycles of 30 sec sonication and 15 sec pulse; Branson Sonifier), the supernatants were purified by Ni- column. The Toxin-Eraser Endotoxin Removal Kit (Genscript) was used to remove LPS and the Toxin-Sensor Chromogenic

LAL Endotoxin Assay Kit (Genscript) was used to detect any residual LPS in the samples. Protein concentrations were measured by Bradford assay, and the purity was monitored by SDS-PAGE (12.5%-acrylamide). Purified recombinant InlA was provided by Marcelo Mendonça (University of Pelotas, Brazil).

Cytokine array and ELISA

A semi-quantitative membrane-based RayBio Human Inflammation Antibody Array kit (Ray Biotech) was used to analyze a panel of 40 inflammatory mediators in Caco-2 cell supernatant infected either with the WT or *lap*$^{-}$ strain (MOI, ~50) at 37°C for 1 h. After killing the extracellular bacteria by gentamicin (50 μg/ml), the Caco-2 cells were incubated for an additional 7 h at 37°C (Jung et al. 1995). Recombinant LAP (1 μg/ml) from ClearColi was incubated for 8 h with Caco-2 cells. After immunoblotting, the reaction intensity was quantified using NIH ImageJ software. The data were normalized and expressed as the mean fold changes as a ratio of *lap*$^{-}$/WT ± SEM. For the ELISA, Caco-2 cell supernatants were centrifuged (2,000 rpm at 4°C for 10 min) following treatment as above, and the quantification of TNF-α and IL-6 in was performed using human TNF-α and IL-6 ELISA kits (Ray Biotech) as per manufacturer's instruction. The quantification of TNF-α and IL-6 protein levels was performed in the ileal tissue lysates from mice using mouse TNF-α and IL-6 ELISA kits (Ray Biotech) as per manufacturer's instruction.

RNA preparation and qRT-PCR

Total RNA was isolated from the mouse ileal tissues using TRIzol reagent (Thermo Fisher Scientific) according to the manufacturer's instructions and treated with the TURBO DNA-free Kit (Thermo Fisher Scientific) to remove residual genomic DNA. The transcript levels were determined using Superscript III Platinum SYBR Green One-Step qRT-PCR kit (Thermo Fisher Scientific). Primers were obtained from IDT (**Table 2.3)** and their recommended thermal cycling

conditions were used. GAPDH was used as a housekeeping gene control for the ileal tissues. The $2^{-\Delta\Delta Ct}$ method was used to calculate the relative changes in gene expression. The relative expression in each figure refers to the induction levels of the gene of interest relative to GAPDH, and these levels were then compared with that of an untreated control calibrator sample.

Histopathology

Thin tissue sections from above were stained with hematoxylin and eosin, and a board-certified veterinary pathologist microscopically examined the slides and the interpretations were based on standard histopathological morphologies. The pathologist, who was blinded to the bacterial strain, compared the ileal sections to the controls. To determine the extent of the inflammation, the mouse ileal tissues were scored on a scale of 0-3 for three parameters yielding a maximum score of 9. The scoring parameters were the amount of polymorphonuclear leukocyte infiltrate, mononuclear infiltrate and involvement of the submucosa. To grade the amount of polymorphonuclear leukocyte infiltrate and mononuclear infiltrate the following histomorphological scale was used: 3= markedly increased, 2= moderately increased, 1 = slightly increased and 0 = normal. To grade the involvement of the submucosa the following histomorphological scale was used: 3= 50% or greater of the submucosal diameter, 2= 10%-50%, 1 = <10% and 0 = normal. The necrosis scores for the livers and spleens were as follows: 1 to ≤3 = microscopic foci, 2 to ≥3 = microscopic foci, and 3 = massive necrosis. The inflammation scores of the livers and spleens were as follows: 1 = mild inflammation, 2 = moderate to marked inflammation associated with the foci of necrosis.

Immunoblotting

To extract the proteins from Caco-2 cells, cells were seeded in 6-well plates for 14-21 days. Following treatment, the cells were washed, scraped from the bottom of 6-well plates, suspended in PBS, and pelleted by centrifugation. Total protein from Caco-2 cells was extracted using the M-PER Extraction Kit (Thermo Fisher Scientific). Detergent-insoluble (membrane) and detergent-soluble (cytosolic) proteins were isolated using a Mem-Per Eukaryotic Protein Extraction Kit (Thermo Fisher Scientific) while the cytosolic and nuclear proteins were extracted using NE-PER Extraction Reagent (Thermo Fisher Scientific). To extract proteins from ileal epithelial cells, the epithelial cell fraction from ileal tissues were isolated as described above (Bou Ghanem et al. 2012) and the detergent-insoluble and the detergent-soluble proteins were isolated using a Mem-Per Eukaryotic Protein Extraction Kit.

To isolate the cell wall-associated proteins bacterial pellets were resuspended in 0.5 ml protein extraction buffer (0.5% SDS, 10 mM Tris at pH 6.9), and incubated at 37°C for 30 min with agitation. The samples were centrifuged (14,000×*g*, 10 min, 4°C), and the supernatants (containing cell wall-associated proteins) were retained. Halt proteases and phosphatase inhibitors (Thermo Fisher Scientific) were used during all of the protein extraction procedures. The protein concentrations were determined by BCA assay (Thermo Fisher Scientific), and separated on SDS-PAGE gels (10-12.5% polyacrylamide) and electro-transferred to polyvinylidene difluoride (PVDF) membrane (Millipore). The membranes were then blocked in 5% nonfat dry milk (NFDM) in 0.1 M Tris-buffered saline, pH 7.5 (TBS) containing 0.1% Tween 20 (TBST) for at least 1 h. All of the primary antibodies were diluted in 5% bovine serum albumin (BSA) or 5% NFDM in TBST and incubated overnight. Secondary antibodies (1:2000 in 5% NFDM in TBST) incubated for 1 h at 37ºC, and a chemiluminescence method was performed using LumiGLO reagent (Cell Signaling). The membranes were exposed to X-ray films or visualized using the Chemi-Doc XRS

system (Bio-Rad). To immunoprobe the same membrane with another antibody, the originally bound antibodies from the membranes were removed by incubating the membranes in Restore Western Blot Stripping Buffer (Thermo Fisher Scientific) according to the manufacturer's protocol. To compare the reaction intensities, the average band densities were determined using Quantity One software (Bio-Rad). Densitometry reports represent the mean ± SEM after normalization to the loading control and are presented as %change of protein with the average for untreated cells (control) set at 100%. Immunoblots and densitometric reports are representative of 3 independent experiments. The antibodies used in this study are listed in **Table 2.1**.

Luciferase assay

The NF-κB Luciferase reporter RAW 264.7 cell line (Novus Biologicals), which expresses an optimized Renilla luciferase reporter gene (RenSP) under the transcriptional control of an NF-κB response element, was used. The cells were seeded (1×10^5 cells/well) into 96-well luminometer-compatible plates for 16 h and then treated with analytes for 6 h or infected with the WT, *lap*$^{-}$, *lap*$^{-}$ *lap*$^{+}$ or the Δ*inlA* strains (MOI ~10, 6h). Media from each well were aspirated, and then 100 µL of ice-cold PBS was added to each well. The plates were then frozen solid at -80°C overnight to completely lyse the cells, thawed back to room temperature, and luciferase assays were performed using the LightSwitch Luciferase assay kit (Novus Biologicals). Luminescence was measured as the relative luminescence units (RLU) using Spectramax (Spectramax, Molecular Devices) and reported as the relative fold change compared with that of the control cells that were treated with media alone. Recombinant human or mouse TNF-α (R&D Systems) and polymyxin B, LPS (*E. coli* Serotype R515, Re, TLR grade), and proteinase K (each from Sigma-Aldrich) were used.

Immunoprecipitation

Caco-2 cells were treated with or without purified LAP (1 µg/ml) for 30 min, rinsed with cold PBS, and lysed in Nondiet P-40 (NP-40) lysis buffer (20 mM Tris HCl, pH 8,137 mM NaCl, 1% NP-40, 2 mM EDTA). The cell lysates were pre-cleared with 10 µl protein G agarose beads (MicroProtein Technologies) for 1 h and the lysates were incubated with 2 µg of anti-IKKβ, 2 µg of anti-Hsp60, normal rabbit serum or normal mouse serum overnight at 4°C. The lysates were further mixed with 20 µl protein G agarose beads for 3 h at 4°C. The beads were washed five times with 1 ml NP-40 lysis buffer. The protein precipitates were analyzed by immunoblotting, and the complexes were visualized by chemiluminescence assay.

Quantification and Statistical Analysis

Experimental data were analyzed using GraphPad Prism (La Jolla, CA) software. For mouse microbial counts, statistical significance was assessed by Mann-Whitney test. In other experiments, comparisons between two data sets were performed using the unpaired Student *t*-test. When comparisons between more than two data sets were performed, a one-way or a two-way analysis of variance with Tukey's multiple-comparison test were performed. All data are representative of at least 3 independent experiments and specific numbers of mice per group are noted in corresponding figure legends. Unless otherwise indicated, data for all experiments are presented as the mean ± standard error of the mean (SEM).

Table 2.1 Key Resource Table

REAGENT or RESOURCE	SOURCE	IDENTIFIER
Antibodies		
Rabbit monoclonal anti-NF-κB p65	Cell Signaling	Cat #8242, RRID: AB_10859369
Rabbit monoclonal anti-Phospho-NF-κB p65 (Ser536)	Cell Signaling	Cat # 3033, RRID: AB_331284
Mouse monoclonal anti-IκBα	Cell Signaling	Cat # 4814, RRID: AB_390781
Mouse monoclonal anti-IKKα	Cell Signaling	Cat # 11930, RRID: AB_2687618
Rabbit monoclonal anti-IKKβ	Cell Signaling	Cat # 8943, RRID: AB_11024092
Rabbit monoclonal anti-phospho-IκB-α (Ser32)	Cell Signaling	Cat # 2859, RRID: AB_561111
Goat anti-rabbit IgG (HRP-linked)	Cell Signaling	Cat # 7074, RRID: AB_2099233
Horse anti-mouse IgG (HRP-linked)	Cell Signaling	Cat # 7076, RRID: AB_330924
Mouse monoclonal anti-Hsp60	Enzo life Science	Cat # ADI-SPA-806F, RRID: AB_11177888
Rabbit monoclonal anti-TATA banding protein	Novus Biologicals	Cat # NBP1-96038. RRID: AB_11015773
Mouse monoclonal anti-β-actin	Santa Cruz Biotechnology	Cat # sc-47778, RRID: AB_626632
Normal rabbit IgG	Santa Cruz Biotechnology	Cat # sc-2027, RRID: AB_737197
Normal mouse IgG	Santa Cruz Biotechnology	Cat # sc-2025, RRID: AB_737182
Mouse monoclonal anti-LAP	Our lab (mAb-H7)	N/A
Mouse monoclonal anti-InlA	Marcelo Mendonca, University of Pelotas, Brazil	N/A
Rabbit polyclonal anti-InlB	Our lab (PAb404)	N/A
Mouse monoclonal anti-ZO-1	Thermo Fisher Scientific	Cat # 3391-00, RRID: AB_2533147
Rabbit polyclonal anti-*Listeria*	Our Lab	N/A
Rabbit polyclonal anti-Hsp60	Our Lab (Burkholder and Bhunia 2010)	N/A
Goat anti-mouse IgG (H+L), F(ab')2 Fragment (Alexa Fluor 555 Conjugate) antibody	Cell Signaling	Cat # 4409, RRID: AB_1904022

Table 2.1 continued

Goat anti-rabbit IgG (H+L), F(ab')2 Fragment (Alexa Fluor 555 Conjugate) antibody	Cell Signaling	Cat # 4413, RRID: AB_10694110
Goat anti-Rabbit IgG (H+L) Cross-Adsorbed- FITC Conjugate	Thermo Fisher Scientific	Cat # F-2765, RRID: AB_2536525
Rabbit polyclonal anti-claudin-1	Thermo Fisher Scientific	Cat # 51-9000, RRID: AB_2533916
Mouse monoclonal anti-claudin-1	Santa Cruz Biotechnology	Cat # sc-166338, RRID: AB_2244863
Rabbit polyclonal anti-occludin	Thermo Fisher Scientific	Cat # 71-1500, RRID:AB_2533977
Mouse monoclonal anti-Beta-catenin	Thermo Fisher Scientific	Cat # MA1-301, RRID: AB_1070649
Rat monoclonal anti- ZO-1	Supernatant from the Anti-ZO-1 hybridoma R40.76	RRID: AB_628459
Rabbit monoclonal anti-pMLC(Ser19)	Santa Cruz Biotechnology	Cat # sc-293109, RRID: AB_10847539
Rabbit polyclonal anti-MLCK	Thermo Fisher Scientific	Cat # PA5-15177, RRID: AB_2298066
Rabbit monoclonal anti-E-cadherin(Human)	Cell Signaling	Cat # 3195, RRID: AB_2291471
Mouse monoclonal anti-E-cadherin(Mouse)	Thermo Fisher Scientific	Cat # 33-4000, RRID: AB_2533118
Rabbit polyclonal anti-MLC-2	Cell Signaling	Cat # 3672, RRID: AB_10692513
Rabbit monoclonal anti-MEK 1/2	Cell Signaling	Cat # 8727, RRID:AB_10829473
Rabbit polyclonal anti-Pan Cadherin	Cell Signaling	Cat # 4068, RRID: AB_10693605
Goat anti-rat IgG (H+L), (Alexa Fluor 555 Conjugate) antibody	Cell Signaling	Cat # 4417, RRID: AB_10696896
Rabbit monoclonal human TNF-α neutralizing antibody	Cell Signaling	Cat # 7321, RRID:AB_10925386

Table 2.1 continued

Rabbit polyclonal human IL-6 neutralizing antibody	Thermo Fisher Scientific	Cat # P620, RRID:AB_223481

Bacterial and Virus Strains		
L. monocytogenes F4244 (WT)	CDC, Atlanta, GA	N/A
L. monocytogenes KB208 (*lap*$^{-}$)	(Jagadeesan et al. 2010)	N/A
L. monocytogenes CKB208 (*lap*$^{-}$*lap*$^{+}$)	(Jagadeesan et al. 2010)	N/A
L. monocytogenes AKB301 (Δ*inlA*)	(Burkholder and Bhunia 2010	N/A
L. monocytogenes AKB302 (Δ*inlA inlA*$^{+}$)	(Burkholder and Bhunia 2010	N/A
L. monocytogenes 10403S	Dr. D.A. Portnoy, UC-Berkeley	N/A
L. monocytogenes DPL2161(ΔLLO)	Dr. D.A. Portnoy, UC-Berkeley	N/A
L. monocytogenes DPL4406(Δ*inlB*)	Dr. D.A. Portnoy, UC-Berkeley	N/A
L. innocua F4248	CDC, Atlanta, GA	N/A
ClearColi BL21(DE3) Electrocompetent Cells	Lucigen Corporation	Cat# 60810
E. coli BL21(DE3) +pET32a-ELAP-2	(Jagadeesan et al. 2010)	N/A
E. coli (ClearColi BL21-DE3)+pET32a-ELAP-2	This Study	N/A
E. coli pET28b-1	Dr. Pascale Cossart (Institut Pasteur, France)	N/A

Biological Samples		
Epithelial cells isolated from ileum of 8-10 week old A/J mice	N/A	N/A

Chemicals, Peptides, and Recombinant Proteins		
Recombinant human TNF-α	R&D Systems	Cat # 210-TA
Recombinant mouse TNF-α	R&D Systems	Cat # 410-MT
LAP from *E. coli* BL21(DE3)	(Jagadeesan et al. 2010)	N/A
LAP from Clear coli BL21(DE3)	This study	N/A
InlA	Dr. Marcelo Mendonca, University of Pelotas, Brazil	N/A
InlB from *E. coli* pET28b-1	Dr. Pascale Cossart (Institut Pasteur, France)	N/A
Modified Oxford agar Base	Neogen Corporation	Cat # 7428
Modified Oxford agar Base supplement	Neogen Corporation	Cat # 7991
Buffered *Listeria* enrichment broth	Neogen Corporation	Cat # 7675
Buffered *Listeria* enrichment broth supplement	Neogen Corporation	Cat # 7980
Collagenase	Worthington BioChem Corp	Cat # LS004188
DNAse 1	Worthington BioChem Corp	Cat # LS002007

Table 2.1 continued

RNAlater	Thermo Fisher Scientific	Cat # AM7021
DAPI	Cell Signaling	Cat # 4083
FITC-labeled 4 kDa dextran	Sigma-Aldrich	Cat # 46944
PDTC	Sigma-Aldrich	Cat # P8765
ML-9	Sigma-Aldrich	Cat # C1172
Dreverse PIK	Dr. J. Turner, Harvard Medical School	N/A
Bay-11-7085	Thermo Fisher Scientific	Cat # 50-101-2177
Cytochalasin-D	Sigma-Aldrich	Cat # C2618
Polymyxin B	Sigma-Aldrich	Cat # 1405-20-5
LPS (*E. coli* Serotype R515, Re, TLR grade)	Enzo Life Sciences	Cat # ALX-581-007
Proteinase K	Sigma-Aldrich	Cat # P2308
Protein G agarose beads	Micro-Protein Technologies	Cat # G100R2

Critical Commercial Assays		
Human Inflammation Antibody Array kit	Ray Biotech	Cat # AAH-INF-3-2
Human TNF-α ELISA kit	Ray Biotech	Cat # ELH-TNFa-1
Human IL-6 ELISA kit	Ray Biotech	Cat # ELH-IL6-1
Mouse TNF-α ELISA kit	Ray Biotech	Cat # ELM-TNFa-1
Mouse IL-6 ELISA kit	Ray Biotech	Cat # ELM-IL6-1
Platinum SYBR Green One-Step qRT-PCR kit	Thermo Fisher Scientific	Cat # 11-736-051
Turbo DNA-free Kit	Thermo Fisher Scientific	Cat # AM1907
BCA assay kit	Thermo Fisher Scientific	Cat # PI23235
M-PER extraction kit	Thermo Fisher Scientific	Cat # PI78501
NE-PER extraction reagent	Thermo Fisher Scientific	Cat # PI78835
Mem-Per Plus Membrane Protein Extraction Kit	Thermo Fisher Scientific	Cat # PI89842
Renilla-firefly Luciferase assay kit	Thermo Fisher Scientific	Cat # PI16185
Chromogenic LAL Endotoxin Assay Kit	Genscript	Cat # L00350
LDH Cytotoxicity Assay Kit	Thermo Fisher Scientific	Cat # PI88954
Toxin-Eraser Endotoxin Removal Kit	Genscript	Cat # L00338
Alexa Fluor 647 Phalloidin	Cell Signaling	Cat # 8940S

Experimental Models: Cell Lines		
Cell line: Caco-2	ATTC	Cat # HTB37
Cell line: Caco-2 presenting stable suppression of *hsp60* mRNA via short hairpin RNA (shRNA) mediated targeting	(Burkholder and Bhunia 2010)	N/A

Table 2.1 continued

Cell line: Caco-2 presenting a non-targeting control shRNA vector	(Burkholder and Bhunia 2010)	N/A
Cell line: RAW 264.7 NF-κB luciferase reporter cell line	Novus Biologicals	Cat # NBP2-26253;

Experimental Models: Organisms/Strains		
Mouse: A/J	The Jackson Laboratory	Stock # 000646
Mouse: C57BL/6	Bred at Purdue transgenic mouse facility	N/A
Mouse: MLCK knockout	(Clayburgh et al. 2005)	N/A

Oligonucleotides		
qPCR Primers for murine *TNF-α*, *IL-6* and *Gapdh* see Table S2	(Gilbert et al. 2012)	N/A

Software and Algorithms		
Bio-Rad quantity one	Bio-Rad	http://www.bio-rad.com/en-ch/product/quantity-one-1-d-analysis-software
ImageJ	NIH	https://imagej.nih.gov/ij/
GraphPad Prism 6.0	GraphPad Software	https://www.graphpad.com/scientific-software/prism/
Microsoft Excel	Microsoft	https://products.office.com/en-us/excel
Nikon Elements	Nikon	https://www.nikoninstruments.com/Products/Software/NIS-Elements-Basic-Research

Table 2.2. Fold Change in 40 Inflammatory Mediators in Caco-2 Cells infected with *L. monocytogenes* F4244 (WT) or *lap*─ mutant.

Inflammatory Markers	**Normalized Fold change in Cytokine Expression levels (Ratio of *lap*⁻/WT)[a]**
Eotaxin	0.69 ± 0.05
Eotaxin-2	0.77 ± 0.08
G-CSF	0.72 ± 0.00
GM-CSF	0.73 ± 0.12
ICAM-1	0.70 ± 0.12
IFN-γ	0.56 ± 0.12
I-309	0.46 ± 0.02
IL-1α	0.43 ± 0.01
IL-1β	1.23 ± 0.23
IL-2	0.95 ± 0.12
IL-3	0.79 ± 0.01
IL-4	0.64 ± 0.00
IL-6	0.53 ± 0.02
IL-6 sR	0.64 ± 0.03
IL-7	0.61 ± 0.00
IL8	0.61 ± 0.02
IL-10	0.70 ± 0.10
IL-11	0.52 ± 0.04
IL12-p40	0.55 ± 0.09
IL12-p70	0.41 ± 0.01
IL-13	0.94 ± 0.08
IL-15	0.86 ± 0.05
IL-16	0.74 ± 0.01
IL17	0.67 ± 0.00
IP-10	0.64 ± 0.05
MCP-1	0.69 ± 0.05
MCP-2	0.67 ± 0.00
M-CSF	0.66 ± 0.02
MIG	0.54 ± 0.05
MIP-1-α	0.48 ± 0.04
MIP-1-β	0.62 ± 0.06
MIP-1-δ	0.60 ± 0.03
RANTES	0.93 ± 0.01
TGF-β1	0.89 ± 0.04
TNF-α	0.74 ± 0.01
TNF-β	0.73 ± 0.08
sTNF-RI	0.59 ± 0.01
sTNF RII	0.56 ± 0.05
PDGF-BB	0.57 ± 0.07
TIMP-2	0.61 ± 0.09

[a]The results are expressed as the ratio of *lap*⁻/WT using semi-quantitative membrane-based RayBio human (RayBiotech Inc.) immunoassay. The intensity of signals was quantified by densitometry from two independent experiments (n = 4) and is reported as fold differences ± SD

Table 2.3. qRT-PCR Primers used in this study.

Gene	Oligonucleotide sequence (5'-3')	References
TNFα (Mouse)	(F)AATGGCCTCCCTCTCATCAGTT (R)CCACTTGGTGGTTTGCTACGA	(Gilbert et al. 2012)
IL-6 (Mouse)	(F)CAAAGCCAGAGTCCTTCAGAGAGATAC (R)GGATGGTCTTGGTCCTTAGCCAC	(Gilbert et al. 2012)
Gapdh (Mouse)	(F)GGTGGGTGGTCCAAGGTTTC (R)TGGTTTGACAATGAATACGGCTAC	(Gilbert et al. 2012)

CHAPTER 3. *LISTERIA* ADHESION PROTEIN PROMOTES *L.MONOCYTOGENES* TRANSLOCATION IN AN INTERNALIN A-PERMISSIVE GERBIL MODEL

Abstract

The crossing of host barriers (intestinal, blood-brain, and placental barrier) is critical step for systemic infections caused by entero-invasive pathogens. *Listeria monocytogenes* is a facultative-intracellular foodborne pathogen that first crosses the intestinal barrier to cause a systemic infection. However, the underlying mechanism is not well understood. Here, we decipher the contribution of *Listeria* Adhesion Protein (LAP) and the bacterial invasion protein Internalin A (InlA) in translocation of the bacterium across the intestinal barrier. We used a Mongolian gerbil model that is relevant to understand the pathophysiology of listeriosis in human as the gerbils are the only small animal model that are permissive to both the invasion proteins InlA-and-Internalin B (InlB)-mediated pathways similar to that in human. Here, we demonstrate that both LAP and InlA promotes *L. monocytogenes* translocation into the lamina propria and systemic dissemination in a gerbil model. Further, we determined the preferential routes for *L. monocytogenes* translocation and show a direct LAP-dependent and InlA-independent pathway for *L. monocytogenes* paracellular translocation across the intestinal epithelial cells that do not express luminally accessible E-cadherin; the host receptor for InlA. Additionally, we show that a functional InlA/E-cadherin interaction pathway that promotes *L. monocytogenes* translocation by targeting cells with luminally accessible E-cadherin such as cell at sites of epithelial cell extrusion, epithelial folds and mucus-expelling goblet cells. Thus, *L. monocytogenes* uses a cooperative action of LAP and InlA to cross the intestinal epithelial barrier for successful infection *in vivo*.

Highlights

1. LAP promotes *L. monocytogenes* translocation and systemic dissemination in an InlA-permissive gerbil model.

2. LAP targets the intestinal epithelial cells that do not express luminally accessible E-cadherin for *L. monocytogenes* paracellular translocation.

3. InlA targets intestinal cells at sites of epithelial cell extrusion, epithelial folds and mucus-expelling goblet for *L. monocytogenes* transcytosis.

4. *L. monocytogenes* uses a cooperative action of LAP and InlA to cross the intestinal epithelial barrier for successful infection *in vivo*.

Introduction

Listeria monocytogenes is a facultative intracellular opportunistic foodborne pathogen that can lead to meningitis, encephalitis, liver abscessation, and abortion in high risk populations; the neonates, elderly, immunocompromised individuals and pregnant women. Among the foodborne pathogens, *L. monocytogenes* has the highest hospitalization and case fatality rate (20-30%) (Scallan et al. 2011; Lomonaco et al. 2015). The bacterium has a remarkable ability to cross host barriers (intestinal, blood-brain, and placental) (Radoshevich and Cossart 2018). The intestinal tract is the primary route for *L. monocytogenes* infection and crossing this barrier represents the first step during the infectious process. *L. monocytogenes* subsequently spreads to deeper tissues to cause systemic infections. The mucosa of the intestines are lined by epithelial cells that provide the first line of defense against infection yet, *L. monocytogenes* can breach this mucosal barrier. However, the underlying mechanisms of how *L. monocytogenes* crosses the gut epithelial barrier is not well understood.

Two *L. monocytogenes* surface invasion proteins, Internalin A (InlA) and Internalin B (InlB) play a major role in the internalization of *L. monocytogenes* into human nonphagocytic cells. However, the interaction of both InlA and InlB with their respective receptors is host species-specific (Disson and Lecuit 2013). InlA interacts with human and guinea pig E-cadherin to promote bacterial transcytosis across the gut epithelium (Mengaud et al. 1996; Nikitas et al. 2011), but not with mouse and rat E-cadherin (Lecuit et al. 1999; Lecuit et al. 2001). InlB interacts with human and mouse Met to accelerate *L. monocytogenes* invasion of the Peyer's patches (Shen et al. 2000; Chiba et al. 2011), but not with a guinea pig or rabbit Met (Khelef et al. 2006). In contrast, the gerbil, like humans, is naturally permissive to both InlA/E-cadherin and InlB/Met interactions (Disson et al. 2008).

E-cadherin is an adherens junction (AJ) protein and is inaccessible to luminal bacteria thus access to E-cadherin is proposed to occur during villous epithelial "cell extrusion" (Pentecost et al. 2006) during which the apical junctional complex proteins are redistributed to the lateral membranes (Marchiando et al. 2011) and near epithelial folds and mucus-expelling goblet cells (Nikitas et al. 2011). Despite the key role of InlA in *L. monocytogenes* crossing the intestinal barrier, the oral inoculation of a Δ*inlA* strain resulted in high bacterial burdens in the small intestine and mesenteric-lymph node (MLN) of wild-type (WT) mice (Bierne et al., 2002; (Drolia et al. 2018) and also in transgenic mice expressing "humanized" E-cadherin (Disson et al. 2008). This suggests that the humanized E-cadherin allele is only relevant to InlA-mediated bacterial invasion and that *L. monocytogenes* uses alternate routes to translocate across the gut mucosa. Importantly, *L. monocytogenes* isolates from clinical human cases have been found expressing a defective InlA (truncated protein) (Cruz et al. 2014; Fravalo et al. 2017) and InlA-defective strains infect human new-borns and fetuses of pregnant guinea pigs after oral dosing

(Holch et al. 2013; Gelbicova et al. 2015) strongly suggesting InlA-independent mechanisms for the crossing of the intestinal barrier in human listeriosis. InlA-independent mechanisms for *L. monocytogenes* intestinal epithelial barrier crossing are understudied and are very relevant to human infection.

Although the Microfold (M) cells in the Peyer's patch aid *L. monocytogenes* to cross the gut epithelial barrier, however, the bacterium is able to cross the intestinal barrier in a Peyer's patch-null mouse (InlA non-permissive) strongly suggesting the presence of alternate pathways for *L. monocytogenes* to cross the intestinal barrier (Chiba et al., 2011; Pron et al., 1998) . InlB plays a role only in colonization of the Peyer's patch in mice, as the Δ*inlB* mutant strain showed an invasion defect through M cells in the Peyer's patch (Chiba et al. 2011) while InlA does not appear to play any role in invasion through M cells (Corr et al. 2006).

As stated above, mice are non-permissive to InlA/E-cadherin-mediated pathway due to an amino acid substitution in the murine E-cadherin sequence (Lecuit et al. 1999). To circumvent the species barrier, previous studies have used *L. monocytogenes* expressing murinized InlA ($InlA^m$), which binds E-cadherin with high affinity for studying *L. monocytogenes* pathogenesis (Wollert et al. 2007; Bou Ghanem et al. 2012). However, a recent study has demonstrated that murinization of InlA extends its receptor repertoire, altering *L. monocytogenes* cell tropism and host response (Tsai et al. 2013). Thus, *L. monocytogenes* expressing $InlA^m$ targets not only goblet cells expressing luminally-accessible E-cadherin but also targets villous M cells, which express luminally-accessible N-cadherin (Tsai et al. 2013). This results in enhanced innate immune response and intestinal barrier damage (Tsai et al. 2013). Therefore, the murinized InlA strain does not closely mimic infection in humans. Alternatively, a few studies have used humanized E-cadherin mice to study *L. monocytogenes* pathogenesis (Disson et al. 2008).

However, the key difference between the pathophysiology of listeriosis in genetically engineered inbred mouse line and human still remains unresolved. Moreover, the humanized E-cadherin mouse is generated on the highly resistant C57BL/6 background (Disson et al. 2008; D'Orazio 2014). Thus, the gerbil is the only small animal model that is naturally permissive to both InlA/E-cadherin and InlB/Met interactions similar to humans.

Our group has demonstrated a key role of *Listeria* adhesion protein (LAP), as an adhesion molecule in *L. monocytogenes* pathogenesis during the intestinal phase of infection (Pandiripally et al. 1999; Jaradat et al. 2003). LAP is a 104-kDa alcohol acetaldehyde dehydrogenase (*Lmo1634*), which contributes to the bacterial adhesion to cell lines of intestinal origin only in pathogenic *Listeria* species (Pandiripally et al. 1999; Jaradat et al. 2003; Jagadeesan et al. 2010; Bailey et al. 2017). We have deciphered the human heat shock protein-60 (Hsp60) as the host epithelial receptor for LAP (Wampler et al. 2004; Jagadeesan et al. 2011). Most recently, we have demonstrated that LAP promotes bacterial translocation into the lamina propria, systemic dissemination by increasing intestinal epithelial permeability *in vivo* in mice and across human enterocyte-like Caco-2 cells (Drolia et al. 2018). We demonstrated that LAP engages its receptor, Hsp60 to activate canonical NF-κB(p65) signaling, thereby promoting the MLCK-mediated opening of the intestinal cell-cell junction via the cellular redistribution of the major junctional proteins, claudin-1, occludin and E-cadherin and bacterial translocation in both model systems (Drolia et al. 2018). However, whether LAP promotes *L. monocytogenes* translocation across the intestinal barrier in an InlA-permissive host (as humans) *in vivo* is not known.

In the present study, we investigated whether LAP promotes the translocation of *L. monocytogenes* across the intestinal barrier *in vivo* in an InlA/E-cadherin and InlB/Met permissive model and determined the respective roles of LAP and InlA in crossing of the

intestinal barrier during the early stage of infection. We used a Mongolian gerbil model that is permissive to both InlA/E-cadherin and InlB/Met systems thus allowing us to study the pathophysiology of listeriosis in animal models relevant to humans. Here, we demonstrate that both LAP and InlA promotes *L. monocytogenes* translocation into the lamina propria and systemic dissemination in a gerbil model. Further, we determined the preferential routes for *L. monocytogenes* translocation and show a direct LAP-Hsp60-mediated, InlA-independent pathway for *L. monocytogenes* paracellular translocation. Additionally, we show a functional InlA/E-cadherin interaction pathway that promotes *L. monocytogenes* translocation by targeting cells with luminally accessible E-cadherin such as cell at sites of epithelial cell extrusion, epithelial folds and mucus-expelling goblet cells. Thus, *L. monocytogenes* uses a cooperative action of LAP and InlA to cross the intestinal epithelial barrier for successful infection *in vivo*.

Results

LAP and InlA Promotes Bacterial Colonization in the Intestine and Systemic Dissemination

To analyze the role of LAP and InlA in virulence, we orally challenged female gerbils with a WT strain F4244 (serotype 4b), an isogenic *lap*⁻ insertion mutant strain (*lap*⁻), and a Δ*inlA* deletion strain and enumerated *L. monocytogenes* counts (Colony Forming Units; CFU's) in the extra-intestinal sites (liver, spleen and MLN) and the intestinal sites (ileum, cecum and colon) at 48 h pi. Relative to the WT strain, the dissemination of *lap*⁻ strain was significantly impaired in the liver (97.76% reduction), spleen (97.86% reduction) and MLN (89.03% reduction) (**Figures 3.1A-3.1C**). The *lap*⁻ strain also exhibited a significant defect in the bacterial burdens that invaded the ileum, cecum and colon (95.75%, 96.25% and 98.8% reduction, respectively) (**Figures 3.1D-3.1F**). As expected, in all organs tested, the Δ*inlA* strain also showed a significant colonization defect (**Figures 3.1A-3.1F**). The bacterial burdens in the liver, spleen, MLN and the colon for the

Δ*inlA* strain were comparable to those for *lap*$^{-}$ strain, while in the cecum and colon the Δ*inlA* strain exhibited a greater colonization defect compared to those for the *lap*$^{-}$ strain. These data suggest that both LAP and InlA promotes *L. monocytogenes* intestinal colonization and systemic dissemination.

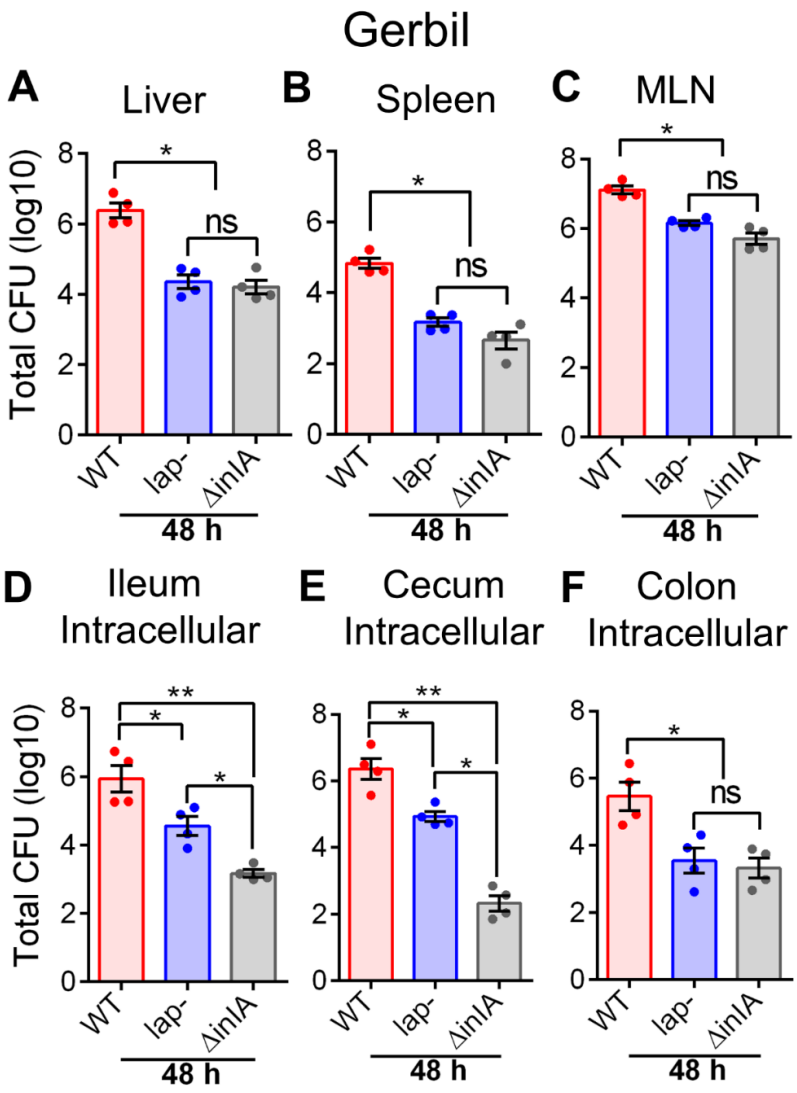

Figure 3.1 LAP and InlA promotes *L. monocytogenes* intestinal colonization and systemic dissemination.

(**A**–**F**) Female gerbils were orally challenged with ~3×10^9 CFU of WT, *lap*$^-$ or Δ*inlA L. monocytogenes* bacteria. The plots show the total CFU obtained from the liver (**A**), spleen (**B**), mesenteric-lymph node(MLN) (**C**), ileum (intracellular) (**D**), cecum (intracellular) (**E**), colon intracellular (**F**) of gerbils (n=4) at 48 h pi from two independent experiments. Bar and brackets represent the mean ± SEM, respectively, for the data points in each group. Dashed horizontal lines indicate the limit of detection for each organ/tissue. All error bars represent mean ± SEM. **p < 0.01; *p < 0.05; ns, no significance.

LAP and InlA Promotes *L. monocytogenes* Translocation into the Underlying Lamina Propria

We next examined the role of LAP and InlA in *L .monocytogenes* crossing of the intestinal barrier by quantifying the amount of the bacteria that were located in the underlying lamina propria of the ileal and colonic mucosa in gerbils challenged with the WT, *lap*⁻ or the Δ*inlA* strain at 48 h pi by using a microscopic approach. Immunostaining of ileal and colonic tissue sections confirmed high bacterial loads in the ileal (**Figures 3.2A and 3.2C**) and colonic (**Figures 3.2B and 3.2D**) lamina propria of the gut mucosa in gerbils challenged with the WT strains. In contrast, significantly fewer *lap*⁻ bacteria were found in the lamina propria of ileal and colonic tissues. The Δ*inlA* strain also exhibited a significant defect in crossing the intestinal barrier; however, the Δ*inlA* strain still crossed the intestinal barrier and were observed in the underlying lamina propria of the ileal and the colonic mucosa.

Next, to determine the extent of the intestinal barrier damage, we analyzed the permeability to the paracellular marker 4-kDa FITC-dextran (FD4), gavaged orally 4–5 hr prior to sacrifice, in *Listeria*-infected gerbils. Relative to the uninfected controls, the FD4 concentrations were significantly increased (~29.8%) in the serum of the WT-challenged gerbil 48 h pi, while the levels in the *lap*⁻ or the Δ*inlA*-challenged gerbils were comparable to uninfected controls (**Figure 3.2E**). These results correlated with histopathologic analysis of ileal tissues which revealed increased numbers of polymorphonuclear and mononuclear cells infiltrating the base of the villous lamina propria in the ileal tissues of gerbils infected with the WT strain (**Figures 3.3A and 3.3B**). Likewise, histopathologic analysis of the colonic tissues revealed significantly increased numbers of polymorphonuclear and mononuclear cells infiltrating the base of the villous lamina propria, crypt cell death, cellular erosion and increased involvement of the submucosa, in gerbils challenged with the WT strain (**Figures 3.3C and 3.3D**). In contrast, ileal and colonic musoca of

gerbils challenged with the *lap*$^{-}$ strain or the Δ*inlA* strain showed significantly lesser alterations as compared to WT-infected gerbils. Taken together, these data suggest that both LAP and InlA promotes *L. monocytogenes* translocation across the intestinal barrier into the underlying lamina propria and the defect in bacterial translocation by the *lap*$^{-}$(*inlA*$^{+}$) bacteria suggest the existence of a LAP-dependent and InlA-independent route for *L. monocytogenes* to cross the intestinal barrier.

Figure 3.2. LAP and InlA promotes *L. monocytogenes* translocation across the intestinal barrier.

(**A, B**) Representative confocal immunofluorescence microscopic images of ileal (**A**) or colonic

(**B**) tissue sections immunostained for ZO-1 (red), *Listeria* (green) and DAPI (blue; nucleus) from WT, *lap*$^{-}$ or Δ*inlA*-challenged gerbils 48 h pi, Bars, 10 µm. Increased *L. monocytogenes* (green) was detected in the lamina propria of ileal (**A**) or colonic (**B**) tissue in WT-challenged gerbils. Very few *L. monocytogenes* was detected in the ileal or colonic lamina propria of the *lap*$^{-}$ or the Δ*inlA*-challenged gerbils (arrows).

(**C, D**) Graph representing quantitative measurements of *L. monocytogenes* counts in the lamina propria from ileal (**C**) or colonic (**D**) villi images (n = 30) from three gerbils for each treatment.

(E) Analysis of 4-kDa FITC-dextran (FD4) permeability through intestinal epithelium of uninfected (control) and *L. monocytogenes*–infected gerbils in serum (**A**) at 48 h pi. FD4 was administered orally 4-5 h before sacrifice. Data represent mean ± SEM of n= 4 gerbils per treatment from two independent experiments.

All error bars represent mean ± SEM. ***$p < 0.001$; **$p < 0.01$; *$p < 0.05$; ns, no significance.

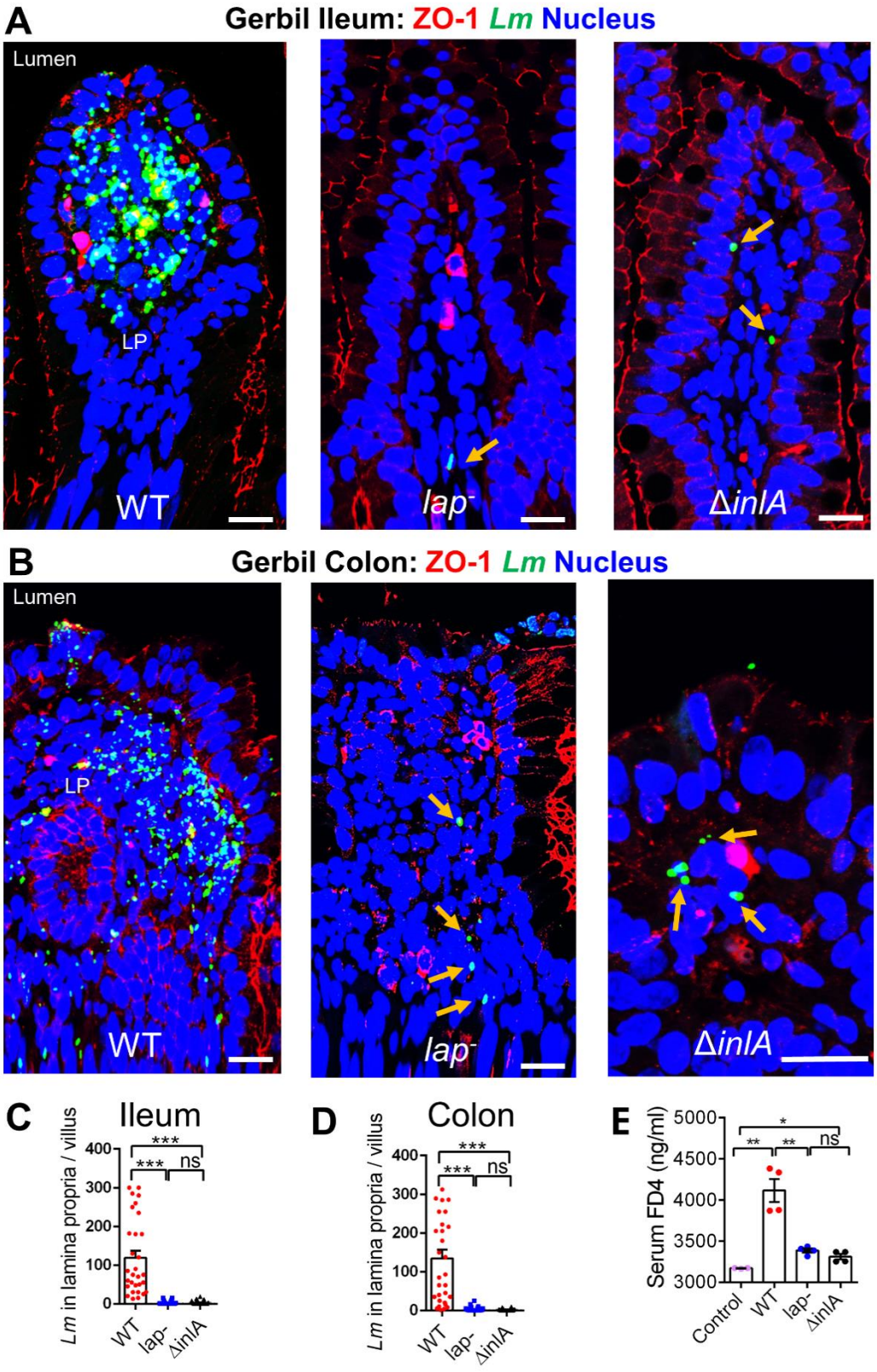
A
Gerbil Ileum: ZO-1 Lm Nucleus
Lumen
LP
WT
lap-
ΔinlA
B
Gerbil Colon: ZO-1 Lm Nucleus
Lumen
LP
WT
lap-
ΔinlA
C
Ileum
Lm in lamina propria / villus
400
300
200
100
0
***
***
ns
WT
lap-
ΔinlA
D
Colon
Lm in lamina propria / villus
400
300
200
100
0
***
***
ns
WT
lap-
ΔinlA
E
Serum FD4 (ng/ml)
5000
4500
4000
3500
3000
*
**
**
ns
Control
WT
lap-
ΔinlA

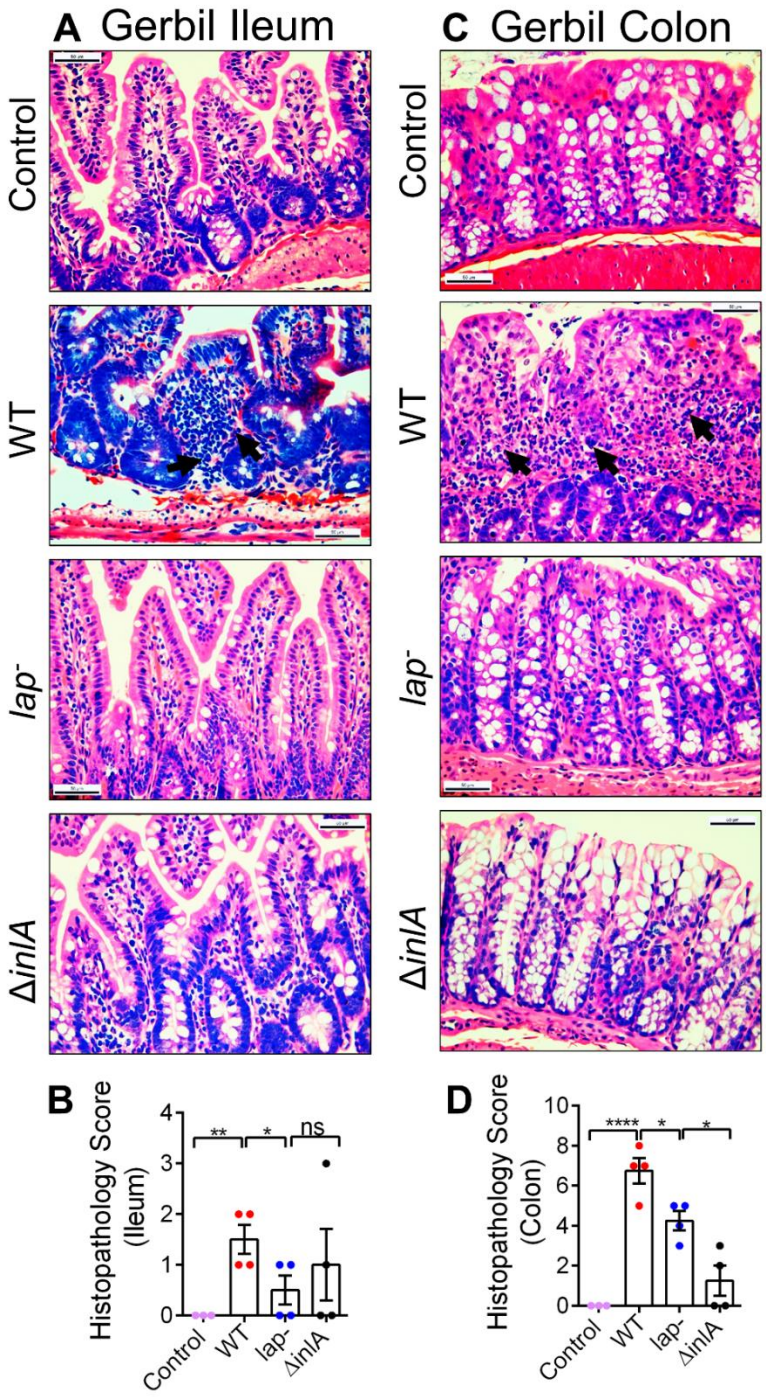

Figure 3.3 Histological analysis of ileal and colonic tissues in *L. monocytogenes* infected gerbils.

(**A**-**D**) Representative H&E stained picto-micrographs(**A and C**) and histological score (**B and D**) of the ileal (**A and B**), and colonic tissues (**C and D**) at 48 h pi (bars, 50 µm) from control uninfected gerbils or gerbils orally infected with ~3×10^9 CFU of *L. monocytogenes* WT, *lap*$^-$ or Δ*inlA* strains. Arrows shows increased polymorphonuclear and mononuclear cells infiltrating the base of the villous lamina propria in gerbils challenged with the WT strain. All error bars represent SEM. ****$p < 0.0001$; **$p < 0.01$; *$p < 0.05$; ns, no significance.

***L. monocytogenes* LAP Targets Intestinal Cells not Expressing Luminally Accessible E-cadherin while InlA Targets Intestinal Cells Expressing Luminally Accessible E-cadherin.**

L. monocytogenes has been shown to translocate through luminally acessible E-cadherin cells of the intestine such as the extruding cells, the enterocytes located in epithelial folds and the mucus-secreting goblet cells (Nikitas et al. 2011). Additionally, *L. monocytogenes* has been shown also translocate through villous M cells (Nikitas et al. 2011). Thus, we next determined the preferential routes for *L. monocytogenes* translocation by analyzing the association of the bacterium with five different cellular targets (a) extruding cells, (b) epithelial folds, (c) goblet cells, (d) villous M cells and (e) other intestinal epithelial cells (IEC's) in the ileal tissues of infected gerbils by selectively immunostaining for M-cells and staining for goblet cell with wheat germ agglutinin (WGA; which binds to sialic acid and N –acetylglucosaminyl carbohydrate residues on the plasma membrane of enterocytes and in mucus of goblet cells, **Figures 3.4A-3.4G)**. Consistent with previous observations (Nikitas et al. 2011), we found *L. monocytogenes* associated with luminally accessible E-cadherin cells such as the extruding cells at the tip of the villi (**Figures 3.4A and 3.4B**), cells at epithelial folds (**Figures 3.4A and 3.4C**) and mucus-secreting goblet cells (**Figures 3.4A and 3.4D**) in gerbils infected with the WT strain at 48 h pi. However, we observed that the majority of *L. monocytogenes* associated with and translocated across other IEC's that do not possess luminally accessible E-cadherin (**Figures 3.4A and 3.4D-F)**.

Next, we determined the relative contribution of LAP and InlA in *L. monocytogenes* association and translocation across these five cellular targets by analyzing the relative association of the bacterium in the ileal mucosa of gerbils infected with either the WT, *lap*$^{-}$ strain or the Δ*inlA* strain at these cellular sites at 48 h pi. We found that the relative association of *L. monocytogenes* at the sites of luminally accessible E-cadherin cells such as extruding cells (**Figures 3.5A and 3.5B)**, enterocytes located in epithelial folds (**Figures 3.5C and 3.5D)** and the mucus-secreting

goblet cells (**Figures 3.5E and 3.5F)** were significantly higher in the ileal mucosa of gerbils infected with the WT and the *lap*¯ strains than in those infected with the Δ*inlA* strain. In contrast, we observed that the WT and the Δ*inlA* strains adhered and translocated across other IECs that do not express luminally accessible E-cadherin at similar rates. Moreover, the relative association of *L. monocytogenes* at these sites were significantly higher in the ileal mucosa of gerbils infected with the WT (~ 10 fold increase) and Δ*inlA* (~8 fold increase) strain relative to those infected with the *lap*¯ strain (**Figures 3.5G and 3.5H)**. As expected, similar rates of *L. monocytogenes* association was observed with the villous M-cells in the ileal mucosa of gerbils infected with either the WT, *lap*¯ or the Δ*inlA* (**Figures 3.5I and 3.5J)**. These observation were consistent with transmission electron microscopic (TEM) analysis; where we observed the WT strain associated with the mucus-secreting goblet cell (**Figure 3.6A)** and in the paracellular space of IEC's **(Figure 3.6B)** that do not express luminally accessible E-cadherin in the ileal mucosa of infected gerbils at 48 h pi**.** Taken together, these data demonstrate that the translocation of *L. monocytogenes* across IECs that do not express luminally accessible E-cadherin is LAP-dependent while the translocation of *L. monocytogenes* across luminally accessible E-cadherin cells such as the extruding cells, cells at epithelial folds and the mucus-secreting goblet cells is InlA-dependent. However, the translocation of *L. monocytogenes* across the villous M-cell is independent of InlA or LAP.

Figure 3.4. *L. monocytogenes* translocate across cells with sites of luminally accessible E-cadherin and luminally inaccessible E-cadherin.

(A) Representative confocal microscopic image of intestinal villi section immunostained for WGA (white), *Lm* (green), M cells (red) and DAPI (blue; nucleus) from *L. monocytogenes* (WT)–infected gerbils at 48 h pi. The panels around the image show enlargements of the boxed areas (Bars, 1 µm) represents *L. monocytogenes* association at and translocation across (yellow arrows) cells that express luminally accessible E-cadherin; at site of epithelial extrusion (**B**, extruded cell at the tip of villi; white arrow), epithelial folds (**C,** white arrows), at goblet cell (**D**; white arrow; goblet cell, *L. monocytogenes*; red arrows) or other intestinal epithelial cells (IECs) do not express luminally accessible E-cadherin (**D- F**). Representing villus M-cell (**G**; white arrows). Microscopy results are representative of at least 3 independent gerbils.

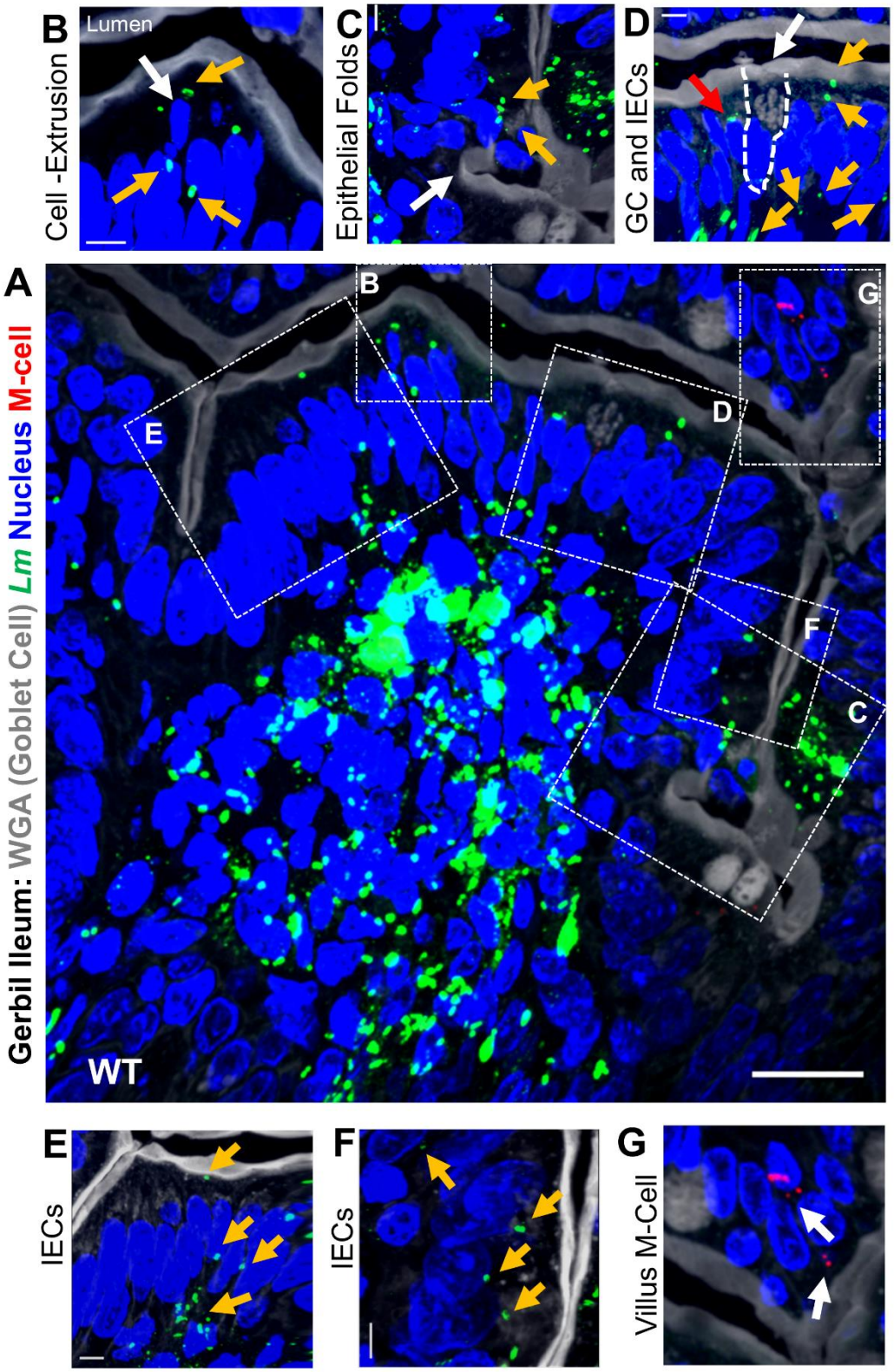
A
Gerbil Ileum: WGA (Goblet Cell) Lm Nucleus M-cell
WT
B
Lumen
Cell -Extrusion
C
Epithelial Folds
D
GC and IECs
E
IECs
F
IECs
G
Villus M-Cell

Figure 3.5. *L. monocytogenes* translocation across cell with luminally accessible E-cadherin is InlA-dependent and across cells with luminally inaccessible E-cadherin in LAP-dependent.

(A, C, E, G and I) Representative confocal microscopic image of ileal sections immunostained for WGA (white), *Lm* (green), M cells (red) and DAPI (blue; nucleus) from *L. monocytogenes* WT, *lap*$^{-}$ or Δ*inlA* –infected gerbils at 48 h pi showing *L. monocytogenes* (yellow arrows) association at and translocation across luminally accessible E-cadherin cells**;** extruded cell at the tip of villi (**A**, white arrow; extruded cell), epithelial folds (**C,** white arrow; epithelial folds), at goblet cell (**E**; white arrow; goblet cell) and luminally inaccessible E-cadherin IECs (**G**) or villus M-cell (**I**; white arrows). **(B, D, F, H and J)** Graph representing quantitative measurements of *L. monocytogenes* infected cells (in each cell type or at each site) of villi images (n = 45) from three gerbil each treatment is presented on the right panels. All error bars represent SEM. ****$p < 0.0001$; **$p < 0.01$; *$p < 0.05$; ns, no significance.

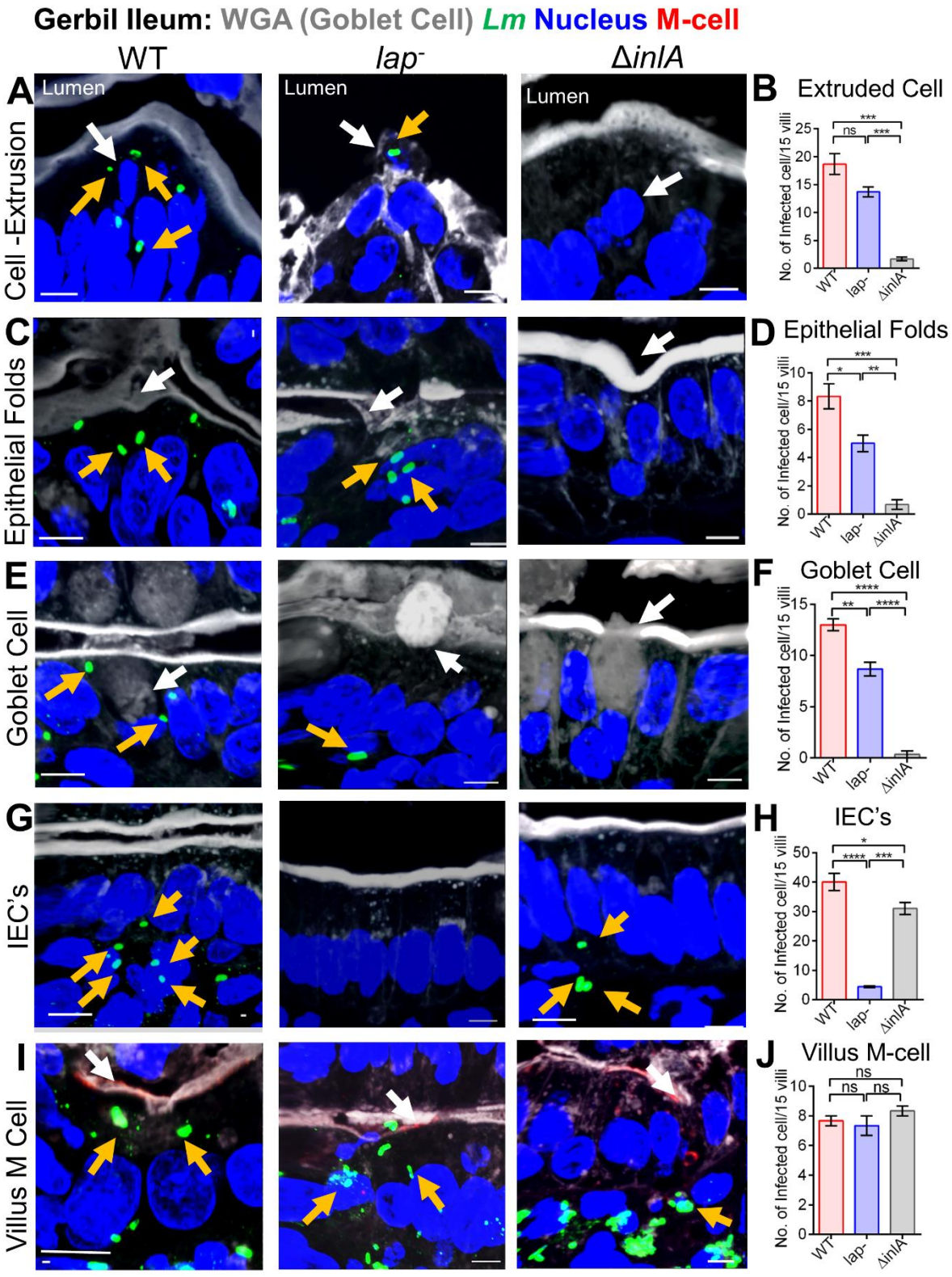
Gerbil Ileum: WGA (Goblet Cell) Lm Nucleus M-cell
WT
lap-
ΔinlA
A
Cell -Extrusion
Lumen
B Extruded Cell
C
Epithelial Folds
D Epithelial Folds
E
Goblet Cell
F Goblet Cell
G
IEC's
H IEC's
I
Villus M Cell
J Villus M-cell
No. of Infected cell/15 villi
ns
WT
lap-
ΔinlA

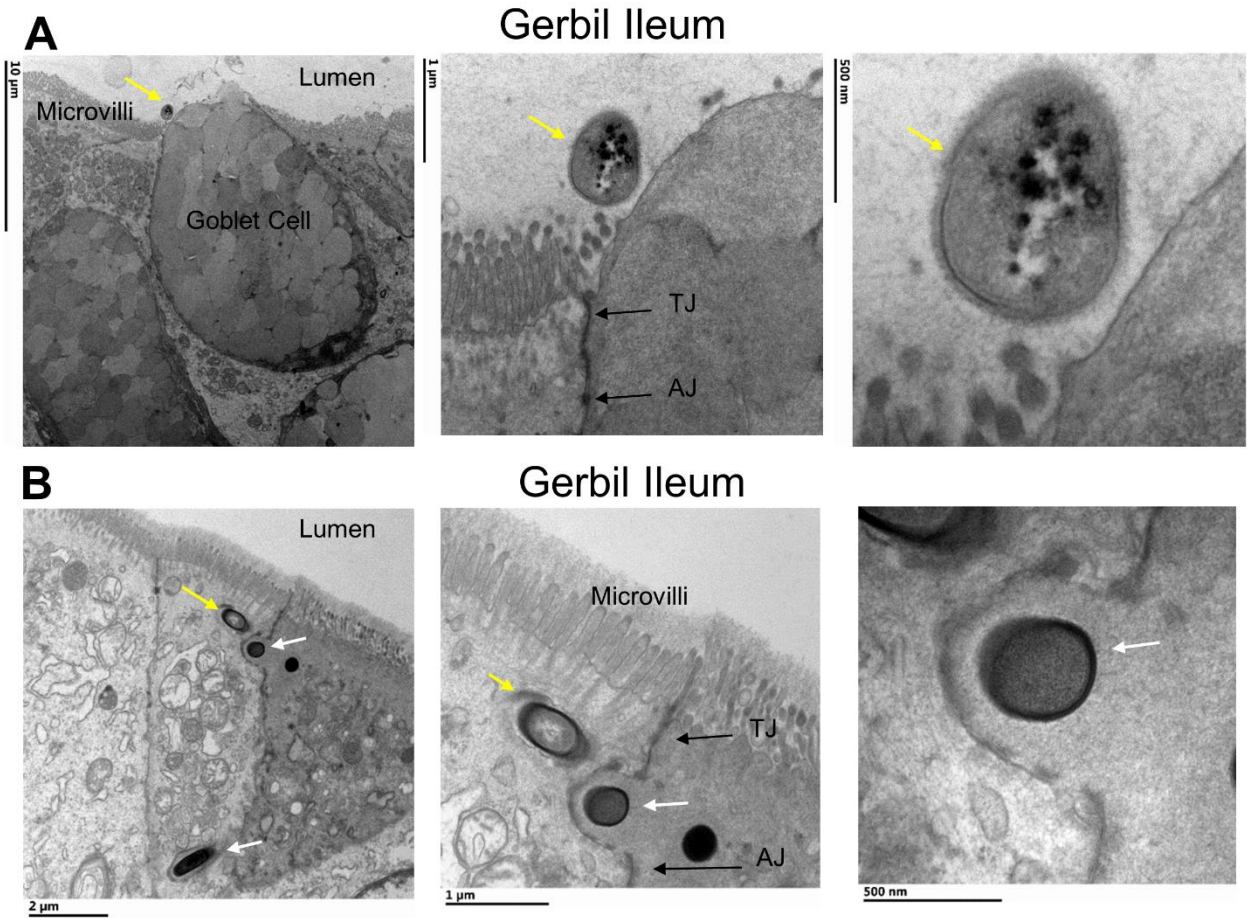

Figure 3.6. Transmission Electron Microscopic (TEM) images of *L. monocytogenes* translocation across intestinal cells.

(A-B) TEM image of ileal sections from *L. monocytogenes* (WT) infected gerbils at 48 h pi showing *L. monocytogenes* (yellow arrows) association at mucus-secreting goblet cell (**A**) and *L. monocytogenes* translocation across the junctional spaces of IEC's (**B,** white arrows) and present in the cytosol (**B**, yellow arrows). The panels on right of the image in A and B show enlargements. This image was acquired by Dr. Shivendra Tenguria.

Discussion

Previous work has demonstrated that *L. monocytogenes* uses the M-cell and the InlA-mediated pathways to invade and cross the intestinal barrier. However, *L. monocytogenes* is able to cross the intestinal barrier in animal models where both these pathways are absent such as the Peyer's patch-null mouse (Chiba et al., 2011; Pron et al., 1998). Additionally, *L. monocytogenes* isolates from clinical human cases have been found expressing a defective InlA (truncated protein) (Cruz et al. 2014; Fravalo et al. 2017) and infect human new-borns and fetuses of pregnant guinea pigs after oral dosing (Holch et al. 2013; Gelbicova et al. 2015). These observations strongly suggest InlA-and M-cell-independent route for *L. monocytogenes* to cross the intestinal barrier.

We have previously reported an InlA-independent translocation of *L .monocytogenes* which requires the engagement of LAP with its receptor Hsp60 leading to the activation of canonical NF-κB(p65) signaling, thereby promoting the MLCK-mediated opening of the intestinal cell-cell junction for bacterial translocation into the lamina propria and systemic dissemination in a mouse model (Drolia et al. 2018). Mice are non-permissive to InlA-E cadherin interactions (Lecuit et al. 1999). Therefore, the relative role of LAP *in vivo* in an InlA-permissive host (as humans) has not been determined. Here, we evaluated the relative contribution of LAP and InlA in *L .monocytogenes* crossing of the intestinal barrier, *in vivo* in a Mongolian gerbil model that is permissive to both InlA/E-cadherin and InlB/Met systems which allowed us to study the pathophysiology of listeriosis in animal models relevant to human listeriosis.

We observed that both the *lap*$^{-}$ strains and the Δ*inlA* were significantly impaired in the ability to cross the intestinal barrier, exit into the underlying lamina propria and disseminate systemically *in vivo* in a gerbil model. These data clearly suggest that both LAP-dependent paracellular translocation and InlA-mediated transcytosis is required for efficient crossing of *L. monocytogenes* across the intestinal barrier.

Previous work has identified that E-cadherin, the receptor for InlA, is accessible to luminally located *L. monocytogenes* around sites of epithelial cell extrusion at the tip of villi, at along villus epithelial folds and at mucus-expelling goblet cells (Nikitas et al. 2011). The interaction of *L. monocytogenes* InlA with accessible E-cadherin at these sites allows rapid (within 30–45 minutes) InlA-dependent translocation of the bacterium in the ligated jejunal loops in transgenic mice expressing human E-cadherin (Nikitas et al. 2011). However, the ability of *L. monocytogenes* to translocate across other possible routes such as by direct targeting of IECs that do not express luminally accessible E-cadherin at later time of infection *in vivo* has not been determined. Consistent with previous studies, we observed a significant defect of the Δ*inlA* strains in adhesion and translocation across cells that express luminally accessible E-cadherin *in vivo* in an InlA-permissive gerbil model of listeriosis. However, we also observed the WT and the Δ*inlA* strains also adhered and translocated across IEC's that do not express luminally accessible E-cadherin while the *lap*⁻ strains showed a significant defect in adhering at and translocating across these sites. These data suggest that *L. monocytogenes* uses LAP to directly target the cell-cell junction of IEC's where E-cadherin in luminally inaccessible for bacterial translocation to gain access to the underlying lamina propria for successful infection. These *in vivo* observations in an InlA-permissive host (gerbils) are consistent with our previous *in vitro* observations in polarized human enterocyte-like Caco-2 cell monolayers and *in vivo* in a mouse model (InlA-non permissive host) where we observed the WT and the Δ*inlA* strains caused the opening of the intestinal cell-cell junction via the cellular redistribution of the major junctional proteins, claudin-1, occludin and E-cadherin to facilitate bacterial translocation. In constrast, Caco-2 cells or mice infected with the *lap*⁻ strain maintained cell-cell junctional protein integrity and were significantly impaired in

translocating across the Caco-2 cells (Burkholder and Bhunia 2010) and the intestinal barrier of mice (Drolia et al. 2018).

Our results from InlA permissive gerbil model suggest that LAP-Hsp60-mediated translocation is an important precursor event for InlA-dependent epithelial translocation that provides access to E-cadherin in the AJ of IEC's that do not express luminally accessible E-cadherin of the InlA-permissive hosts (**Figure 3.7)**. Additionally, LAP-Hsp60-mediated paracellular translocation across IECs that do not express luminally accessible E-cadherin also serves as an active mechanism for InlA-independent translocation in InlA-permissive hosts such as humans, rabbits, guinea pigs, and gerbils in addition to epithelial invasion via ''villous cell extrusion'' (Pentecost et al. 2006) at the epithelial folds and the empty goblet cell junction (Nikitas et al. 2011) (**Figure 3.7)**.

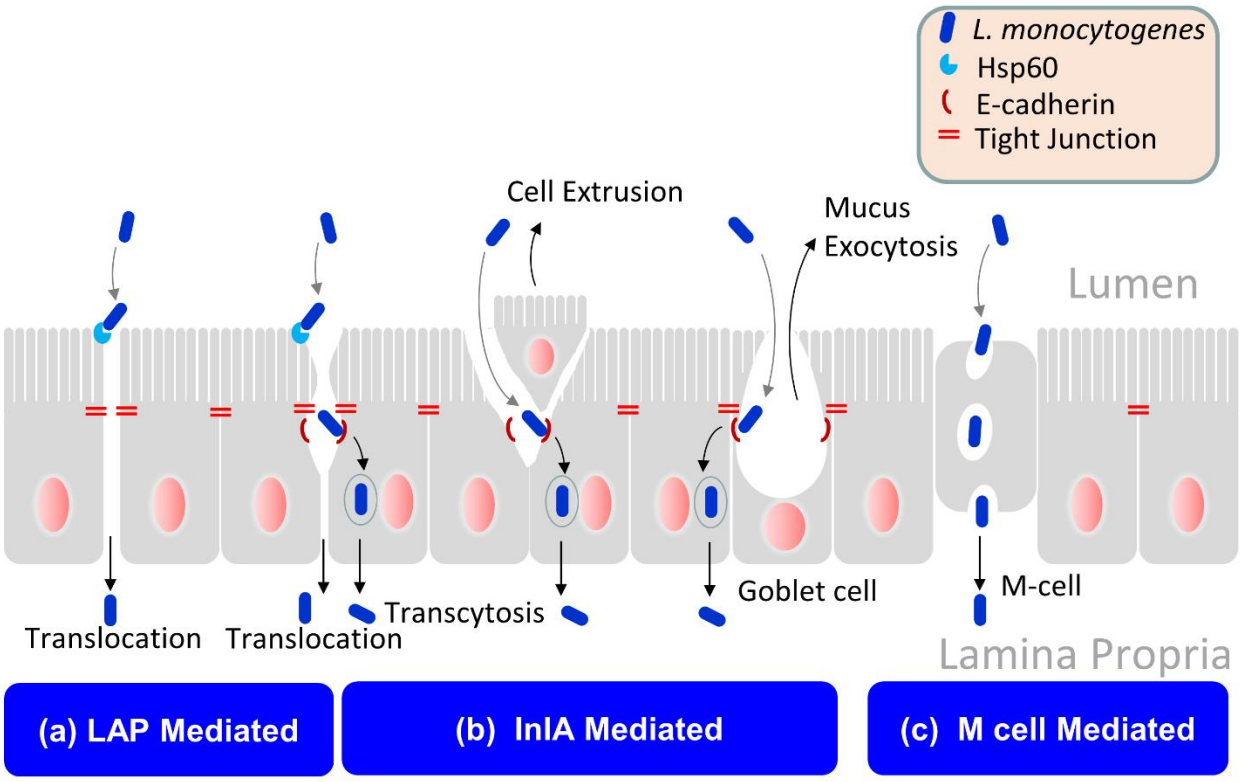

Figure 3.7. Schematic representation showing different routes used by *L. monocytogenes* to cross the gut epithelial barrier.

(**a**) *Listeria* adhesion protein (LAP)-mediated *L. monocytogenes* translocation involves the interaction of LAP with epithelial Hsp60 at IEC's that do not express luminally inaccessible E-cadherin for redistribution of the tight junction proteins (claudin-1 and occludin) the adherens junction protein E-cadherin, as well as the subsequent bacterial translocation.

(**b**) InlA/E-cadherin-mediated *L. monocytogenes* transcytosis, which occurs during epithelial cell extrusion or goblet cell mucus exocytosis, providing access of InlA to E-cadherin at the adherens junction.

(**c**) M cell-mediated *L. monocytogenes* translocation occurs in the Peyer's patches and at villus M-cells independently of LAP or InlA.

Author Contributions

Rishi Drolia and Dr. Arun K. Bhunia designed the experiments, performed the experiments, interpreted the data and wrote the manuscript. Dr. Shivendra Tenguria acquired the TEM images and assisted with animal experiments.

Experimental Model and Subject Details

Gerbil. Female Mongolian gerbils weighing 51-60 g (~8-10 week-old) were obtained from Charles River (stain 243). Following arrival, the gerbils were housed in a group of two gerbil/cage and provided mouse chow and water at libidum. On the day of the challenge, food and water were removed from the cages 12 h prior to oral gavage to prevent mechanical blockage of the *Listeria* inoculum by food in the stomach, which may cause the inoculum to aspirate into the lungs. The 12-h grown *L. monocytogenes* WT, *lap*$^{-}$, and *ΔinlA* strains, each resuspended in 200 µl of phosphate-buffered saline (PBS, pH 7.4) containing approximately 3×10^9 CFU were administered orally to randomly selected gerbil using a stainless steel ball-end feeding needle (Popper). The control gerbil received only PBS. The food was returned 1 h pi, and the gerbils were sacrificed 48 h pi using CO_2 asphyxiation. All animal procedure (IACUC Protocol no. 1201000595) was approved by the Purdue University Animal Care and Use Committee, who adheres to the recommendations of the Guide for the Care and Use of Laboratory Animals published by the National Institutes of Health.

Bacterial strains and growth conditions. The bacterial strains are listed in the **Key Resources Table 3.1** *L. monocytogenes* F4244 (WT) serovar 4b, the isogenic *lap*-deficient insertion mutant KB208 (*lap*$^{-}$) (Jagadeesan et al. 2010), and the Δ*inlA* in-frame deletion mutant (AKB301) (Burkholder and Bhunia 2010), were used. All of the *L. monocytogenes* strains were grown in

Tryptic soy broth containing 0.6% yeast extract (TSBYE; BD Bioscience) at 37°C with shaking for 12-16 h unless otherwise indicated. The *lap*$^{-}$ strain was grown in TSBYE containing erythromycin (Em; 5 µg/ml) at 42°C.

Method Details

Enumeration of *L. monocytogenes* in gerbil organs

To enumerate *Listeria* in the extra-intestinal sites, the organs were harvested aseptically following oral infection (48 h pi) and homogenized using a tissue homogenizer in 4.5 ml (spleen, and MLN) or 9 ml (liver) of buffered- *Listeria* enrichment broth (BLEB; Neogen) containing 0.1% Tween 20 and selective antimicrobial agents (Neogen). The samples were serially diluted in PBS and plated onto modified Oxford (MOX; Neogen) agar plates containing selective antimicrobial agents (Neogen). To enumerate *Listeria*, in the intestinal sites, the luminal contents from the harvested intestinal segments (ileum, cecum and colon) were gently removed. The segments were rinsed three times in a Perti-dish containing 10ml Dulbecco's Modified Eagle's medium (DMEM). The sections were then incubated for 2 h in 15ml of DMEM containing 100 µg/ml of gentamycin sulphate to kill the extracellular bacteria in the lumen. The sections were then rinsed three more times in 15 ml of DMEM and homogenized in a round-bottom tube using a tissue homogenizer in 1 ml BLEB. The samples were serially diluted in PBS and plated onto MOX agar plates supplemented with antimicrobial agents. In specific experiments, small sections of ileal and colonic tissues samples (1 cm) were cut and fixed overnight in 10% formalin for histopathology or immunostaining.

Immunofluorescence staining and confocal microscopy

The gerbil ileal and colonic tissue sections were collected and fixed with 10% formalin and embedded in paraffin. The tissues were sectioned (5 µm- thick), deparaffinized, and rehydrated for antigen retrieval by immersing the slides in boiling sodium citrate buffer (10 mM, pH 6.0) for 10 min. The tissue sections were permeabilized and blocked with PBS containing 0.3% Triton X-100 (Sigma-Aldrich) and 5% normal goat serum (Cell signaling) and immunostained with specific antibodies (**see Key Resources Table 3.1**) by incubating overnight at 4°C followed by Alexa Fluor-488, Alexa Fluor-555 conjugated secondary antibody with or without Alexa Fluor-647 conjugated-wheat germ agglutinin (WGA, which binds to sialic acid and N –acetylglucosaminyl carbohydrate residues on the plasma membrane of enterocytes and in mucus of goblet cells) for 2 h at room temperature followed by washing three times with PBS (3 cycles, 5 min). The nuclei were stained with DAPI (1 µg/ml; Cell signaling) and slides were mounted in ProLong antifade reagent (Cell Signaling).

All images were acquired using a Nikon A1R confocal microscope (equipped with 405nm/Argon/561nm lasers) using a Plan APO VC 60X/1.40 NA oil immersion objective with the Nikon Elements software (Nikon Instruments Inc.) at the Purdue Bindley Bioscience Imaging Facility. The X-Z and Y-Z cross-sections were produced by orthogonal reconstructions from z-stack scanning at 0.2µm intervals taken with 60X objective in 5 µm thick paraffin embedded tissue section. Three-dimensional reconstructions were performed using Nikon elements software (Nikon Instruments Inc.).

To enumerate the number infected cell types the number of *L. monocytogenes* positive cells from each of the following cell type: a) extruding cells, (b) epithelial folds, (c) goblet cells, (d) villous M cells and (e) other intestinal epithelial cells (IEC's) were counted from immunostained

images from 45 intact villi (15 villi each from 3 gerbil/ treatment) and expressed as number of infected cell/15 villi.

Analysis of *in vivo* intestinal permeability

Gerbils were orally gavaged with non-metabolizable 4 kDa FITC-labeled dextran (FD4; 36 mg/100 µl, Sigma-Aldrich) 4-5 h prior to sacrifice. Serum (50 µl each), collected above, were mixed with an equal volume of PBS, and fluorescence was measured (Em: 485 nm; Ex: 520 nm; Spectramax, Molecular Devices) and the FD4 concentration was calculated using a standard curve generated by serially diluting FD4 in PBS. The serum from the gerbil that were uninfected were used to determine the control levels.

Histopathology

Thin tissue sections from above were stained with hematoxylin and eosin, and a board-certified veterinary pathologist microscopically examined the slides and the interpretations were based on standard histopathological morphologies. The pathologist, was blinded to the bacterial strain, compared the ileal or the colonic sections to the controls.

To determine the extent of the inflammation, the gerbil ileal tissues were scored on a scale of 0-3 for two parameters yielding a maximum score of 6. The scoring parameters were the amount of polymorphonuclear leukocyte infiltrate and mononuclear infiltrate.

To determine the extent of the inflammation and damage, the gerbil colonic tissues were scored on a scale of 0-3 for five parameters yielding a maximum score of 15. The scoring parameters were the amount of polymorphonuclear leukocyte infiltrate, mononuclear infiltrate crypt cell death, erosion and submusoca involvement.

To grade the amount of polymorphonuclear leukocyte infiltrate and mononuclear infiltrate the following histomorphological scale was used: 3= markedly increased, 2= moderately increased,

1 = slightly increased and 0 = normal. To grade the involvement of the submucosa the following histomorphological scale was used: 3= 50% or greater of the submucosal diameter, 2= 10%-50%, 1 = <10% and 0 = normal.

Transmission Electron Microscopy (TEM)

Ileal tissue samples were washed thoroughly and fixed in 2.5% glutaraldehyde in 0.1 M sodium cacodylate buffer, post-fixed in buffered 1% osmium tetroxide containing 0.8% potassium ferricyanide, and en bloc stained with 1% aqueous uranyl acetate. Samples were then dehydrated with a graded series of acetonitrile and embedded in EMbed-812 resin. Thin sections (80 nm) were cut on a Leica EM UC6 ultramicrotome and stained with 2% uranyl acetate and lead citrate. Images were acquired on an FEI Tecnai G2 20 electron microscope equipped with a LaB6 source and operating at 100 kV.

Quantification and Statistical Analysis

Experimental data were analyzed using GraphPad Prism (La Jolla, CA) software. For gerbil microbial counts, statistical significance was assessed by Mann-Whitney test. In other experiments, comparisons between two data sets were performed using the unpaired Student *t*-test. When comparisons between more than two data sets were performed, a one-way or a two-way analysis of variance with Tukey's multiple-comparison test were performed. All data are representative of at least 2-3 independent experiments and specific numbers of gerbil per group are noted in corresponding figure legends. Unless otherwise indicated, data for all experiments are presented as the mean ± standard error of the mean (SEM).

Table 3.1 Key Resource Table

REAGENT or RESOURCE	SOURCE	IDENTIFIER
Antibodies		
Rat anti-Microfold (M) cell pure, mouse antibody	Miltenyi Biotec	Cat # 130-096-148, RRID: AB_2660297
Rat monoclonal anti- ZO-1	Supernatant from the Anti-ZO-1 hybridoma R40.76	RRID: AB_628459
Rabbit polyclonal anti-*Listeria*	Our Lab (Geng et al. 2004)	N/A
Goat anti-rat IgG (H+L), (Alexa Fluor 555 Conjugate) antibody	Cell Signaling	Cat # 4417, RRID: AB_10696896
Goat anti-mouse IgG (H+L), F(ab')2 Fragment (Alexa Fluor 555 Conjugate) antibody	Cell Signaling	Cat # 4409, RRID: AB_1904022
Goat anti-rabbit IgG (H+L), F(ab')2 Fragment (Alexa Fluor 488 Conjugate) antibody	Cell Signaling	Cat # 4412, RRID: AB_1904025
Bacterial and Virus Strains		
L. monocytogenes F4244 (WT)	CDC, Atlanta, GA	N/A
L. monocytogenes KB208 (*lap*$^{-}$)	(Jagadeesan et al. 2010)	N/A
L. monocytogenes AKB301 (Δ*inlA*)	(Burkholder and Bhunia 2010)	N/A
Chemicals, Peptides, and Recombinant Proteins		
Modified Oxford agar Base	Neogen Corporation	Cat # 7428
Modified Oxford agar Base supplement	Neogen Corporation	Cat # 7991
Buffered *Listeria* enrichment broth	Neogen Corporation	Cat # 7675
Buffered *Listeria* enrichment broth supplement	Neogen Corporation	Cat # 7980
DAPI	Cell Signaling	Cat # 4083
FITC-labeled 4 kDa dextran	Sigma-Aldrich	Cat # 46944
WGA-Alexa Fluor 647 conjugate	Thermo Fisher Scientific	Cat # W32466
Experimental Models: Organisms/Strains		
Gerbil: Mangolian	Charles River	Strain # 243
Software and Algorithms		
GraphPad Prism 6.0	GraphPad Software	https://www.graphpad.com/scientific-software/prism/
Microsoft Excel	Microsoft	https://products.office.com/en-us/excel

Table 3.1 continued

Nikon Elements	Nikon	https://www.nikoninstruments.com/Products/Software/NIS-Elements-Basic-Research

CHAPTER 4. CONCLUSIONS AND FUTURE PRESPECTIVE

The following chapter is under revision for publication and is modified from: Drolia, R. and Bhunia, A.K. Crossing the Intestinal Barrier Via *Listeria* Adhesion Protein and Internalin A Trends in Microbiology TIMI-D-18-00177.

Summary

The intestinal epithelial cell lining provides the first line of defense, yet foodborne pathogen such as *Listeria monocytogenes* can overcome this barrier; however, the underlying mechanism is not well understood. Though the host M cells in the Peyer's patch and the bacterial invasion protein Internalin A (InlA) are involved, *L. monocytogenes* can cross the gut barrier in their absence. The interaction of *Listeria* adhesion protein (LAP) with host cell receptor (heat shock protein 60) disrupts the epithelial barrier, promoting bacterial translocation. InlA aids *L. monocytogenes* transcytosis via interaction with E-cadherin receptor, which is facilitated by epithelial cell extrusion and goblet cell exocytosis; however, LAP-induced cell junction opening may be an alternate bacterial strategy for InlA access to E-cadherin and its translocation. Here, we summarize the strategies *L. monocytogenes* employs to circumvent the intestinal epithelial barrier. Additionally, we provide implications of recent findings for food safety regulations.

Highlights

1. Intestinal epithelial cells are the first line of defense against enteric pathogens.

2. Bacterial pathogens such as *L. monocytogenes* have evolved sophisticated mechanisms to breach this barrier.

3. *L. monocytogenes* invasion protein Internalin A (InlA) targets its basolateral receptor, E-cadherin, by host intrinsic mechanisms: the epithelial cell extrusion and goblet cell exocytosis allowing its transcytosis across the intestinal barrier.

4. The *Listeria* adhesion protein (LAP) engages its surface receptor; Hsp60, and initiates a complex signaling cascade leading to cellular redistribution of cell-to-cell junctional proteins for *L. monocytogenes* translocation.

5. *L. monocytogenes* capitalizes on two most dominant pathways: LAP-mediated and InlA-mediated for by-passing the critical intestinal barrier and successful infection.

LAP Promotes *L. monocytogenes* Translocation *In Vivo*

LAP induces intestinal barrier dysfunction for *L. monocytogenes* translocation across the epithelial barrier *in vivo*. In orally infected mice (non-permissive to InlA/E-cadherin interaction) and gerbils (permissive to InlA/E-cadherin interaction), the translocation of the *lap*-deficient *L. monocytogenes* strain from the lumen to the underlying lamina propria of the intestinal epithelium and to the MLN, liver, and spleen is significantly impaired (Drolia et al. 2018). In contrast, the Δ*inlA* strain translocated as efficiently as the WT strain in a mouse model (Drolia et al. 2018). However, mice infected intraperitoneally, a route that bypasses the intestinal barrier; both the WT and the *lap*-deficient *L. monocytogenes* strain translocate to liver almost in equal numbers [80] suggesting that LAP has an important role in the intestinal phase of infection but not in the late stages of infection. LAP increases intestinal epithelial permeability, which positively correlates with translocation of *Listeria* into the underlying lamina propria. In mouse ileal tissue, *L. monocytogenes* WT and Δ*inlA* cells were co-localized with ZO-1, which is a TJ protein, and these strains were observed to exit into the lamina propria while the *lap*$^{-}$ strain remained confined to the gut lumen (Drolia et al. 2018) (**Figures 4.1A and 4.1B**).

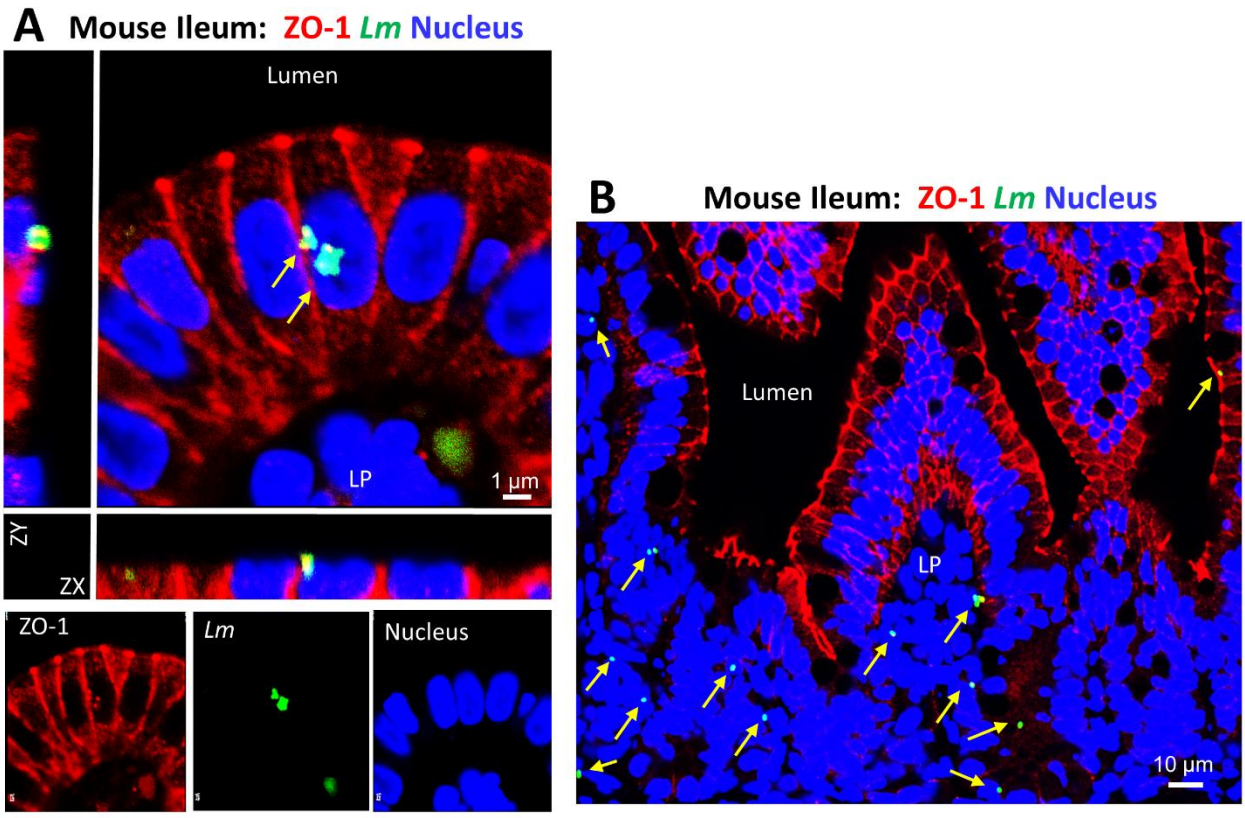

Figure 4.1. *Listeria monocytogenes* translocation through the intestinal epithelium.

(A) Confocal microscopic images showing wild-type *L. monocytogenes* (F4244) localization in the mouse ileal epithelial cell junction (48 h post-infection) immunostained for ZO-1 (red), *L. monocytogenes* (*Lm*, green, arrows), and nucleus (blue). *L. monocytogenes* (arrows) is observed exiting the epithelial cell into the underlying lamina propria (LP) and co-localized with ZO-1 (ZY axis and ZX axis images). Scale bar, 1 µm. Bottom panel displays separate channels individually.

(B) Confocal microscopic images of ileal villi immunostained for ZO-1 (red), *L. monocytogenes* F4244 (*Lm*) (green, arrows), and nucleus (blue) of mice orally infected with wild-type *L. monocytogenes* for 48 h post-infection. *L. monocytogenes* (green, arrows) cells are visible in the lamina propria (LP). Scale bar, 10 µm.

Exploiting the Epithelial Innate Immunity

LAP activates canonical NF-κB signaling, a central regulator of innate immunity (Elewaut et al. 1999) in Caco-2 cells and mouse ileum for increased epithelial permeability (Elewaut et al. 1999; Drolia et al. 2018). The dynamics of LAP-mediated NF-κB and MLCK activation is well studied and is dependent on the engagement of LAP with its surface receptor Hsp60**.** The

interaction of LAP with Hsp60 leads to the internalization of surface Hsp60 to bind with the IκB kinase (IKK) complex. This activates IKK which induces the degradation of inhibitors of kB (IkB)-α and facilitates the activation, nuclear translocation and phosphorylation of NF-κB (p65) (**Figure 4.2**). The LAP-mediated increase in epithelial permeability correlates with the increased expression of the NF-κB-regulated pro-inflammatory cytokines TNF-α and IL-6. Furthermore, NF-κB inhibitors significantly reduce LAP-mediated NF-κB activation, epithelial permeability, and *L. monocytogenes* translocation across polarized Caco-2 cells (Drolia et al. 2018). Additionally, in the mouse ileal villi, Hsp60 localizes at the plasma membrane of epithelial cells and is thus accessible to bacteria located in the intestinal lumen. Therefore, *L. monocytogenes* uses LAP to exploit epithelial innate defenses and induce intestinal barrier dysfunction.

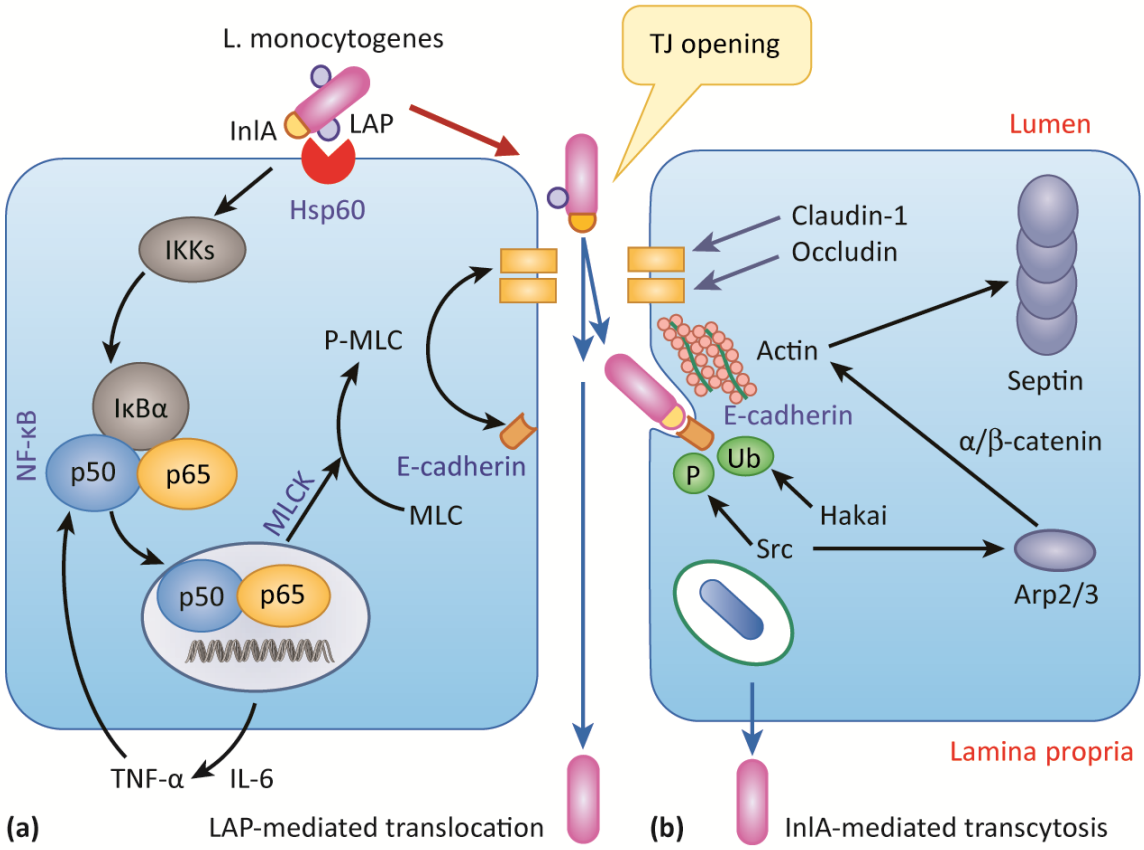

Figure 4.2. Detailed schematic showing the dynamics of *L. monocytogenes* epithelial barrier crossing strategies.

(a) Dynamics of the LAP/Hsp60 interaction. LAP binds to its epithelial receptor Hsp60 in the plasma membrane. Upon engagement of its surface receptor Hsp60, it is redistributed to the cytosol to directly interact with IKK, which leads to the activation of the canonical NF-κB pathway. NF-κB activation results in the secretion of proinflammatory cytokines TNFα and IL-6, leading to increased epithelial permeability. Activated NF-κB induces activation of myosin light chain kinase (MLCK), which phosphorylates myosin light chain (MLC). Phosphorylated MLC triggers the redistribution of junctional proteins (claudin-1, occludin, and E-cadherin) for junctional opening, which allows for subsequent bacterial translocation. The LAP-Hsp60-mediated junctional opening may also facilitate InlA access to E-cadherin at the AJ for InlA-mediated translocation.

(b) Dynamics of the InlA/E-cadherin interaction. Upon interaction of InlA with E-cadherin at the AJ, the junctional machinery is activated leading to caveolin-dependent clustering of E-cadherin. Two post translational modifications occur at this stage: Src-dependent phosphorylation of E-cadherin followed by Hakai dependent ubiquitination of E-cadherin. This results in a recruitment of clathrin and multiple components of the endocytic machinery, which works with the actin machinery to promote bacterial uptake. Two pathways link E-cadherin to actin polymerization: (a) direct interaction of α-catenin and β-catenin (b) Src-dependent activation of the Arp2/3 complex followed by recruitment of septin at the site of entry. These events lead to the generation of caveolin and clathrin-coated pit for bacterial internalization as well as epithelial barrier crossing by transcytosis.

E-cadherin Dilemma-in the Epithelial Barrier Architecture

It is now clear that *L. monocytogenes* uses the LAP-mediated pathway to establish infection by directly shifting junctional protein composition. InlA employs E-cadherin as the receptor, but *L. monocytogenes* redistributes E-cadherin to facilitate bacterial translocation during infection (Drolia et al. 2018), raising an intriguing question: at what stage during the infection process does InlA interact with E-cadherin? If the initial LAP-mediated interaction causes a redistribution of membrane E-cadherin to be endocytosed for cell junction opening, there are possibly remnants of membrane E-cadherin left to interact with InlA to proceed with InlA-mediated bacterial uptake and invasion. Since earlier studies reported that InlA-mediated transcytosis takes place only after 48-72 hpi (Wollert et al. 2007; Chiba et al. 2011; Bou Ghanem et al. 2012; Bergmann et al. 2013), it is possible that during the early infection phase, *L. monocytogenes* capitalizes on the LAP-Hsp60-mediated translocation pathway to gain access for successful infection. This flexibility may make the bacterium far less susceptible to clearance by the innate immune defense by providing easier access to the lamina propria early in the infection process. Furthermore, LAP-Hsp60-mediated translocation may also serve as an important precursor event for InlA-dependent epithelial translocation that provides access to E-cadherin in the adherens junction of the permissive hosts such as gerbils, guinea pigs, and humans in addition to epithelial invasion via villous cell extrusion (Pentecost et al. 2006) and at the empty goblet cell junction (Nikitas et al. 2011) as the infection continues (**Figure 4.3**).

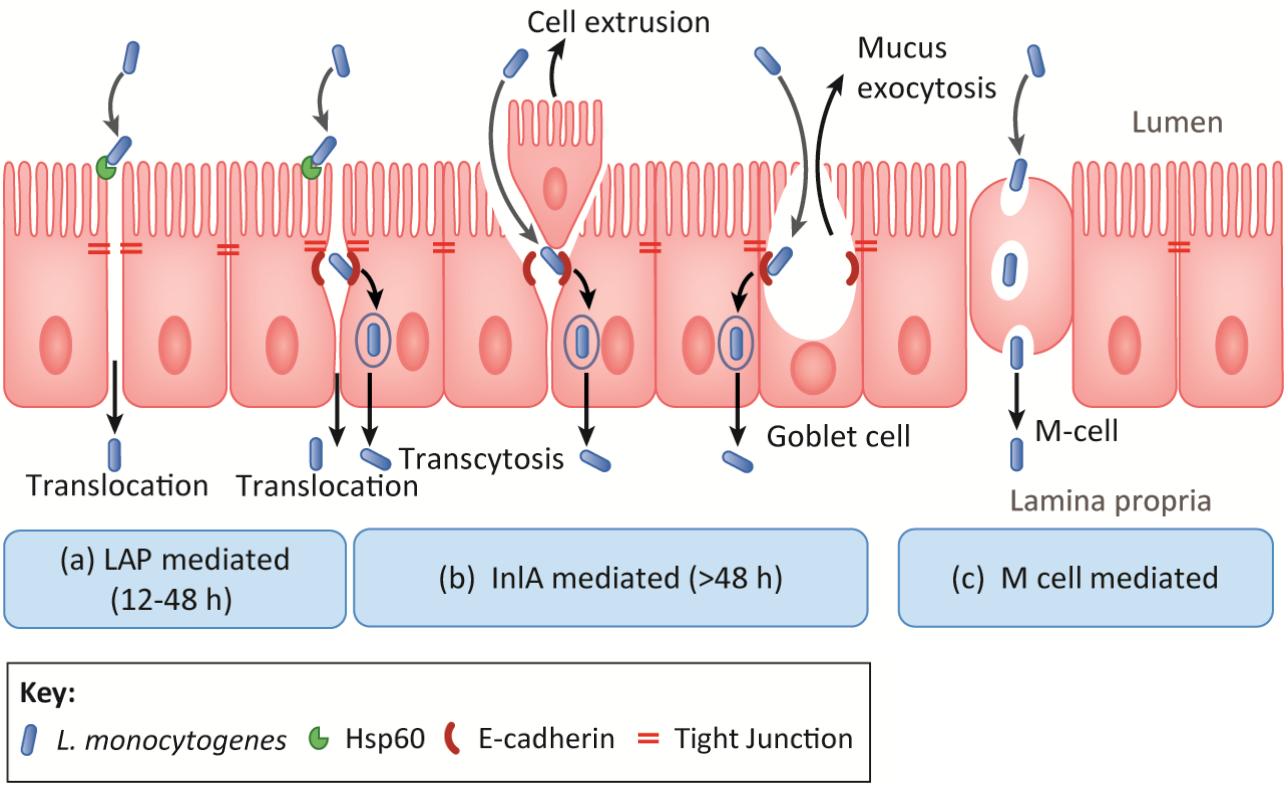

Figure 4.3. Detailed schematic showing *L. monocytogenes* epithelial barrier crossing routes. **(a)** *Listeria* adhesion protein (LAP)-mediated *L. monocytogenes* translocation involves the interaction of LAP with epithelial Hsp60 for redistribution of the tight junction proteins claudin-1 and occludin) the adherens junction protein E-cadherin, as well as the subsequent bacterial translocation. **(b)** InlA/E-cadherin-mediated *L. monocytogenes* transcytosis, which occurs during epithelial cell extrusion or goblet cell mucus exocytosis, providing access of InlA to E-cadherin at the adherens junction. (**c**) M cell-mediated *L. monocytogenes* translocation occurs in the Peyer's patches.

Concluding Remarks and Future Perspective

The epithelial cells in the gastrointestinal tract provide the first line of defense against luminal microbes from crossing the gut wall. In healthy humans, the epithelial barrier is tightly controlled, and it allows selective passage of nutrients, drugs, and small molecules, but it prevents passage of luminal microbes including pathogens. *L. monocytogenes* being a foodborne pathogen has to cross the gut barrier to enter the blood circulation and disseminate to the MLN, liver, spleen, brain, and placenta (in pregnant women) for successful infection. It has been well-

established that for *L. monocytogenes* to cross the epithelial barrier, InlA is responsible and it is considered the most important protein for epithelial cell invasion (Radoshevich and Cossart 2018). However, some *L. monocytogenes* isolates from the environment or food sources naturally carry truncated InlA with a premature stop codon, and these isolates were considered less invasive (Olier et al. 2003; Nightingale et al. 2005; Van Stelten et al. 2011). Conversely, in recent years, *L. monocytogenes* strains with defective InlA were responsible for neonatal listeriosis in humans (Cruz et al. 2014; Gelbicova et al. 2015; Fravalo et al. 2017), mice, and guinea pigs after oral challenge (Holch et al. 2013). Other virulence factors such as Vip (Cabanes et al. 2005) and LapB (Reis et al. 2010) have been described in the literature and help *Listeria* to invade cells, but their contribution in *L. monocytogenes* crossing of the intestinal epithelial barrier has not been well defined.

LAP aids *L. monocytogenes* in crossing the gut epithelial barrier during the early stage of infection. LAP is an house-keeping enzyme (alcohol acetaldehyde dehydrogenase) required for bacterial growth under anaerobic conditions (Burkholder et al. 2009; Jagadeesan et al. 2010; Mueller-Herbst et al. 2014) and at the same time, it helps *L. monocytogenes* to attach to the intestinal cells by interacting with the cellular receptor Hsp60; thus, LAP is considered a prototypical moonlight protein (Henderson et al. 2013). LAP orchestrates a complex cell signaling event to activate regulatory molecules, NF-κB, and MLCK to regulate the opening of the epithelial cell–cell junction (Drolia et al. 2018). The intestinal cell junction opening allows *L. monocytogenes* to cross the gut barrier very early in the infection process (in a few hours) as soon as the bacterium reaches the intestine when the immune system is not very active. It is clear that *L. monocytogenes* uses two dominant pathways, LAP-mediated (Drolia et al. 2018) followed by InlA-mediated (Wollert et al. 2007; Disson et al. 2008; Bou Ghanem et al. 2012) or their

cooperative action (**Figures 4.2 and 4.3**), to enter the host tissues, thus making this bacterium a very successful infective foodborne pathogen, especially in high-risk immunocompromised individuals. However, the role of other *Listeria* proteins, the gut microbiota and the immune status of the host cannot be ignored since the bacterium may employ several virulence factors (Camejo et al. 2011) and multiple independent routes (Zhang et al. 2017) to be highly invasive (**see Outstanding Questions**). This may also explain why *L. monocytogenes* has such a low infectious dose (Pouillot et al. 2016; Buchanan et al. 2017) and the highest hospitalization and mortality rate among the foodborne pathogens (Scallan et al. 2011). Thus, RTE foods containing even a few *L. monocytogenes* cells such as <100 CFU/g as defined in food regulations by the European Union (Ricci et al. 2018) would be a huge risk to the growing worldwide population with underlying chronic health conditions including diabetes mellitus, cancer, HIV/AIDS, alcoholism, cirrhosis, opioid addiction, malnutrition, and diseases related to smoking (McNeill et al. 2017). Future research focused on deeper understanding of the molecular and cellular mechanisms that *L. monocytogenes* and other bacterial foodborne pathogens employ to cross the intestinal barrier will help in drug design and therapeutics for preventing fatal systemic infections.

Outstanding Questions

1. Does interaction of LAP with Hsp60 initiate other signaling pathway(s) besides NF-κB and MLCK?

2. Does immunocompromised condition increase susceptibility to listeriosis by enhancing enterocyte Hsp60 expression?

3. Does *L. monocytogenes* target other tight junction components such as tricellulin and desmosomes for cell junction breach?

4. What other mechanism(s), besides bacteriocin does *L. monocytogenes* employ to modulate the host gut microbiota

GLOSSARY

Goblet cells: A specialized secretory cell that synthesize and secrete mucin glycoproteins and other components of the mucus.

Enterocytes: Columnar epithelial cells with apical microvilli and are most abundant cells in the small intestine. Forms a major barrier to the resident intestinal microbiota and to pathogens in the gastrointestinal tract.

Mucins: A high molecular weight, heavily glycosylated proteins that coats the surfaces of cells that line the respiratory, digestive and urogenital tracts. Rich in complex O-linked oligosaccharides.

Mucus: A viscous, fluid layer that overlies the mucosal surface and contains secreted mucin glycoproteins and other molecules involved in host defense against infection.

Tight Junction (TJ): Also known as the zonula occludens. It is the most apical junction along the lateral surface that create a barrier and regulates the diffusion of ions and solutes.

Adherens Junction (AJ): Also known as zonula adherens. Located below the tight junction between adjoining epithelial cells. It is an adhesive junction that maintains cell-cell adhesion and is composed of cadherin and transmembrane adhesion molecules connected to the actin cytoskeleton.

Desmosome: Also known as macula adherens. Located beneath the apical junctional complex. Desmosomes is composed of transmembrane cadherins of two subtypes, desmoglein and desmocollin and adaptor protein plakoglobin, plakophillin and desmoplakin.

Apical Junctional Complex: Three types of intercellular junctions (TJ, AJ and desmosomes) comprise the apical junctional complex. It consists of a network of transmembrane, scaffolding, and signaling proteins, and serves as a barrier, adhesion site, and signaling complex to control cell polarity, proliferation, and differentiation.

Myosin Light Chain Kinase: The Ca^{2+}–calmodulin-dependent kinase that phosphorylates myosin II regulatory light chain at serine 19 and threonine 18 to activate myosin ATPase.

E-cadherin: Belongs to the family of classical cadherins. A Ca^{2+}-dependent cell–cell adhesion molecule that mediates the formation of adherens junctions between polarized epithelial cells and plays an important role in cell sorting during development.

Lamina Propria: Located beneath the basement membrane and contains immune cells, including macrophages, dendritic cells, plasma cells, lymphocytes and neutrophils.

Macropinocytosis: An invagination of the cell membrane to form a vesicle at highly ruffled regions of the plasma membrane. The internalized vesicle fuses with lysosomes or endosomes.

Clathrin: A molecular scaffold for vesicular uptake of cargo at the plasma membrane.

Caveolin: Specialized invaginations of the plasma membrane that contains caveolin-1 protein and cholesterol. The caveolin aids in the uptake of some extracellular materials and are involved in cell signaling.

M Cells: Specialized epithelial cells of the MALT that transport antigens, bacteria and viruses from the lumen to the underlying immune cells, thereby initiating a systemic immune response or tolerance.

Peyer's Patch: Organized lymphoid follicles that form the interface between the **GALT** and the luminal microenvironment. Peyer's Patch plays an important role in the immune surveillance of the intestinal lumen and facilitates the generation of the immune response within the mucosa.

Hsp60: A mitochondrial chaperonin that is responsible for the transportation and refolding of proteins from the cytoplasm into the mitochondrial matrix.

microRNA (miRNA): Small non-coding, naturally occurring RNA molecules. These are complementary to one or more messenger RNA (mRNA) molecules and functions to downregulate gene expression by translational repression, mRNA cleavage, and deadenylation.

Toll-like receptors (TLR): The first identified family of pattern recognition receptors (PRRs) and are expressed either on the cell surface or associated with intracellular vesicles.

Nucleotide-binding oligomerization domain 2 (NOD2): An intracellular pattern recognition receptor (PRR) that senses bacterial peptidoglycan in cytosol and elicits host immune response.

Mucosa-associated lymphoid tissue (MALT): MALT contains an array of lymphocytes such as B cells, T cells, plasma cells, and dendritic cells and macrophages. MALT is found in the mucosal linings of organs such as the gastrointestinal tract, lungs, salivary glands and conjunctiva.

Gut-associated lymphoid tissue (GALT): GALT consists of both isolated and aggregated lymphoid follicles and is part of the MALT that is comprised of lymphoid tissues and organs located directly beneath the mucosal epithelium.

Nuclear factor–κB (**NF-κB):** Transcription factor proteins that play pivotal role in regulating the expression of genes in many biological processes including innate and adaptive immunity, inflammation, stress responses, B-cell development, and lymphoid organogenesis. These proteins consist of five family members; NF-κB2 (p52/p100), NF-κB1 (p50/p105), c-Rel, RelA/p65, and RelB.

REFERENCES

Abreu, M.T., Thomas, L.S., Arnold, E.T., Lukasek, K., Michelsen, K.S. and Arditi, M. (2003) TLR signaling at the intestinal epithelial interface. *J Endotox Res* **9**, 322-330.

Al Nabhani, Z., Dietrich, G., Hugot, J.-P. and Barreau, F. (2017) Nod2: the intestinal gate keeper. *PLoS Pathog* **13**, e1006177.

Alnabhani, Z., Montcuquet, N., Biaggini, K., Dussaillant, M., Roy, M., Ogier-Denis, E., Madi, A., Jallane, A., Feuilloley, M. and Hugot, J.-P. (2015) *Pseudomonas fluorescens* alters the intestinal barrier function by modulating IL-1β expression through hematopoietic NOD2 signaling. *Inflamm Bowel Dis* **21**, 543-555.

Alto, N.M., Shao, F., Lazar, C.S., Brost, R.L., Chua, G., Mattoo, S., McMahon, S.A., Ghosh, P., Hughes, T.R. and Boone, C. (2006) Identification of a bacterial type III effector family with G protein mimicry functions. *Cell* **124**, 133-145.

Amieva, M.R., Vogelmann, R., Covacci, A., Tompkins, L.S., Nelson, W.J. and Falkow, S. (2003) Disruption of the epithelial apical-junctional complex by *Helicobacter pylori* CagA. *Science* **300**, 1430-1434.

Archambaud, C., Nahori, M.-A., Soubigou, G., Bécavin, C., Laval, L., Lechat, P., Smokvina, T., Langella, P., Lecuit, M. and Cossart, P. (2012) Impact of lactobacilli on orally acquired listeriosis. *Proc Nat Acad Sci USA* **109**, 16684-16689.

Archambaud, C., Sismeiro, O., Toedling, J., Soubigou, G., Bécavin, C., Lechat, P., Lebreton, A., Ciaudo, C. and Cossart, P. (2013) The intestinal microbiota interferes with the microRNA response upon oral Listeria infection. *mBio* **4**, e00707-00713.

Bailey, T.W., do Nascimento, N.C. and Bhunia, A.K. (2017) Genome sequence of *Listeria monocytogenes* strain F4244, a 4b serotype. *Genome Announcements* **5**, e01324-01317.

Baldwin, D.N., Vanchinathan, V., Brown, P.O. and Theriot, J.A. (2003) A gene-expression program reflecting the innate immune response of cultured intestinal epithelial cells to infection by *Listeria monocytogenes*. *Genome Biol* **4**, art. no.-R2.

Barreau, F. and Hugot, J.P. (2014) Intestinal barrier dysfunction triggered by invasive bacteria. *Curr Opin Microbiol* **17**, 91-98.

Batz, M., Hoffmann, S. and Morris Jr, J.G. (2014) Disease-outcome trees, EQ-5D scores, and estimated annual losses of quality-adjusted life years (QALYs) for 14 foodborne pathogens in the United States. *Foodborne Pathog Dis* **11**, 395-402.

Becattini, S., Littmann, E.R., Carter, R.A., Kim, S.G., Morjaria, S.M., Ling, L., Gyaltshen, Y., Fontana, E., Taur, Y. and Leiner, I.M. (2017) Commensal microbes provide first line defense against *Listeria monocytogenes* infection. *J Exp Med* **214**, 1973-1989.

Becattini, S. and Pamer, E.G. (2017) Multifaceted defense against *Listeria monocytogenes* in the gastro-intestinal lumen. *Pathogens* **7**, 1.

Berger, E., Rath, E., Yuan, D., Waldschmitt, N., Khaloian, S., Allgäuer, M., Staszewski, O., Lobner, E.M., Schöttl, T. and Giesbertz, P. (2016) Mitochondrial function controls intestinal epithelial stemness and proliferation. *Nat Comm* **7**, 13171.

Bergmann, S., Beard, P.M., Pasche, B., Lienenklaus, S., Weiss, S., Gahan, C.G., Schughart, K. and Lengeling, A. (2013) Influence of internalin a murinisation on host resistance to orally acquired listeriosis in mice. *BMC Microbiol* **13**, 90.

Bierne, H. and Cossart, P. (2007) *Listeria monocytogenes* surface proteins: from genome predictions to function. *Microbiol Mol Biol Rev* **71**, 377-397.

Bierne, H., Garandeau, C., Pucciarelli, M.G., Sabet, C., Newton, S., Garcia-del Portillo, F., Cossart, P. and Charbit, A. (2004) Sortase B, a new class of sortase in *Listeria monocytogenes*. *J Bacteriol* **186**, 1972-1982.

Bierne, H., Mazmanian, S.K., Trost, M., Pucciarelli, M.G., Liu, G., Dehoux, P., Jansch, L., Garcia-del Portillo, F., Schneewind, O. and Cossart, P. (2002) Inactivation of the srtA gene in *Listeria monocytogene*s inhibits anchoring of surface proteins and affects virulence. *Mol Microbiol* **43**, 869-881.

Bierne, H., Milohanic, E. and Kortebi, M. (2018) To be cytosolic or vacuolar: the double life of *Listeria monocytogenes*. *Front Cell Infect Microbiol* **8**, 136.

Boller, K., Vestweber, D. and Kemler, R. (1985) Cell-adhesion molecule uvomorulin is localized in the intermediate junctions of adult intestinal epithelial cells. *J Cell Biol* **100**, 327-332.

Bonazzi, M., Veiga, E., Pizarro-Cerda, J. and Cossart, P. (2008) Successive post-translational modifications of E-cadherin are required for InlA-mediated internalization of *Listeria monocytogenes*. *Cell Microbiol* **10**, 2208-2222.

Bou Ghanem, E.N., Jones, G.S., Myers-Morales, T., Patil, P.D., Hidayatullah, A.N. and D'Orazio, S.E. (2012) InlA promotes dissemination of *Listeria monocytogenes* to the mesenteric lymph nodes during food borne infection of mice. *PLoS Pathog* **8**, e1003015.

Boyle, E.C., Brown, N.F. and Finlay, B.B. (2006) *Salmonella enterica* serovar Typhimurium effectors SopB, SopE, SopE2 and SipA disrupt tight junction structure and function. *Cell Microbiol* **8**, 1946-1957.

Brandl, K., Plitas, G., Schnabl, B., DeMatteo, R.P. and Pamer, E.G. (2007) MyD88-mediated signals induce the bactericidal lectin RegIIIγ and protect mice against intestinal *Listeria monocytogenes* infection. *J Exp Med* **204**, 1891-1900.

Braun, L., Dramsi, S., Dehoux, P., Bierne, H., Lindahl, G. and Cossart, P. (1997) InIB: An invasion protein of *Listeria monocytogenes* with a novel type of surface association. *Mol Microbiol* **25**, 285-294.

Brugere-Picoux, J. (2008) Ovine listeriosis. *Small Ruminant Res* **76**, 12-20.

Buchanan, R.L., Gorris, L.G., Hayman, M.M., Jackson, T.C. and Whiting, R.C. (2017) A review of *Listeria monocytogenes*: An update on outbreaks, virulence, dose-response, ecology, and risk assessments. *Food Control* **75**, 1-13.

Burkholder, K.M. and Bhunia, A.K. (2010) *Listeria monocytogenes* uses *Listeria* adhesion protein (LAP) to promote bacterial transepithelial translocation, and induces expression of LAP receptor Hsp60. *Infect Immun* **78**, 5062-5073.

Burkholder, K.M., Kim, K.-P., Mishra, K., Medina, S., Hahm, B.-K., Kim, H. and Bhunia, A.K. (2009) Expression of LAP, a SecA2-dependent secretory protein, is induced under anaerobic environment. *Microbes Infect* **11**, 859-867.

Cabanes, D., Sousa, S., Cebria, A., Lecuit, M., Garcia-del Portillo, F. and Cossart, P. (2005) Gp96 is a receptor for a novel *Listeria monocytogenes* virulence factor, Vip, a surface protein. *EMBO J* **24**, 2827-2838.

Camejo, A., Carvalho, F., Reis, O., Leitao, E., Sousa, S. and Cabanes, D. (2011) The arsenal of virulence factors deployed by *Listeria monocytogenes* to promote its cell infection cycle. *Virulence* **2**, 379-394.

Chiba, S., Nagai, T., Hayashi, T., Baba, Y., Nagai, S. and Koyasu, S. (2011) Listerial invasion protein internalin B promotes entry into ileal Peyer's patches in vivo. *Microbiol Immunol* **55**, 123-129.

Chun, J.N., Choi, B., Lee, K.W., Lee, D.J., Kang, D.H., Lee, J.Y., Song, I.S., Kim, H.I., Lee, S.-H., Kim, H.S., Lee, N.K., Lee, S.Y., Lee, K.-J., Kim, J. and Kang, S.W. (2010) Cytosolic Hsp60 is involved in the NF-kappa B-dependent survival of cancer cells via IKK regulation. *PLoS One* **5**, e9422.

Clayburgh, D.R., Barrett, T.A., Tang, Y., Meddings, J.B., Van Eldik, L.J., Watterson, D.M., Clarke, L.L., Mrsny, R.J. and Turner, J.R. (2005) Epithelial myosin light chain kinase–dependent barrier dysfunction mediates T cell activation–induced diarrhea in vivo. *J Clin Invest* **115**, 2702-2715.

Corr, S., Hill, C. and Gahan, C.G.M. (2006) An in vitro cell-culture model demonstrates internalin- and hemolysin-independent translocation of *Listeria monocytogenes* across M cells. *Microb Pathog* **41**, 241-250.

Corr, S.C., Gahan, C.C. and Hill, C. (2008) M- cells: origin, morphology and role in mucosal immunity and microbial pathogenesis. *Pathog Dis* **52**, 2-12.

Cruz, C.D., Pitman, A.R., Harrow, S.A. and Fletcher, G.C. (2014) *Listeria monocytogenes* associated with New Zealand seafood production and clinical cases: unique sequence types, truncated InlA and attenuated invasiveness. *Appl Environ Microbiol* **80**, 1489-1497.

Czuprynski, C.J., Faith, N.G. and Steinberg, H. (2003) A/J mice are susceptible and C57BL/6 mice are resistant to *Listeria monocytogenes* infection by intragastric inoculation. *Infect Immun* **71**, 682-689.

D'Orazio, S.E. (2014) Animal models for oral transmission of *Listeria monocytogenes*. *Front Cell Infect Microbiol* **4**.

de Noordhout, C.M., Devleesschauwer, B., Angulo, F.J., Verbeke, G., Haagsma, J., Kirk, M., Havelaar, A. and Speybroeck, N. (2014) The global burden of listeriosis: a systematic review and meta-analysis. *Lancet Infect Dis* **14**, 1073-1082.

Denizot, J., Sivignon, A., Barreau, F., Darcha, C., Chan, C.H.F., Stanners, C.P., Hofman, P., Darfeuille-Michaud, A. and Barnich, N. (2011) Adherent-invasive *Escherichia coli* induce claudin-2 expression and barrier defect in CEABAC10 mice and Crohn's disease patients. *Inflam Bowel Dis* **18**, 294-304.

Deriu, E., Liu, J.Z., Pezeshki, M., Edwards, R.A., Ochoa, R.J., Contreras, H., Libby, S.J., Fang, F.C. and Raffatellu, M. (2013) Probiotic bacteria reduce *Salmonella* Typhimurium intestinal colonization by competing for iron. *Cell Host & Microbe* **14**, 26-37.

Disson, O., Grayo, S., Huillet, E., Nikitas, G., Langa-Vives, F., Dussurget, O., Ragon, M., Le Monnier, A., Babinet, C., Cossart, P. and Lecuit, M. (2008) Conjugated action of two species-specific invasion proteins for fetoplacental listeriosis. *Nature* **455**, 1114-1118.

Disson, O. and Lecuit, M. (2013) In vitro and in vivo models to study human listeriosis: mind the gap. *Microbes Infect* **15**, 971-980.

Dramsi, S., Biswas, I., Maguin, E., Braun, L., Mastroeni, P. and Cossart, P. (1995) Entry of *Listeria monocytogenes* into hepatocytes requires expression of InlB, a surface protein of the internalin multigene family. *Mol Microbiol* **16**, 251-261.

Drolia, R., Tenguria, S., Durkes, A.C., Turner, J.R. and Bhunia, A.K. (2018) *Listeria* adhesion protein induces intestinal epithelial barrier dysfunction for bacterial translocation. *Cell Host & Microbe* **23**, 470-484.

Dziewanowska, K., Carson, A.R., Patti, J.M., Deobald, C.F., Bayles, K.W. and Bohach, G.A. (2000) Staphylococcal fibronectin binding protein interacts with heat shock protein 60 and integrins: Role in internalization by epithelial cells. *Infect Immun* **68**, 6321-6328.

Elewaut, D., DiDonato, J.A., Kim, J.M., Truong, F., Eckmann, L. and Kagnoff, M.F. (1999) NF-κB is a central regulator of the intestinal epithelial cell innate immune response induced by infection with enteroinvasive bacteria. *J Immunol* **163**, 1457-1466.

Elmi, A., Nasher, F., Jagatia, H., Gundogdu, O., Bajaj- Elliott, M., Wren, B. and Dorrell, N. (2016) *Campylobacter jejuni* outer membrane vesicle- associated proteolytic activity promotes bacterial invasion by mediating cleavage of intestinal epithelial cell E-cadherin and occludin. *Cell Microbiol* **18**, 561-572.

Farber, J., Ross, W. and Harwig, J. (1996) Health risk assessment of *Listeria monocytogenes* in Canada. *Int J Food Microbiol* **30**, 145-156.

Fravalo, P., Cherifi, T., Feliciano, K.D.N., Letellier, A., Fairbrother, J.-H. and Bekal, S. (2017) Characterisation of InlA truncation in *Listeria monocytogenes* isolates from farm animals and human cases in the province of Quebec. *Vet Rec Open* **4**, e000199.

Freitag, N.E., Port, G.C. and Miner, M.D. (2009) *Listeria monocytogenes* from saprophyte to intracellular pathogen. *Nat Rev Microbiol* **7**, 623-628.

Gaillard, J.L., Berche, P., Frehel, C., Gouin, E. and Cossart, P. (1991) Entry of *L. monocytogenes* into cells is mediated by internalin, a repeat protein reminiscent of surface-antigens from Gram-positive cocci. *Cell* **65**, 1127-1141.

Gelbicova, T., Kolackova, I., Pantucek, R. and Karpiskova, R. (2015) A novel mutation leading to a premature stop codon in inlA of *Listeria monocytogenes* isolated from neonatal listeriosis. *New Microbiol* **38**, 293-296.

Geng, T., Morgan, M.T. and Bhunia, A.K. (2004) Detection of low levels of *Listeria monocytogenes* cells by using a fiber-optic immunosensor. *Appl Environ Microbiol* **70**, 6138-6146.

Gessain, G., Tsai, Y.-H., Travier, L., Bonazzi, M., Grayo, S., Cossart, P., Charlier, C., Disson, O. and Lecuit, M. (2015) PI3-kinase activation is critical for host barrier permissiveness to *Listeria monocytogenes*. *J Exp Med* **212**, 165-183.

Ghosh, P., Halvorsen, E.M., Ammendolia, D.A., Mor-Vaknin, N., O'Riordan, M.X., Brumell, J.H., Markovitz, D.M. and Higgins, D.E. (2018) Invasion of the brain by *Listeria monocytogenes* is mediated by InlF and host cell vimentin. *mBio* **9**, e00160-00118.

Gilbert, S., Zhang, R., Denson, L., Moriggl, R., Steinbrecher, K., Shroyer, N., Lin, J. and Han, X. (2012) Enterocyte STAT5 promotes mucosal wound healing via suppression of myosin light chain kinase- mediated loss of barrier function and inflammation. *EMBO Mol Med* **4**, 109-124.

Goldblum, S.E., Rai, U., Tripathi, A., Thakar, M., De Leo, L., Di Toro, N., Not, T., Ramachandran, R., Puche, A.C. and Hollenberg, M.D. (2011) The active Zot domain (aa 288–293) increases ZO-1 and myosin 1C serine/threonine phosphorylation, alters interaction between ZO-1 and its binding partners, and induces tight junction disassembly through proteinase activated receptor 2 activation. *FASEB J* **25**, 144-158.

Gouin, E., Adib-Conquy, M., Balestrino, D., Nahori, M.-A., Villiers, V., Colland, F., Dramsi, S., Dussurget, O. and Cossart, P. (2010) The *Listeria monocytogenes* InlC protein interferes with innate immune responses by targeting the I kappa B kinase subunit IKK alpha. *Proc Nat Acad Sci USA* **107**, 17333-17338.

Guichard, A., Cruz-Moreno, B., Aguilar, B., van Sorge, N.M., Kuang, J., Kurkciyan, A.A., Wang, Z., Hang, S., de Chambrun, G.P.P. and McCole, D.F. (2013) Cholera toxin disrupts barrier function by inhibiting exocyst-mediated trafficking of host proteins to intestinal cell junctions. *Cell Host & Microbe* **14**, 294-305.

Hase, K., Kawano, K., Nochi, T., Pontes, G.S., Fukuda, S., Ebisawa, M., Kadokura, K., Tobe, T., Fujimura, Y. and Kawano, S. (2009) Uptake through glycoprotein 2 of $FimH^+$ bacteria by M cells initiates mucosal immune response. *Nature* **462**, 226.

Hecht, G., Pestic, L., Nikcevic, G., Koutsouris, A., Tripuraneni, J., Lorimer, D.D., Nowak, G., Guerriero, V., Elson, E.L. and deLanerolle, P. (1996) Expression of the catalytic domain of myosin light chain kinase increases paracellular permeability. *Am J Physiol Cell Physiol* **271**, C1678-C1684.

Henderson, B., Fares, M.A. and Lund, P.A. (2013) Chaperonin 60: a paradoxical, evolutionarily conserved protein family with multiple moonlighting functions. *Biol Rev* **88**, 955-987.

Hisamatsu, T., Suzuki, M., Reinecker, H.C., Nadeau, W.J., McCormick, B.A. and Podolsky, D.K. (2003) CARD15/NOD2 functions as an antibacterial factor in human intestinal epithelial cells. *Gastroenterology* **124**, 993-1000.

Hoffmann, S., Batz, M.B. and Morris Jr, J.G. (2012) Annual cost of illness and quality-adjusted life year losses in the United States due to 14 foodborne pathogens. *J Food Prot* **75**, 1292-1302.

Holch, A., Ingmer, H., Licht, T.R. and Gram, L. (2013) *Listeria monocytogenes* strains encoding premature stop codons in inlA invade mice and guinea pig fetuses in orally dosed dams. *J Med Microbiol* **62**, 1799-1806.

Jagadeesan, B., Fleishman Littlejohn, A.E., Amalaradjou, M.A.R., Singh, A.K., Mishra, K.K., La, D., Kihara, D. and Bhunia, A.K. (2011) N-Terminal Gly_{224} - Gly_{411} domain in *Listeria* adhesion protein interacts with host receptor Hsp60. *PLoS One* **6**, e20694.

Jagadeesan, B., Koo, O.K., Kim, K.P., Burkholder, K.M., Mishra, K.K., Aroonnual, A. and Bhunia, A.K. (2010) LAP, an alcohol acetaldehyde dehydrogenase enzyme in *Listeria* promotes bacterial adhesion to enterocyte-like Caco-2 cells only in pathogenic species. *Microbiology* **156**, 2782-2795.

Jaradat, Z.W. and Bhunia, A.K. (2002) Glucose and nutrient concentrations affect the expression of a 104-kilodalton *Listeria* adhesion protein in *Listeria monocytogenes*. *Appl Environ Microbiol* **68**, 4876-4883.

Jaradat, Z.W. and Bhunia, A.K. (2003) Adhesion, invasion and translocation characteristics of *Listeria monocytogenes* serotypes in Caco-2 cell and mouse models. *Appl Environ Microbiol* **69**, 3640-3645.

Jaradat, Z.W., Wampler, J.W. and Bhunia, A.K. (2003) A *Listeria* adhesion protein-deficient *Listeria monocytogenes* strain shows reduced adhesion primarily to intestinal cell lines. *Med Microbiol Immunol* **192**, 85-91.

Jones, G.S., Bussell, K.M., Myers-Morales, T., Fieldhouse, A.M., Ghanem, E.N.B. and D'Orazio, S.E. (2015) Intracellular *Listeria monocytogenes* comprises a minimal but vital fraction of the intestinal burden following foodborne infection. *Infect Immun* **83**, 3146-3156.

Jones, G.S. and D'Orazio, S.E. (2017) Monocytes are the predominant cell type associated with *Listeria monocytogenes* in the gut, but they do not serve as an intracellular growth niche. *J Immunol* **198**, 2796-2804.

Jonquieres, R., Bierne, H., Fiedler, F., Gounon, P. and Cossart, P. (1999) Interaction between the protein InIB of *Listeria monocytogenes* and lipoteichoic acid: a novel mechanism of protein association at the surface of Gram-positive bacteria. *Mol Microbiol* **34**, 902-914.

Jung, H.C., Eckmann, L., Yang, S.-K., Panja, A., Fierer, J., Morzycka-Wroblewska, E. and Kagnoff, M. (1995) A distinct array of proinflammatory cytokines is expressed in human colon epithelial cells in response to bacterial invasion. *J Clin Invest* **95**, 55-65.

Kawai, T. and Akira, S. (2011) Toll-like receptors and their crosstalk with other innate receptors in infection and immunity. *Immunity* **34**, 637-650.

Kayal, S., Lilienbaum, A., Join-Lambert, O., Li, X.X., Israel, A. and Berche, P. (2002) Listeriolysin O secreted by *Listeria monocytogenes* induces NF-kappa B signalling by activating the I kappa B kinase complex. *Mol Microbiol* **44**, 1407-1419.

Keeney, K.M. and Finlay, B.B. (2011) Enteric pathogen exploitation of the microbiota-generated nutrient environment of the gut. *Curr Opin Microbiol* **14**, 92-98.

Khelef, N., Lecuit, M., Bierne, H. and Cossart, P. (2006) Species specificity of the *Listeria monocytogenes* InlB protein. *Cell Microbiol* **8**, 457-470.

Kim, H. and Bhunia, A.K. (2013) Secreted *Listeria* adhesion protein (Lap) influences Lap-mediated *Listeria monocytogenes* paracellular translocation through epithelial barrier. *Gut Pathog* **5**, 16.

Kobayashi, K.S., Chamaillard, M., Ogura, Y., Henegariu, O., Inohara, N., Nunez, G. and Flavell, R.A. (2005) Nod2-dependent regulation of innate and adaptive immunity in the intestinal tract. *Science* **307**, 731-734.

Kocks, C., Gouin, E., Tabouret, M., Berche, P., Ohayon, H. and Cossart, P. (1992) *L. monocytogenes* -induced actin assembly requires the *actA* gene product, a surface protein. *Cell* **68**, 521-531.

Kommineni, S., Bretl, D.J., Lam, V., Chakraborty, R., Hayward, M., Simpson, P., Cao, Y., Bousounis, P., Kristich, C.J. and Salzman, N.H. (2015) Bacteriocin production augments niche competition by enterococci in the mammalian gastrointestinal tract. *Nature* **526**, 719.

Lamond, N.M. and Freitag, N.E. (2018) Vertical transmission of *Listeria monocytogenes:* Probing the balance between protection from pathogens and fetal tolerance. *Pathogens* **7**, 52.

Lecuit, M., Dramsi, S., Gottardi, C., Fedor-Chaiken, M., Gumbiner, B. and Cossart, P. (1999) A single amino acid in E-cadherin responsible for host specificity towards the human pathogen *Listeria monocytogenes*. *EMBO J* **18**, 3956 - 3963.

Lecuit, M., Sonnenburg, J., Cossart, P. and Gordon, J. (2007) Functional genomic studies of the intestinal response to a foodborne enteropathogen in a humanized gnotobiotic mouse model. *J Biol Chem* **282**, 15065 - 15072.

Lecuit, M., Vandormael-Pournin, S., Lefort, J., Huerre, M., Gounon, P., Dupuy, C., Babinet, C. and Cossart, P. (2001) A transgenic model for listeriosis: role of internalin in crossing the intestinal barrier. *Science* **292**, 1722 - 1725.

Liao, A.P., Petrof, E.O., Kuppireddi, S., Zhao, Y., Xia, Y., Claud, E.C. and Sun, J. (2008) *Salmonella* type III effector AvrA stabilizes cell tight junctions to inhibit inflammation in intestinal epithelial cells. *PLoS One* **3**, e2369.

Lin, Z., Zhang, Y.-G., Xia, Y., Xu, X., Jiao, X. and Sun, J. (2016) *Salmonella* Enteritidis effector AvrA stabilizes intestinal tight junctions via the JNK pathway. *J Biol Chem* **291**, 26837-26849.

Lindén, S., Bierne, H., Sabet, C., Png, C., Florin, T., McGuckin, M. and Cossart, P. (2008) *Listeria monocytogenes* internalins bind to the human intestinal mucin MUC2. *Arch Microbiol* **190**, 101-104.

Lomonaco, S., Nucera, D. and Filipello, V. (2015) The evolution and epidemiology of Listeria monocytogenes in Europe and the United States. *Infect Gen Evol* **35**, 172-183.

Ma, T.Y., Boivin, M.A., Ye, D., Pedram, A. and Said, H.M. (2005) Mechanism of TNF-a modulation of Caco-2 intestinal epithelial tight junction barrier: Role of myosin light-chain kinase protein expression. *Am J Physiol Gastrointest Liver Physiol* **288**, G422-G430.

Ma, T.Y., Iwamoto, G.K., Hoa, N.T., Akotia, V., Pedram, A., Boivin, M.A. and Said, H.M. (2004) TNF-a induced increase in intestinal epithelial tight junction permeability requires NF-kB activation. *Am J Physiol Gastrointes Liver Physiol* **286**, G367-G376.

MacCallum, A., Hardy, S.P. and Everest, P.H. (2005) *Campylobacter jejuni* inhibits the absorptive transport functions of Caco-2 cells and disrupts cellular tight junctions. *Microbiology* **151**, 2451-2458.

Madi, A., Svinareff, P., Orange, N., Feuilloley, M.G.J. and Connil, N. (2010) *Pseudomonas fluorescens* alters epithelial permeability and translocates across Caco-2/TC7 intestinal cells. *Gut Pathog* **2**, 16.

Maijala, R., Lyytikäinen, O., Johansson, T., Autio, T., Aalto, T., Haavisto, L. and Honkanen-Buzalski, T. (2001) Exposure of *Listeria monocytogenes* within an epidemic caused by butter in Finland. *Int J Food Microbiol* **70**, 97-109.

Maldonado-Contreras, A., Birtley, J.R., Boll, E., Zhao, Y., Mumy, K.L., Toscano, J., Ayehunie, S., Reinecker, H.-C., Stern, L.J. and McCormick, B.A. (2017) *Shigella* depends on SepA to destabilize the intestinal epithelial integrity via cofilin activation. *Gut Microbes* **8**, 544-560.

Maltby, R., Leatham-Jensen, M.P., Gibson, T., Cohen, P.S. and Conway, T. (2013) Nutritional basis for colonization resistance by human commensal *Escherichia coli* strains HS and Nissle 1917 against *E. coli* O157: H7 in the mouse intestine. *PLoS One* **8**, e53957.

Mansell, A., Braun, L., Cossart, P. and O'Neill, L.A.J. (2000) A novel function of InIB from *Listeria monocytogenes*: activation of NF-kappa B in J774 macrophages. *Cell Microbiol* **2**, 127-136.

Mansell, A., Khelef, N., Cossart, P. and O'Neill, L.A.J. (2001) Internalin B activates nuclear factor-kappa B via Ras, phosphoinositide 3-kinase, and Akt. *J Biol Chem* **276**, 43597-43603.

Marchiando, A.M., Shen, L., Graham, W.V., Edelblum, K.L., Duckworth, C.A., Guan, Y., Montrose, M.H., Turner, J.R. and Watson, A.J. (2011) The epithelial barrier is maintained by in vivo tight junction expansion during pathologic intestinal epithelial shedding. *Gastroenterology* **140**, 1208-1218. e1202.

Marco, A.J., Altimira, J., Prats, N., Lopez, S., Dominguez, L., Domingo, M. and Briones, V. (1997) Penetration of *Listeria monocytogenes* in mice infected by the oral route. *Microb Pathog* **23**, 255-263.

Mariscotti, J.F., Quereda, J.J., García-del Portillo, F. and Pucciarelli, M.G. (2014) The *Listeria monocytogenes* LPXTG surface protein Lmo1413 is an invasin with capacity to bind mucin. *Int J Med Microbiol* **304**, 393-404.

Marra, A. and Isberg, R.R. (1997) Invasin-dependent and invasin-independent pathways for translocation of *Yersinia pseudotuberculosis* across the Peyer's patch intestinal epithelium. *Infect Immun* **65**, 3412-3421.

Martens, E.C., Neumann, M. and Desai, M.S. (2018) Interactions of commensal and pathogenic microorganisms with the intestinal mucosal barrier. *Nat Rev Microbiol* **16**, 457-470.

McGuckin, M.A., Lindén, S.K., Sutton, P. and Florin, T.H. (2011) Mucin dynamics and enteric pathogens. *Nat Rev Microbiol* **9**, 265-278.

McNamara, B.P., Koutsouris, A., O'Connell, C.B., Nougayréde, J.-P., Donnenberg, M.S. and Hecht, G. (2001) Translocated EspF protein from enteropathogenic *Escherichia coli* disrupts host intestinal barrier function. *J Clin Invest* **107**, 621-629.

McNeill, C., Sisson, W. and Jarrett, A. (2017) Listeriosis: A resurfacing menace. *J Nurse Practice* **13**, 647-654.

Meinzer, U., Barreau, F., Esmiol-Welterlin, S., Jung, C., Villard, C., Léger, T., Ben-Mkaddem, S., Berrebi, D., Dussaillant, M. and Alnabhani, Z. (2012) *Yersinia pseudotuberculosis* effector YopJ subverts the Nod2/RICK/TAK1 pathway and activates caspase-1 to induce intestinal barrier dysfunction. *Cell Host Microbe* **11**, 337-351.

Melton-Witt, J.A., Rafelski, S.M., Portnoy, D.A. and Bakardjiev, A.I. (2012) Oral infection with signature-tagged *Listeria monocytogenes* reveals organ-specific growth and dissemination routes in guinea pigs. *Infect Immun* **80**, 720-732.

Mengaud, J., Ohayon, H., Gounon, P., Mege, R.M. and Cossart, P. (1996) E-cadherin is the receptor for internalin, a surface protein required for entry of *L. monocytogenes* into epithelial cells. *Cell* **84**, 923-932.

Mishra, K.K., Mendonca, M., Aroonnual, A., Burkholder, K.M. and Bhunia, A.K. (2011) Genetic organization and molecular characterization of *secA2* locus in *Listeria* species. *Gene* **489**, 76-85.

Morampudi, V., Graef, F.A., Stahl, M., Dalwadi, U., Conlin, V.S., Huang, T., Vallance, B.A., Hong, B.Y. and Jacobson, K. (2016) Tricellular tight junction protein tricellulin is targeted by the enteropathogenic *E. coli* effector EspG1 leading to epithelial barrier disruption. *Infect Immun*, IAI. 00700-00716.

Mueller-Herbst, S., Wustner, S., Muhlig, A., Eder, D., Fuchs, T.M., Held, C., Ehrenreich, A. and Scherer, S. (2014) Identification of genes essential for anaerobic growth of *Listeria monocytogenes*. *Microbiology* **160**, 752-765.

Murray, E.G.D., Webb, R.A. and Swann, M.B.R. (1926) A disease of rabbits characterised by a large mononuclear leucocytosis, caused by a hitherto undescribed bacillus *Bacterium monocytogenesis* (n.sp.). *J Pathol Bacteriol* **29**, 407-439.

NicAogáin, K. and O'Byrne, C.P. (2016) The role of stress and stress adaptations in determining the fate of the bacterial pathogen *Listeria monocytogenes* in the food chain. *Front Microbiol* **7**, 1865.

Nightingale, K., Windham, K., Martin, K., Yeung, M. and Wiedmann, M. (2005) Select *Listeria monocytogenes* subtypes commonly found in foods carry distinct nonsense mutations in inlA, leading to expression of truncated and secreted internalin A, and are associated with a reduced invasion phenotype for human intestinal epithelial cells. *Appl Environ Microbiol* **71**, 8764-8772.

Nikitas, G., Deschamps, C., Disson, O., Niault, T., Cossart, P. and Lecuit, M. (2011) Transcytosis of *Listeria monocytogenes* across the intestinal barrier upon specific targeting of goblet cell accessible E-cadherin. *J Exp Med* **208**, 2263-2277.

Nishikawa, S., Hirasue, M., Miura, T., Yamada, K., Sasaki, S. and Nakane, A. (1998) Systemic dissemination by intrarectal infection with *Listeria monocytogenes* in mice. *Microbiol Immunol* **42**, 325-327.

Odenwald, M.A. and Turner, J.R. (2017) The intestinal epithelial barrier: a therapeutic target? *Nat Rev Gastroenterol Hepatol* **14**, 9-21.

Oeckinghaus, A., Hayden, M.S. and Ghosh, S. (2011) Crosstalk in NF-[kappa]B signaling pathways. *Nat Immunol* **12**, 695-708.

Ohno, H. (2015) Intestinal M cells. *J Biochem (Tokyo)* **159**, 151-160.

Olier, M., Pierre, F., Rousseaux, S., Lemaître, J.-P., Rousset, A., Piveteau, P. and Guzzo, J. (2003) Expression of truncated internalin A is involved in impaired internalization of some *Listeria monocytogenes* isolates carried asymptomatically by humans. *Infect Immun* **71**, 1217-1224.

Ortega, F.E., Rengarajan, M., Chavez, N., Radhakrishnan, P., Gloerich, M., Bianchini, J., Siemers, K., Luckett, W.S., Lauer, P. and Nelson, W.J. (2017) Adhesion to the host cell surface is sufficient to mediate *Listeria monocytogenes* entry into epithelial cells. *Mol Biol Cell* **28**, 2945-2957.

Owens, S.-E., Graham, W.V., Siccardi, D., Turner, J.R. and Mrsny, R.J. (2005) A strategy to identify stable membrane-permeant peptide inhibitors of myosin light chain kinase. *Pharm Res* **22**, 703-709.

Pägelow, D., Chhatbar, C., Beineke, A., Liu, X., Nerlich, A., van Vorst, K., Rohde, M., Kalinke, U., Förster, R. and Halle, S. (2018) The olfactory epithelium as a port of entry in neonatal neurolisteriosis. *Nat Comm* **9**, 4269.

Pandiripally, V.K., Westbrook, D.G., Sunki, G.R. and Bhunia, A.K. (1999) Surface protein p104 is involved in adhesion of *Listeria monocytogenes* to human intestinal cell line, Caco-2. *J Med Microbiol* **48**, 117-124.

Pentecost, M., Kumaran, J., Ghosh, P. and Amieva, M.R. (2010) *Listeria monocytogenes* Internalin B activates junctional endocytosis to accelerate intestinal invasion. *PLoS Pathog* **6**, e1000900.

Pentecost, M., Otto, G., Theriot, J.A. and Amieva, M.R. (2006) *Listeria monocytogenes* invades the epithelial junctions at sites of cell extrusion. *PLoS Pathog* **2**, e3.

Perdomo, O., Cavaillon, J., Huerre, M., Ohayon, H., Gounon, P. and Sansonetti, P. (1994) Acute inflammation causes epithelial invasion and mucosal destruction in experimental shigellosis. *J Exp Med* **180**, 1307-1319.

Pizarro-Cerdá, J., Kühbacher, A. and Cossart, P. (2012) Entry of *Listeria monocytogenes* in mammalian epithelial cells: An updated view. *Cold Spring Harb Perspect Med* **2**, a010009.

Pockley, A.G. and Henderson, B. (2018) Extracellular cell stress (heat shock) proteins—immune responses and disease: an overview. *Phil Trans R Soc B* **373**, 20160522.

Popowska, M., Krawczyk-Balska, A., Ostrowski, R. and Desvaux, M. (2017) InlL from *Listeria monocytogenes* is involved in biofilm formation and adhesion to mucin. *Front Microbiol* **8**, 660.

Portnoy, D.A., Chakraborty, T., Goebel, W. and Cossart, P. (1992) Molecular determinants of *Listeria monocytogenes* pathogenesis. *Infect Immun* **60**, 1263-1267.

Portnoy, D.A., Jacks, P.S. and Hinrichs, D.J. (1988) Role of hemolysin for the intracellular growth of *Listeria monocytogenes*. *J Exp Med* **167**, 1459-1471.

Pouillot, R., Klontz, K.C., Chen, Y., Burall, L.S., Macarisin, D., Doyle, M., Bally, K.M., Strain, E., Datta, A.R. and Hammack, T.S. (2016) Infectious dose of *Listeria monocytogenes* in outbreak linked to ice cream, United States, 2015. *Emerg Infect Dis* **22**, 2113-2119.

Pron, B., Boumaila, C., Jaubert, F., Sarnacki, S., Monnet, J., Berche, P. and Gaillard, J. (1998) Comprehensive study of the intestinal stage of listeriosis in a rat ligated ileal loop system. *Infect Immun* **66**, 747-755.

Quereda, J.J., García- del Portillo, F. and Pucciarelli, M.G. (2016) *Listeria monocytogenes* remodels the cell surface in the blood- stage. *Environ Microbiol Reports* **8**, 641-648.

Radoshevich, L. and Cossart, P. (2018) *Listeria monocytogenes*: towards a complete picture of its physiology and pathogenesis. *Nat Rev Microbiol* **16**, 32-46.

Rajabian, T., Gavicherla, B., Heisig, M., Müller-Altrock, S., Goebel, W., Gray-Owen, S.D. and Ireton, K. (2009) The bacterial virulence factor InlC perturbs apical cell junctions and promotes cell-to-cell spread of *Listeria*. *Nat Cell Biol* **11**, 1212-1218.

Regan, T., Nally, K., Carmody, R., Houston, A., Shanahan, F., MacSharry, J. and Brint, E. (2013) Identification of TLR10 as a key mediator of the inflammatory response to *Listeria monocytogenes* in intestinal epithelial cells and macrophages. *J Immunol* **191**, 6084-6092.

Reis, O., Sousa, S., Camejo, A., Villiers, V.r., Gouin, E., Cossart, P. and Cabanes, D. (2010) LapB, a novel *Listeria monocytogenes* LPXTG surface adhesin, required for entry into eukaryotic cells and virulence. *J Infect Dis* **202**, 551-562.

Ricci, A., Allende, A., Bolton, D., Chemaly, M., Davies, R., Fernández Escámez, P.S., Girones, R., Herman, L., Koutsoumanis, K. and Nørrung, B. (2018) *Listeria monocytogenes* contamination of ready- to- eat foods and the risk for human health in the EU. *EFSA J* **16**, 5134.

Roxas, J.L., Monasky, R.C., Roxas, B.A.P., Agellon, A.B., Mansoor, A., Kaper, J.B., Vedantam, G. and Viswanathan, V.K. (2018) Enteropathogenic *Escherichia coli* EspH-mediated Rho GTPase inhibition results in desmosomal perturbations. *Cell Mol Gastroenterol Hepatol* **6**, 163-180.

Saadat, I., Higashi, H., Obuse, C., Umeda, M., Murata-Kamiya, N., Saito, Y., Lu, H., Ohnishi, N., Azuma, T. and Suzuki, A. (2007) *Helicobacter pylori* CagA targets PAR1/MARK kinase to disrupt epithelial cell polarity. *Nature* **447**, 330-333.

Sakaguchi, T., Köhler, H., Gu, X., McCormick, B.A. and Reinecker, H.-C. (2002) *Shigella flexneri* regulates tight junction-associated proteins in human intestinal epithelial cells. *Cell Microbiol* **4**, 367-381.

Santiago, N.I., Zipf, A. and Bhunia, A.K. (1999) Influence of temperature and growth phase on expression of a 104-kilodalton *Listeria* adhesion protein in *Listeria monocytogenes*. *Appl Environ Microbiol* **65**, 2765-2769.

Scallan, E., Hoekstra, R.M., Angulo, F.J., Tauxe, R.V., Widdowson, M.A., Roy, S.L., Jones, J.L. and Griffin, P.M. (2011) Foodborne illness acquired in the United States—major pathogens. *Emerg Infect Dis* **17**, 7-15.

Schlech, W., Lavigne, P., Bortolussi, R., Allen, A., Haldane, E., Wort, A., Hightower, A., Johnson, S., King, S., Nicholls, E. and Broome, C. (1983) Epidemic listeriosis--evidence for transmission by food. *N Engl J Med* **308**, 203 - 206.

Shen, Y., Naujokas, M., Park, M. and Ireton, K. (2000) InlB-dependent internalization of *Listeria* is mediated by the Met receptor tyrosine kinase. *Cell* **103**, 501-510.

Simovitch, M., Sason, H., Cohen, S., Zahavi, E.E., Melamed- Book, N., Weiss, A., Aroeti, B. and Rosenshine, I. (2010) EspM inhibits pedestal formation by enterohaemorrhagic Escherichia coli and enteropathogenic *E. coli* and disrupts the architecture of a polarized epithelial monolayer. *Cell Microbiol* **12**, 489-505.

Singh, A.P., Sharma, S., Pagarware, K., Siraji, R.A., Ansari, I., Mandal, A., Walling, P. and Aijaz, S. (2018) Enteropathogenic *E. coli* effectors EspF and Map independently disrupt tight junctions through distinct mechanisms involving transcriptional and post-transcriptional regulation. *Sci Rep* **8**, 3719.

Smith, M., Takeuchi, K., Anderson, G., Ware, G., McClure, H., Raybourne, R., Mytle, N. and Doyle, M. (2008) Dose-response model for *Listeria monocytogenes*-induced stillbirths in nonhuman primates. *Infect Immun* **76**, 726 - 731.

Speth, C., Prohaszka, Z., Mair, M., Stockl, G., Zhu, X.J., Jobstl, B., Fust, G. and Dierich, M.P. (1999) A 60 kD heat-shock protein-like molecule interacts with the HIV transmembrane glycoprotein gp41. *Mol Immunol* **36**, 619-628.

Stavru, F., Archambaud, C. and Cossart, P. (2011) Cell biology and immunology of *Listeria monocytogenes* infections: novel insights. *Immunol Rev* **240**, 160-184.

Stevenson, B.R. and Begg, D.A. (1994) Concentration-dependent effects of cytochalasin D on tight junctions and actin filaments in MDCK epithelial cells. *J Cell Sci* **107**, 367-375.

Swaminathan, B. and Gerner-Smidt, P. (2007) The epidemiology of human listeriosis. *Microbes Infect* **9**, 1236-1243.

Tapia, R., Kralicek, S.E. and Hecht, G.A. (2017) EPEC effector EspF promotes Crumbs3 endocytosis and disrupts epithelial cell polarity. *Cell Microbiol* **19**, e12757.

Tegtmeyer, N., Wessler, S., Necchi, V., Rohde, M., Harrer, A., Rau, T.T., Asche, C.I., Boehm, M., Loessner, H., Figueiredo, C., Naumann, M., Palmisano, R., Solcia, E., Ricci, V. and Backert, S. (2017) *Helicobacter pylori* employs a unique basolateral type IV secretion mechanism for CagA delivery. *Cell Host & Microbe* **22**, 552-560.e555.

Thanabalasuriar, A., Koutsouris, A., Weflen, A., Mimee, M., Hecht, G. and Gruenheid, S. (2010) The bacterial virulence factor NleA is required for the disruption of intestinal tight junctions by enteropathogenic *Escherichia coli*. *Cell Microbiol* **12**, 31-41.

Tilney, L. and Portnoy, D. (1989) Actin filaments and the growth, movement, and spread of the intracellular bacterial parasite, *Listeria monocytogenes*. *J Cell Biol* **109**, 1597-1608.

Toledo-Arana, A., Dussurget, O., Nikitas, G., Sesto, N., Guet-Revillet, H., Balestrino, D., Loh, E., Gripenland, J., Tiensuu, T., Vaitkevicius, K., Barthelemy, M., Vergassola, M., Nahori, M.-A., Soubigou, G., Regnault, B., Coppee, J.-Y., Lecuit, M., Johansson, J. and Cossart, P. (2009) The *Listeria* transcriptional landscape from saprophytism to virulence. *Nature* **459**, 950-956.

Tsai, Y.-H., Disson, O., Bierne, H. and Lecuit, M. (2013) Murinization of internalin extends its receptor repertoire, altering *Listeria monocytogenes* cell tropism and host responses. *PLoS Pathog* **9**, e1003381.

Tsuchiya, K., Kawamura, I., Takahashi, A., Nomura, T., Kohda, C. and Mitsuyama, M. (2005) Listeriolysin O-induced membrane permeation mediates persistent interleukin-6 production in Caco-2 cells during *Listeria monocytogenes* infection *in vitro*. *Infect Immun* **73**, 3869-3877.

Turner, J.R. (2009) Intestinal mucosal barrier function in health and disease. *Nat Rev Immunol* **9**, 799-809.

Turner, J.R., Rill, B.K., Carlson, S.L., Carnes, D., Kerner, R., Mrsny, R.J. and Madara, J.L. (1997) Physiological regulation of epithelial tight junctions is associated with myosin light-chain phosphorylation. *Am J Physiol* **273**, C1378-C1385.

Utech, M., Mennigen, R. and Bruewer, M. (2009) Endocytosis and recycling of tight junction proteins in inflammation. *Biomed Res Int* **2010**, Article ID 484987.

Vabulas, R.M., Ahmad-Nejad, P., da Costa, C., Miethke, T., Kirschning, C.J., Häcker, H. and Wagner, H. (2001) Endocytosed HSP60s use toll-like receptor 2 (TLR2) and TLR4 to activate the toll/interleukin-1 receptor signaling pathway in innate immune cells. *J Biol Chem* **276**, 31332-31339.

Van Der Flier, L.G. and Clevers, H. (2009) Stem cells, self-renewal, and differentiation in the intestinal epithelium. *Annu Rev Physiol* **71**, 241-260.

Van Stelten, A., Simpson, J.M., Chen, Y., Scott, V.N., Whiting, R.C., Ross, W.H. and Nightingale, K.K. (2011) Significant shift in median guinea pig Infectious dose shown by an outbreak-associated *Listeria monocytogenes* epidemic clone strain and a strain carrying a premature stop codon mutation in *inlA*. *Appl Environ Microbiol* **77**, 2479-2487.

Vázquez-Boland, J.A., Krypotou, E. and Scortti, M. (2017) *Listeria* placental infection. *mBio* **8**, e00949-00917.

Wampler, J.L., Kim, K.P., Jaradat, Z. and Bhunia, A.K. (2004) Heat shock protein 60 acts as a receptor for the Listeria adhesion protein in Caco-2 cells. *Infect Immun* **72**, 931-936.

Welshimer, H.J. and Donker-Voet, J. (1971) *Listeria monocytogenes* in Nature. *Appl Microbiol* **21**, 516-519.

Wollert, T., Pasche, B., Rochon, M., Deppenmeier, S., van den Heuvel, J., Gruber, A.D., Heinz, D.W., Lengeling, A. and Schubert, W.D. (2007) Extending the host range of *Listeria monocytogenes* by rational protein design. *Cell* **129**, 891-902.

Wroblewski, L.E., Piazuelo, M.B., Chaturvedi, R., Schumacher, M., Aihara, E., Feng, R., Noto, J.M., Delgado, A., Israel, D.A. and Zavros, Y. (2014) *Helicobacter pylori* targets cancer-associated apical-junctional constituents in gastroids and gastric epithelial cells. *Gut*, gutjnl-2014-307650.

Wroblewski, L.E., Shen, L., Ogden, S., Romero–Gallo, J., Lapierre, L.A., Israel, D.A., Turner, J.R. and Peek Jr, R.M. (2009) *Helicobacter pylori* dysregulation of gastric epithelial tight junctions by urease-mediated myosin II activation. *Gastroenterology* **136**, 236-246.

Wu, Z., Nybom, P. and Magnusson, K.E. (2000) Distinct effects of *Vibrio cholerae* haemagglutinin/protease on the structure and localization of the tight junction- associated proteins occludin and ZO- 1. *Cell Microbiol* **2**, 11-17.

Xanthoudakis, S., Roy, S., Rasper, D., Hennessey, T., Aubin, Y., Cassady, R., Tawa, P., Ruel, R., Rosen, A. and Nicholson, D.W. (1999) Hsp60 accelerates the maturation of pro-caspase-3 by upstream activator proteases during apoptosis. *EMBO J* **18**, 2049-2056.

Yuhan, R., Koutsouris, A., Savkovic, S.D. and Hecht, G. (1997) Enteropathogenic *Escherichia coli*-induced myosin light chain phosphorylation alters intestinal epithelial permeability. *Gastroenterology* **113**, 1873-1882.

Zeng, M.Y., Cisalpino, D., Varadarajan, S., Hellman, J., Warren, H.S., Cascalho, M., Inohara, N. and Núñez, G. (2016) Gut microbiota-induced immunoglobulin G controls systemic infection by symbiotic bacteria and pathogens. *Immunity* **44**, 647-658.

Zhang, T., Abel, S., Abel zur Wiesch, P., Sasabe, J., Davis, B.M., Higgins, D.E. and Waldor, M.K. (2017) Deciphering the landscape of host barriers to *Listeria monocytogenes* infection. *Proc Nat Acad Sci U S A* **114**, 6334-6339.

APPENDIX

Analysis of LAP Expression in Glycerol and under Anaerobic Growth Conditions

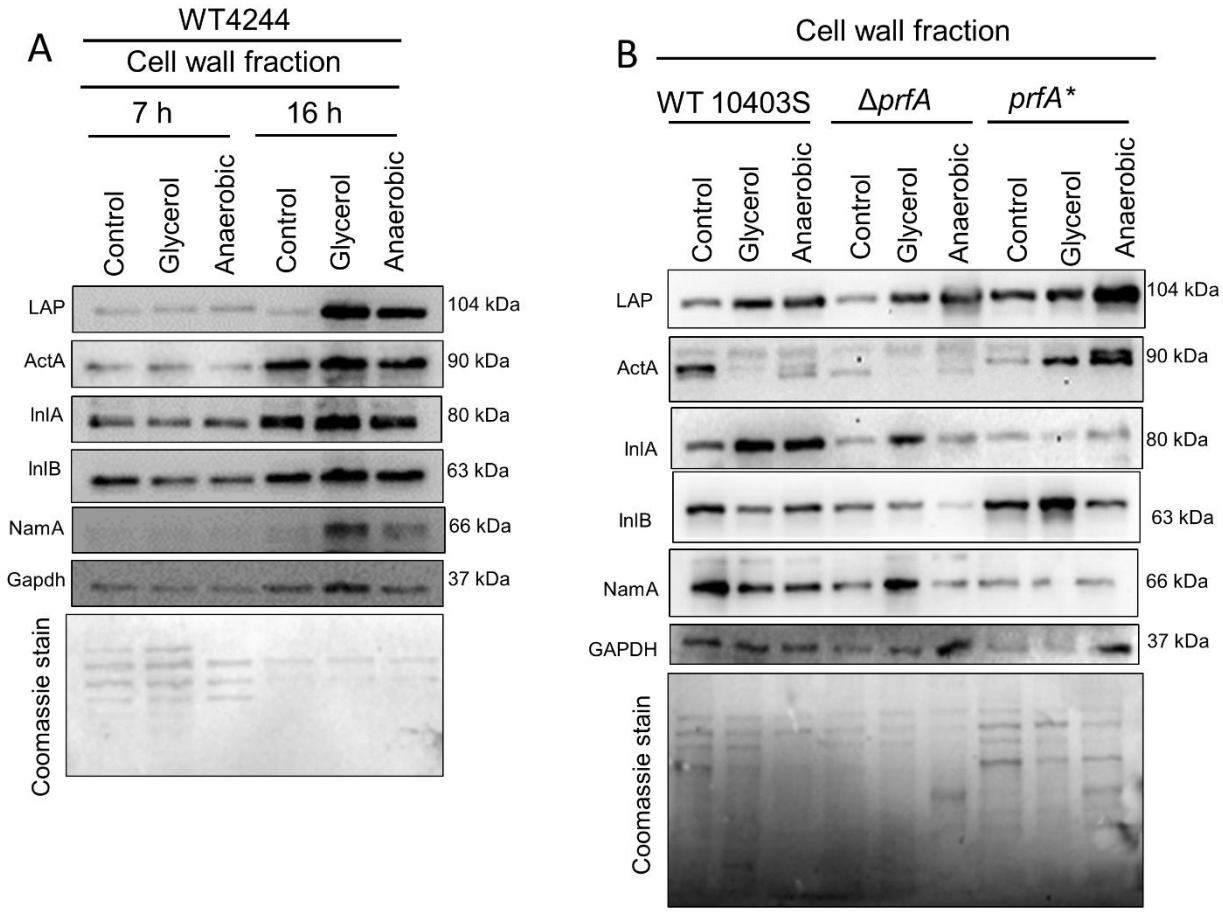

NF-L1166: (prfA L140F)or prfA*
NF-L890:Δ*prfA*

Complementation of *lap⁻ adh⁺ and lap⁻ aldh⁺* strains

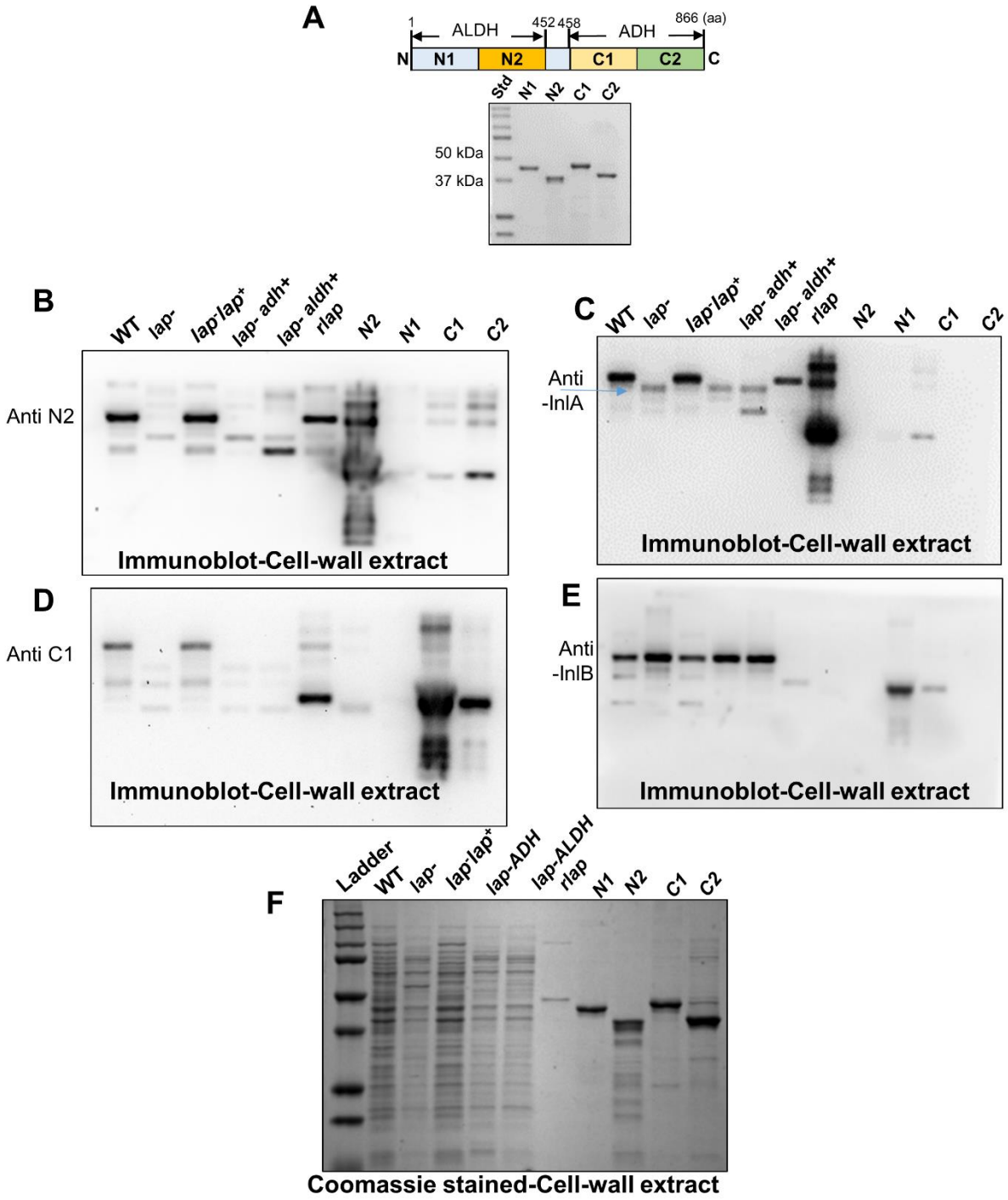

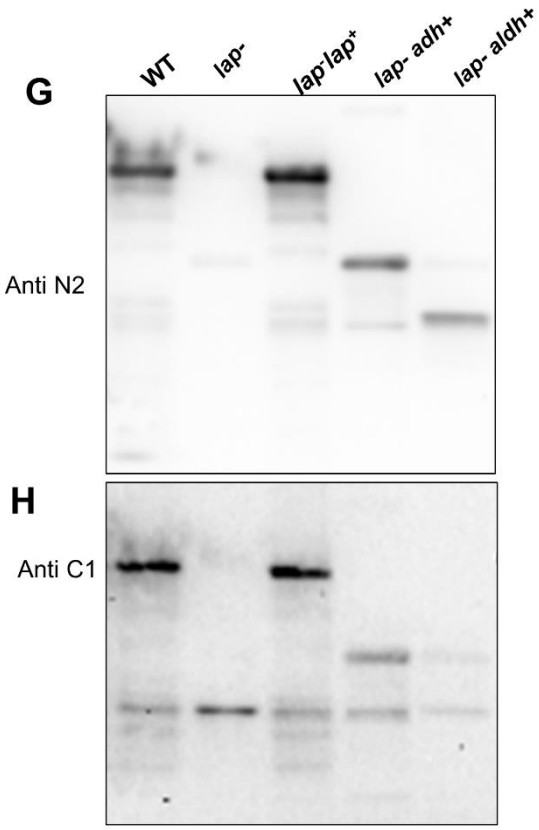

Immunoblot-Intracellular fraction

L. monocytogenes infection increases epithelial Hsp60 expression *in vitro* and *in vivo*

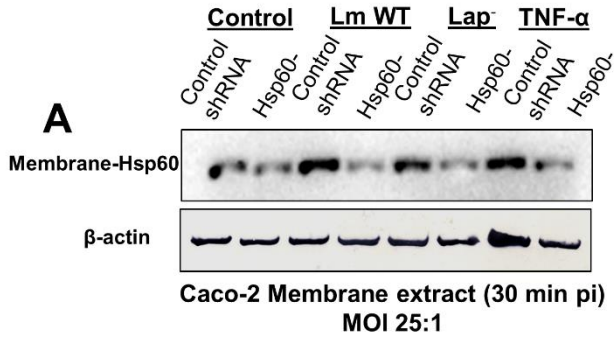

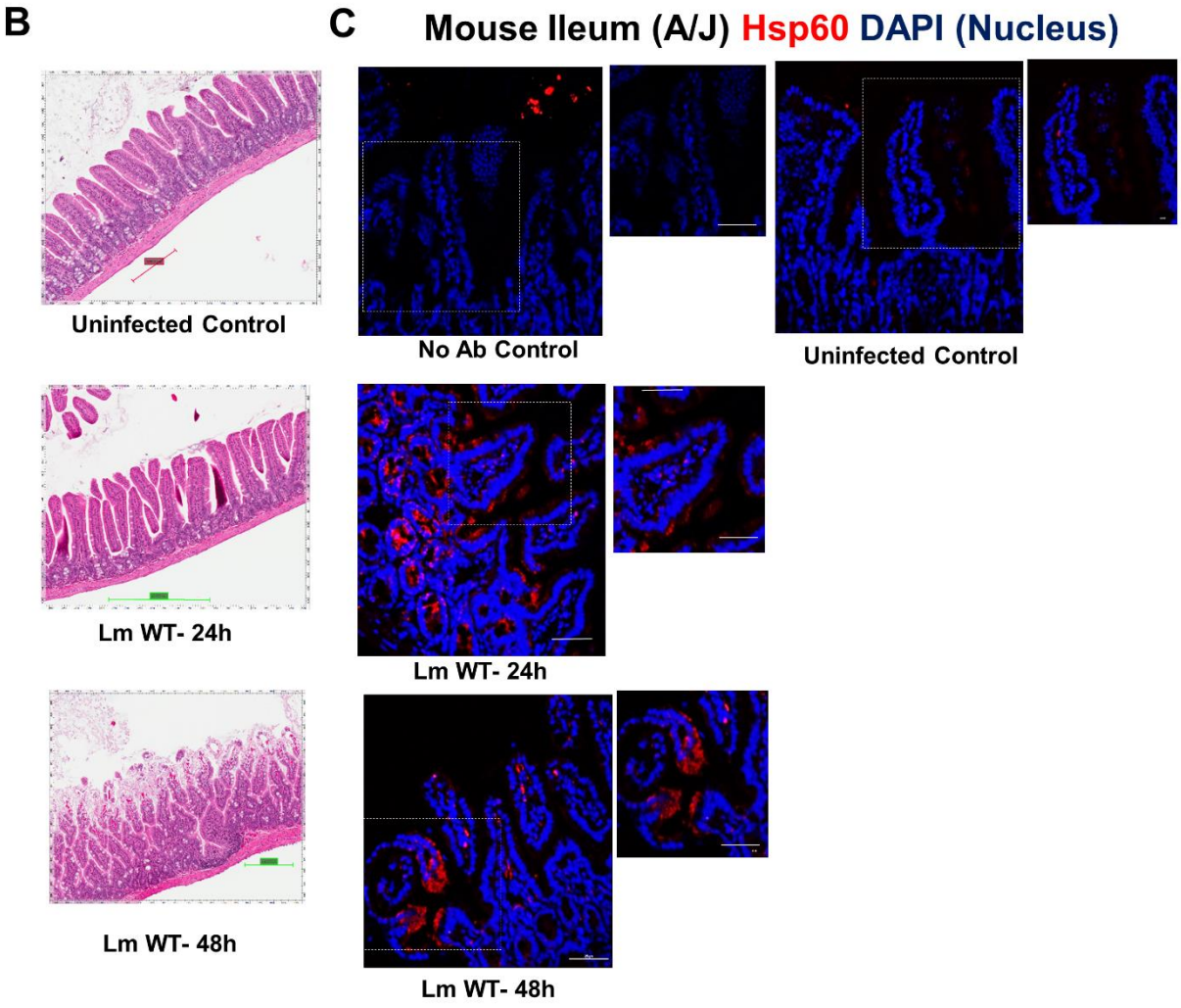

Transmission electron microscopic examination of cell-cell junction ultrastructure of ileal tissue sections from control mice or mice challenged with *L. monocytogenes* WT, *lap*$^{-}$ or Δ*inlA* strains.

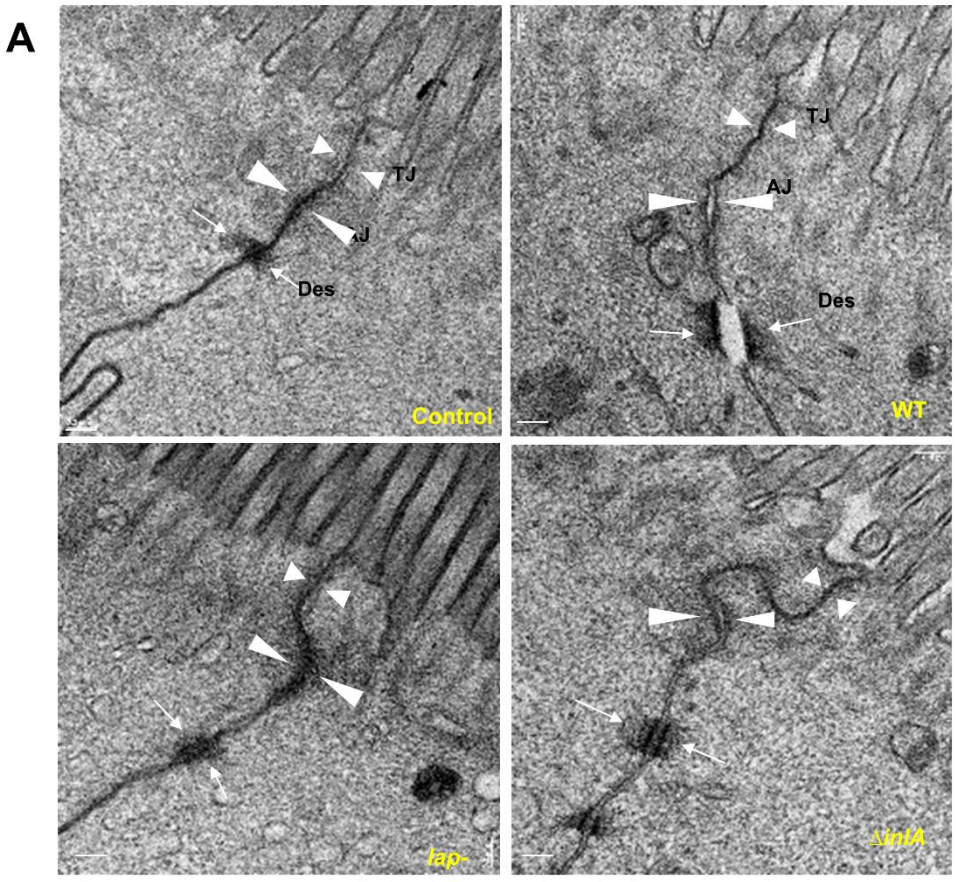

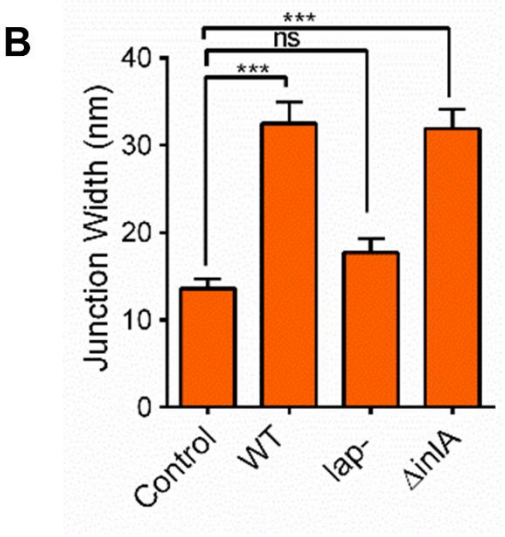

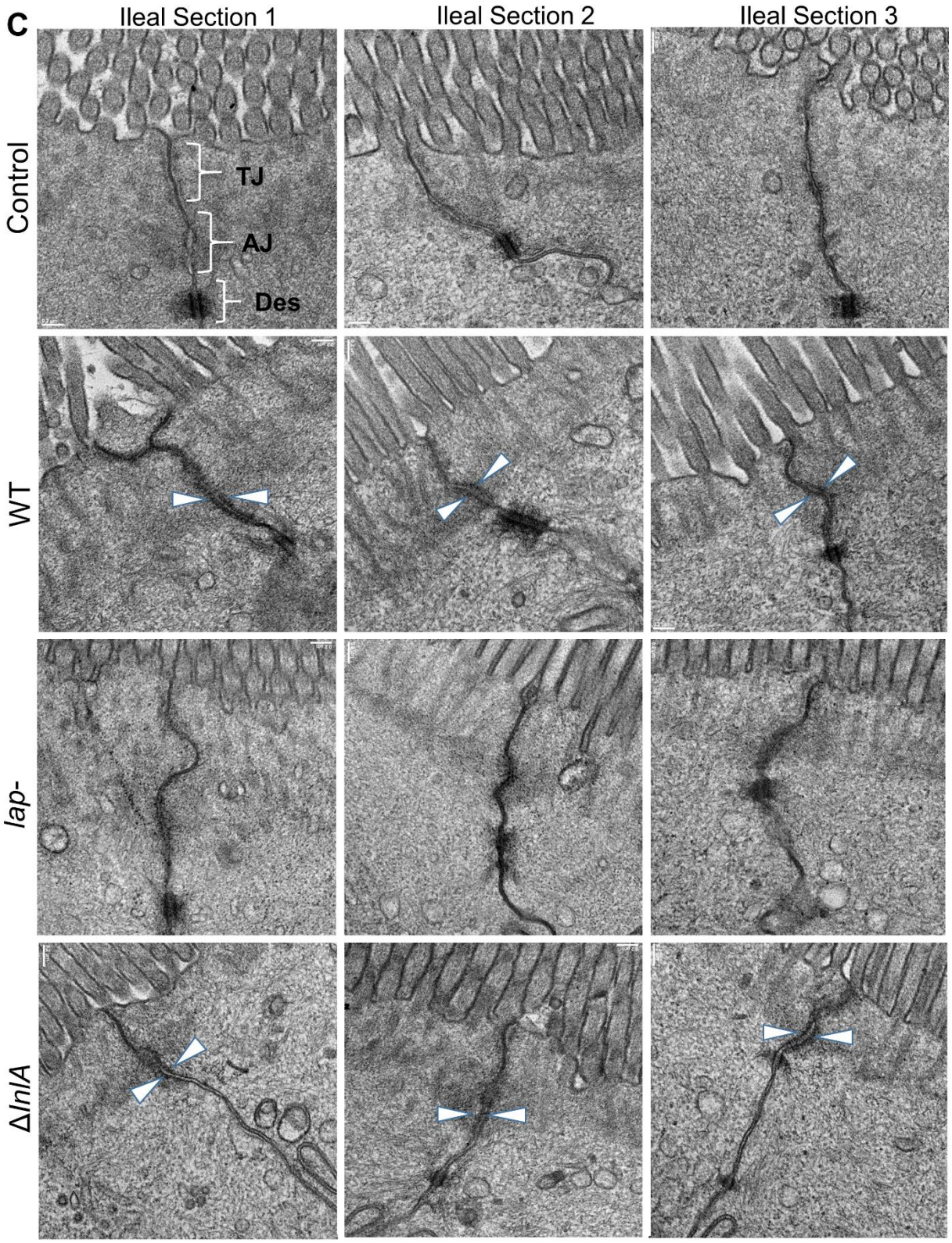
C
Ileal Section 1
Ileal Section 2
Ileal Section 3
Control
WT
lap-
ΔInlA
TJ
AJ
Des

VITA

RISHI DROLIA

Department of Food Science, Purdue University,
745 Agriculture Mall Drive,
West Lafayette, IN 47907

EDUCATION

Date	Institution	Degree
2012-Present	**Purdue University,** West Lafayette, IN 47907 Advisor: Arun K. Bhunia ▪ Dissertation Title: "Cellular and Molecular Mechanism of *Listeria* Adhesion Protein-Mediated Bacterial Crossing of the Intestinal Barrier" ▪ Expected graduation: December 2018	Ph. D (Food Science, Concentration: Cellular and Molecular Microbiology)
2009-2012	**Kansas State University,** Manhattan, KS 66506 Advisor: Stephen K. Chapes ▪ Thesis Title: "*Ehrlichia chaffeensis* Replication Sites in Adult *Drosophila melanogaster"*	M.S.(Biology)
2007-2009	**University of Pune,** Maharashtra, India 411004 ▪ Thesis Title: "Molecular Analysis Through the Sequencing of 16S rRNA Gene of Cutaneous Microflora of Human Skin in Diabetic (Type 1) Patients"	M.Sc.(Biochemistry)
2004-2007	**Bharati Vidyapeeth University** Pune, Maharashtra, India 411038	B.Sc.(Microbiology)
2004-2008	**Bharati Vidyapeeth University** Pune, Maharashtra, India 411038	Advanced Diploma (Industrial Microbiology)

PROFESSIONAL APPOINTMENTS

Graduate Research Assistant, Purdue University, Department of Food Science

August 2012-Present

- Elucidation of *Listeria monocytogenes* pathogenesis in mouse, gerbil and cell culture models
- Utilize a next-generation probiotic approach for combating *Listeria* infection *in vivo*
- Analyze the effect of antibiotic resistance on bacterial pathogenesis and virulence
- Evaluate the role of heat-stressed protein in bacterial pathogenesis and antibiotic response
- Assessment of coinfection and virulence-gene associated mutant bacterial colonies using optical sensor
- Write grants, manuscripts and reports.

Graduate Teaching Assistant, Purdue University, Department of Food Science

Spring 2016 and Spring 2018

- Taught a **graduate level** course (FS 566, 2 credit) for Ph.D. and masters students in molecular food microbiology and microbial techniques for food pathogens.

Graduate Research Assistant, Kansas State University, Division of Biology

August 2009-June 2012

- Elucidated *Erhlichia chaffeensis* pathogenesis in adult *Drosophila* model
- Wrote manuscripts and reports.

Graduate Teaching Assistant, Kansas State University, Division of Biology

August 2009- December 2011 (Every Fall and Spring Semesters)

- Taught a general microbiology laboratory class (BIOL 455, 3 credit) for senior and junior undergraduate students.

PUBLICATIONS IN PEER-REVIEWED JOURNALS (Google Scholar)

Drolia, R., Von Ohlen, T., and Chapes, S.K. **2013**. *Ehrlichia chaffeensis* replication sites in adult Drosophila melanogaster. **International Journal of Medical Microbiology.** 303(1):40-49. **(IF: 3.298)**

Singh, A.K., **Drolia, R**., Bai, X., and Bhunia, A.K. **2015**. Streptomycin Induced stress response in *Salmonella enterica* serovar Typhimurium shows distinct colony scatter signature. **PloS ONE.** 10(8):e0135035. **(IF: 2.766)**

Singh, A.K., Leprun, L., **Drolia, R**., Bai, X., Kim, H., Aroonnual, A., Bae, E., Mishra, K.K., and Bhunia, A.K. **2016**. Virulence Gene-Associated Mutant Bacterial Colonies Generate Differentiating 2-D Laser Scatter Fingerprints. **Applied and Environmental Microbiology.** 82(11): 3256-3268. **(IF: 3.633)**

Drolia, R., Tenguria, S., Durkes, A.C., Turner, J.R., and Bhunia, A.K. **2018**. *Listeria* Adhesion Protein Induces Intestinal Epithelial Barrier Dysfunction for Bacterial Translocation. **Cell Host & Microbe.** 23(4): 470-484.e7 **(IF: 17.872)**

Zhu, X., Liu, D., Singh, A.K., **Drolia, R.,** Bai, X., Tenguria, S., and Bhunia, A.K. **2018**. Tunicamycin Mediated Inhibition of Wall Teichoic Acid Affects *Staphylococcus aureus* and *Listeria monocytogenes* Cell Morphology, Biofilm Formation and Virulence. **Frontiers in Microbiology.** 9:1352 **(IF: 4.019)**

MANUSCRIPT IN REVIEW/PREPARATION

Drolia, R., and Bhunia, A.K. Crossing the Intestinal Barrier via *Listeria* Adhesion Protein and Internalin A. Manuscript # TIMI-D-18-00177, **In Review**, **Trends in Microbiology (IF: 11.776)**

Drolia, R., Tenguria, S., and Bhunia, A.K. Gerbil Model of Listeriosis. Manuscript under preparation.

Amalaradjou, M.A.R*., **Drolia, R***., Ryan, V., Tenguria, S., Liu, D., Bai, X., Singh, A.K., Bailey, T., dos Santos, A.P., Durkes, A.C., et al. Lactobacillus Expressing *Listeria* Adhesion Protein from a Nonpathogenic Bacterium Improves Gut Health and Protects Mice from Pathogen. Manuscript under preparation (*equal contribution)

Tenguria, S., **Drolia, R.,** and Bhunia, A.K. Gastroenteritis with *Listeria monocytogenes* In Mouse Models. Manuscript under preparation

Bai, X., Liu, D., Xu, L., **Drolia, R**., Bailey, T., Durkes, A.C., and Bhunia, A.K. Biofilm-Isolated *Listeria monocytogenes* Exhibits Lower Intestinal and Extra-Intestinal Dissemination than Planktonic Cells Very Early in the Oral Infection of Mouse. Manuscript under preparation

Liu, D., Bailey, T.W., Zhu, X., **Drolia, R.,** Singh, A.K., Seleem, M., and Bhunia, A.K. 2018. Re-association of the Secreted LAP on Cell Wall of *Listeria monocytogenes* is Facilitated by Multiple Anchoring Partners. Manuscript under preparation

PATENTS

- Drolia, R., Samaddar, M., Bhunia, A. K. Enhanced Drug Delivery across Epithelial Barrier. PRF No. 67963-01. **Utility Patent Filed**, Oct 4, 2018

DISCLOSURES

- Amalaradjou, M. A., **Drolia, R.,** Koo, O. K., Bhunia, A. K. Next Generation Probiotic that Improves Gut Health and Provides Protection against Enteric Pathogens.
  PRF No. 68291-01. **Provisional Disclosure Issued**, Jul 2, 2018**.**

RESEARCH GRANTS

Funded grant:

Agency: Purdue Research Foundation (PRF) research grants

Title: *Listeria* Adhesion Protein Disrupts Innate Defense to Promote Intestinal Epithelial Paracellular Permeability in Mouse.

PI, Dr. Arun K. Bhunia; Graduate student, **Rishi Drolia**

Duration of funding - May 2016- July 2017, Amount ~$30,000 for providing half-time support for graduate students employed as graduate research assistants

Assisted grant: Played key role in writing, reviewing and submitting the grant

Agency: National Institute of Health (NIH) for a R21 grant: Topics in Bacterial Pathogenesis Special Emphasis Panel IDM-B (81), 1 R21-AI144778-01

Title: Investigation on the Intestinal Phase of Listeriosis in a Gerbil Model.

PI: Dr. Arun K. Bhunia; Co-PI: Dr. Abigail C. Durkes; Collaborator: Dr. Jerrold R. Turner.

Assisted grant: Played key role in writing, reviewing and submitting the grant.

Agency: National Institute of Food and Agriculture (NIFA), Agriculture and Food Research Initiative (AFRI)

Title: Novel Next-Generation Probiotic Approach to Prevent *Listeria monocytogenes* Colonization and Infection in Swine.

PI: Dr. Arun K. Bhunia; Co-PI's: Dr. Cindy H, Nakatsu, Dr. Kalapo Ajuown, Dr. Abigail Durkes, Dr. Shivendra Tenguria.

CONFERENCE PRESENTATIONS

Kinney, T.*, Nichols, R.*****, **Drolia, R.**, Von Ohlen,T. Chapes, S.K. (2011). Screening of Host Gene Requirements of *Ehrlichia chaffeensis* Using *Drosophila melanogaster*. Undergraduate Research Forum, Kansas State University, Manhattan, KS (Poster Presentation). ***** Presented by mentored undergraduate students.

Drolia, R., Kim, H., Bhunia, A. K. (2014). *Listeria* Adhesion Protein Interaction with Mammalian Chaperone 60 Promotes Epithelial Paracellular Permeability through NF-κB Activation. American Society for Microbiology General Meeting, Boston, Massachusetts. Poster No. 2477, May 17-20, 2014. (Poster presentation)

Drolia, R., Tenguria, S., Durkes, A.C., Turner, J.R., and Bhunia, A.K. (2018). LAP Induces Intestinal Epithelial Barrier Dysfunction by Activating NF-κB and MLCK for *Listeria monocytogenes* Translocation in Caco-2 and Mouse Models. American Society for Microbiology General Meeting, Atlanta, GA. Abstract No. 88, June 8-11, 2018. (Poster presentation)

Bai, X., Liu, D., Xu, L., **Drolia, R**., Bailey, T., Durkes, A.C., and Bhunia, A.K. (2018). Biofilm-Isolated *Listeria monocytogenes* Exhibits Lower Intestinal and Extra-Intestinal Dissemination than

Planktonic Cells Very Early in the Oral Infection of Mouse. American Society for Microbiology General Meeting, Atlanta, GA. Abstract No. 29, June 8-11, 2018. (Poster presentation).

Liu, D., Bailey, T.W., Zhu, X., **Drolia, R.,** Singh, A.K., Seleem, M., and Bhunia, A.K. (2018). Re-association of the Secreted LAP on Cell Wall of *Listeria monocytogenes* is Facilitated by Multiple Anchoring Partners. American Society for Microbiology General Meeting, Atlanta, GA. Abstract No. 1101, June 8-11, 2018. (Poster presentation).

Tenguria, S., **Drolia, R.,** Durkes, A.C., and Bhunia, A.K. (2018). *Listeria monocytogenes* Induced Gastroenteritis in a Mouse Model. American Society for Microbiology General Meeting, Atlanta, GA. Abstract No. 13, June 8-11, 2018. (Poster presentation).

TEACHING EXPERIENCE

Purdue University, West Lafayette, IN

Department of Food Science

Spring semester, 2016 and 2018

- Taught laboratory and class sessions of molecular food microbiology; microbial techniques for food pathogens (FS 566, 2 credit) to class of 11 graduate students (MS and Ph.D.) in 2016, and 6 graduate students in 2018.

Kansas State University, Manhattan, KS

Division of Biology

Fall 2009, Spring 2010, Fall 2010, Spring 2011, Fall 2011

- Taught laboratory and class sessions for a general microbiology class (BIOL 455, 3 credit) for five semesters to ~ 25-35 undergraduate enrolled students each semester.

Student Evaluations:

Student evaluations for Fall 2010 and Spring 2011. The group median ratings are shown.

N = number of students who completed the evaluation forms.

The rating scale is 5 = Excellent, 4 = Good, 3 = Fair, 2 = Poor, 1 = Very Poor

Evaluation questions	**Fall 2010 (N = 29)**	**Spring 2011 (N= 29)**
Overall effectiveness as a teacher	4.7	4.7
Increased desire to learn about the subject	4.2	4.2
Amount learned in the course	4.2	4.4

GUEST LECTURES

Delivered lecture on "Real time PCR" for a biotechnology course to a class of 8 undergraduate students on February 24 & 26, 2015 at the Department of Biotechnology, Ivy Tech Community College. Invited by Dr. K.K Mishra.

MENTORING EXPERIENCE / SUPERVISION

Actively engaged in mentoring/supervising following BS and high school students in their research that included planning experiments, analyzing data, and writing report/manuscript:

- **Irene Bhunia (2018):** Mentored an 8th grade West Lafayette junior/senior high school student for a poster presentation titled "Renal microbe mishap: Microbial imbalance's effect on the formation of kidney stones". Awarded gold medals for poster presentation in each Biochemistry, and Biomedical Sciences division.

- **Jingyi Ren (2016):** Mentored a senior undergraduate student at Purdue University for 3 research credits in summer and fall 2016 on a project titled" Hsp60, the receptor for *Listeria* Adhesion Protein (LAP), is distinctly expressed in the large intestine.

- **Wen Lv (2016):** Mentored a senior undergraduate student at Purdue University for 2 research credits in spring and fall 2016 on a project titled "Identify the host proteins that interact with *Listeria* Adhesion Protein (LAP) in human colonic cells (Caco-2) during *Listeria monocytogenes* infection.

- **Allison Guthrie (2013-2014):** Mentored a junior undergraduate student at Purdue University for 2 research credits in fall 2013 and spring 2014 on a project titled "Identify the host signaling cascades activated by *Listeria* Adhesion Protein (LAP) in human colonic cells (Caco-2) to during *Listeria monocytogenes* infection.

- **Taylor Kinney (2011):** Mentored a senior undergraduate student at Kansas State University for 2 research credits in fall 2011 on a project titled "Screening of host gene requirements of *Ehrlichia chaffeensis* using *Drosophila melanogaster*.

- **Racheal Nichols (2011):** Mentored a senior undergraduate student at Kansas State University for 2 research credits in spring 2011 on a project titled "Screening of host gene requirements of *Ehrlichia chaffeensis* using *Drosophila melanogaster"*.

RESEARCH NEWS

- Purdue research news:
  Researchers Find Alternate Path for *Listeria* to Sicken People
- Medical Xpress research news:
  Researchers Find Alternate Path for *Listeria* to Sicken People
- Purdue research news:
  Laser Tool Effective at Identifying Mutant *Listeria* Bacteria

ACADEMIC AWARDS / RECOGNITIONS

- Selected as a Spotlight Graduate Student in the College of Agriculture, Purdue University September 2018. Link
- Graduate Student Spotlight in Purdue Agriculture In Focus Newsletter
  September 2018. Link
- American Society for Microbiology Travel Award, 2018
- Graduate Research Assistantship: Purdue University, 2012-current
- Graduate Research/Teaching Assistantship: Kansas State University, 2009-2012
- Ranked Third College Level (M.Sc. Biochemistry) GPA 3.92/4

RELATED PROFESSIONAL SKILLS

- **Animal handling and infection:** Restraining and control of rodents (mouse, rat, gerbils and guinea pigs), oral gavage, animal euthanasia and dissection, animal breeding, *in vivo* permeability assays.
- **Biochemistry:** Cell and tissue protein extraction**,** cell fractionation**,** affinity, ion exchange and size exclusion chromatography, immunoblotting, immunofluorescence and dot-blot
- **Microscopy:** High resolution confocal, immunofluorescence, three-dimensional fluorescence and light microscopy imaging
- **Tissue culture and Microbiology:** Mammalian cell culture of adherent cells**,** insect cell culture of suspension cells, bacterial cultures and mutant construction for application in molecular biology techniques
- **Insect Work:** *Drosophila melanogaster* care, injection *of D. melanogaster* with nano-injector
- **Molecular Biology:** PCR optimization, primer design RT-PCR, qRT-PCR, Agarose and polyacrylamide gel electrophoresis, bacterial transformation, transfection of mammalian cells, gene silencing using SiRNA and ShRNA in mammalian cells extraction of plasmid, genomic DNA and RNA, quantification of nucleic acid and protein.

PROFESSIONAL ORGANIZATION MEMBERSHIP

- American Society for Microbiology (ASM).